

**Derivation of autothermal pyrolysis reaction kinetics**

by

**Chad Alan Peterson**

A dissertation submitted to the graduate faculty  
in partial fulfillment of the requirements for the degree of

**DOCTOR OF PHILOSOPHY**

Major: Mechanical Engineering

Program of Study Committee:  
Robert Brown, Major Professor  
Brent Shanks  
Jean-Philippe Tessonier  
Shankar Subramaniam  
Song-Charng Kong

The student author, whose presentation of the scholarship herein was approved by the program of study committee, is solely responsible for the content of this dissertation. The Graduate College will ensure this dissertation is globally accessible and will not permit alterations after a degree is conferred.

Iowa State University

Ames, Iowa

2020

Copyright © Chad Alan Peterson, 2020. All rights reserved.

## TABLE OF CONTENTS

	Page
ACKNOWLEDGMENTS .....	v
ABSTRACT.....	vii
CHAPTER 1. INTRODUCTION .....	1
Lignocellulose as a renewable feedstock.....	1
Thermochemical Processing of Biomass.....	2
Overview of Autothermal Pyrolysis .....	3
Autothermal Processing at Iowa State University .....	4
Initial Modeling of Autothermal Pyrolysis.....	7
Dissertation Organization .....	8
References .....	9
CHAPTER 2. OXIDATION KINETICS OF BIOCHAR FROM WOODY AND HERBACEOUS BIOMASS .....	12
Abstract.....	12
Introduction .....	13
Materials and methods.....	17
Biochar production .....	17
Acid washing of biochar.....	18
Biochar characterization .....	18
Experiments to determine chemical kinetics of biochar oxidation .....	19
Fluidized bed experiments.....	21
Results .....	24
Biochar elemental and compositional analysis .....	24
Oxidation rates from TGA experiments .....	25
Char oxidation rates from fluidized bed experiments .....	34
Estimating the effect of particle attrition on biochar oxidation kinetics .....	41
Conclusions .....	43
Acknowledgements .....	44
Declaration of Competing Interest .....	45
References .....	45
CHAPTER 3. LOW TEMPERATURE OXIDATION KINETICS OF THE PRODUCTS OF BIOMASS PYROLYSIS .....	49
Abstract.....	49
Introduction .....	49
Methods .....	54
Continuous reactor system .....	54
Hydrodynamic model .....	55
Derivation of decomposition rates .....	57
Oxidation rate derivation.....	58
Reactor repeatability.....	59

Results .....	60
Two phase theory validation .....	60
Oxidation rate of select pyrolysis products .....	61
Heat of combustion calculations .....	68
Conclusions .....	69
Acknowledgements .....	69
References: .....	70
 CHAPTER 4. OXIDATION OF PHENOLIC COMPOUNDS DURING AUTOTHERMAL PYROLYSIS OF LIGNOCELLULOSE .....	73
Abstract.....	73
Introduction .....	73
Methods .....	79
Pyrolysis of red oak and recovery of bio-oil fractions .....	79
Bio-oil analysis.....	80
Micropyrolysis experiments of model phenolic compounds .....	83
Results .....	84
Effect of oxygen on the elemental composition of phenolic oligomers.....	84
Effect of oxygen on the molecular weight of phenolic oligomers .....	85
Effect of oxygen on phenolic oligomer functional groups.....	87
Influence of oxygen functionality on polymerization of model compounds .....	90
Effect of oxygen functionality on phenolic oligomer bonds.....	92
Conclusions .....	97
Acknowledgements .....	97
References .....	98
 CHAPTER 5. EFFECT OF TEMPERATURE ON PYROLYSIS OF FERROUS SULFATE PRETREATED CORN STOVER .....	103
Abstract.....	103
Introduction .....	104
Methods .....	107
Biomass pretreatment .....	107
Continuous pyrolysis reactor and fractional recovery.....	107
Product analysis.....	109
Results .....	113
Influence of temperature on grouped pyrolysis products.....	113
Temperature effects on bio-oil heavy ends .....	117
Temperature effect on bio-oil light ends .....	124
Comparison of pyrolysis co-products.....	126
Conclusions .....	129
Acknowledgements .....	130
References .....	130
 CHAPTER 6. GENERAL CONCLUSION.....	134
Chapter 1.....	134
Chapter 2.....	134
Chapter 3.....	135

Chapter 4.....	136
Chapter 5.....	136
Future Work.....	137
APPENDIX A. Nomenclature Chapter 3.....	138
APPENDIX B. Supplemental Information Chapter 3 .....	139
Reactor model.....	139

## ACKNOWLEDGMENTS

I would like to thank my advisor, Dr. Robert Brown, for all the advice and helpful guidance over my graduate career. My research and growth would not have been the same without his exceptional tutelage. After my first tour of the Bioeconomy Institute back in Fall 2015, I knew that I wanted to be a part of his research group. I am extremely grateful Dr. Brown took me on as a graduate student and supported me throughout my studies.

I would also like to thank all my committee members, Dr. Brent Shanks, Dr. Jean-Philippe (JP) Tessonnier, Dr. Song-Charng Kong, and Dr. Shankar Subramaniam, for their helpful advice and support.

In addition, thank you to all of the staff at the Bioeconomy Institute and BioCentury Research Farm. I have had the honor of working with world-class staff that significantly advanced my studies. In no particular order, the work of Ryan Smith, Patrick Johnston, Lysle Whitmer, Marge Rover, Brad Koenig, Preston Gable, John Stanford, and Andrew Friend, all provided tremendous support and I am truly grateful. Likewise, my undergraduate assistants, Malachi Hornbuckle and Charles Fields made my life so much easier and advanced my research tremendously, to which I owe them greatly.

I have had the support of numerous friends during my time at Iowa State. To all my friends, thanks for being awesome these past four years. To avoid unintentionally forgetting a name, I will not even attempt to make a list, but thanks again. Likewise, I want to give a shout-out to my friends from undergrad (607/731 represent) that accidentally pushed me down this extremely rewarding path. My parents (John and Kathy) were always supportive, so thanks for that. Also, my three brothers (Aaron, Brian, and Darin) were always willing to help me out, so thanks again.

Now, saving the best for last. My longtime partner, Megan Wettlaufer, thanks for the continued support over the years. This work is as much yours as mine. I am truly grateful to have shared our time together at Iowa State and look forward to our continued adventures.

**ABSTRACT**

The conversion of lignocellulosic material to higher value chemicals and fuels offers a renewable feedstock for carbon-based products. Fast pyrolysis offers one potential route to convert raw biomass into higher value products. As pyrolysis bio-refineries become available, technical challenges will exist providing sufficient thermal energy to support this endothermic process at large scales. Fortunately, autothermal pyrolysis can solve these heat transfer limitations as thermal energy can now be generated within the reactor. However, given the low temperature (400-600°C) operation of these autothermal pyrolyzers, relevant oxidation kinetics are not available. Consequently, this absence in knowledge is addressed in this work determining relevant oxidation kinetics to autothermal pyrolysis.

This work primarily focuses on the derivation of oxidation kinetics pertaining to autothermal pyrolysis. In depth kinetic studies were subsequently conducted for bio-oil products and char oxidation, deriving valuable reaction data. Additional work analyzed autothermal produced phenolic oil, finding subtle partial oxidation reactions occurred to this lignin derived fraction. Finally, a temperature study was conducted under autothermal conditions to determine the effect of temperature. The derived kinetic data from this work will undoubtedly improve the operation and scale-up of autothermal pyrolyzers.

## CHAPTER 1. INTRODUCTION

### **Lignocellulose as a renewable feedstock**

Carbon is used in nearly every aspect of our modern society for transportation fuels, plastics, and chemicals. The majority of this carbon is provided through fossil carbon, thus being a finite resource. In addition, there are negative environmental impacts from the usage of this sequestered carbon. The consumption of sequestered carbon for transportation fuels releases CO<sub>2</sub> into the atmosphere, causing a greenhouse effect, and single use plastics are quickly accumulating in the environment [1]. Consequently, finding renewable resources to replace fossil carbon is an urgent matter.

Biorenewables offer a promising alternative to traditional fossil carbon. Among these, biomass can be used as a direct replacement for fossil carbon with proper processing. According to the most recent Billion Ton Study, the upwards of 30% of fossil fuels could be replaced with biomass in the United States [2]. Among the many forms of biomass, lignocellulose appears promising to produce fuels and higher value chemicals. However, unlike conventional hydrocarbons, lignocellulosic biomass contains a significant amount of oxygen that complicates its conversion to traditional products [3].

Lignocellulose is composed of three primary components: cellulose, hemicellulose, and lignin. Cellulose is repeating homopolymer chain of D-glucose units bonded by  $\beta$  (1-4) glycosidic bonds. Typical chain length of cellulose is on the order of 1000-3000 repeating units. Cellulose is generally 40-50 wt.% of herbaceous and wood feedstocks, though can exceed 90 wt.% in cotton. The next component, hemicellulose, is often defined as a repeating five carbon sugar, xylose, though includes other components including acetyl groups, mannose, and even trace amounts of glucose. Hemicellulose composition varies among feedstocks, though it is



approximately 15-30 wt. % [4]. Finally, lignin is complex three-dimensional structure consisting of phenolic monomers. Lignin acts to provide rigidity and as a binder for the polysaccharides (cellulose and hemicellulose). The lignin structure is composed of three monolignol blocks: paracoumaryl alcohol, coniferyl alcohol, and sinapyl alcohol. The respective blocks differ by methoxy groups and are more commonly referred to as p-hydroxyphenyl (H), guaiacyl (G), and syringyl (S) units. Lignin composition varies between feedstocks but is generally 10-25 wt.% [4].

Utilization of lignocellulosic biomass offers a promising route forward to reduce dependence on non-renewable sources of carbon. However, given the recalcitrant structure and varying composition of biomass, a conversion process is needed to turn the material into higher value products.

### **Thermochemical Processing of Biomass**

Thermochemical conversion of biomass offers one promising route to produce useful renewable products. These processes use some combination of heat, pressure, and catalyst to transform organic material into chemicals, fuels, and power. Thermochemical conversions are typically divided into four subgroups: pyrolysis, gasification, combustion, and solvent liquefaction [5]. While each offer their own benefits, fast pyrolysis has emerged as a promising approach to convert lignocellulosic biomass into a suitable product for upgrading to fuels and chemicals [6]. Fast pyrolysis is conventionally defined as the rapid decomposition of biomass in the absence of oxygen, to produce bio-oil, char, and non-condensable gases (NCG). This rapid decomposition occurs in a matter of seconds at temperatures between 400-600°C at atmospheric pressure. The primary product, bio-oil, is produced at up to 75 wt. %, containing hundreds of carbohydrate-derived compounds, including ketones, aldehydes, and acids, as well as lignin-derived phenolic monomers and oligomers [7]. The other valuable product, biochar, often retains

the original shape of the biomass particle and is used for a variety of applications [3]. Finally, NCG is mainly comprised of carbon monoxide and carbon dioxide, with trace amounts of methane, ethane, and other light hydrocarbon gases.

During pyrolysis, thermal energy is required to heat the organic material and for the decomposition reactions. This enthalpy for pyrolysis, including the sensible energy to raise the biomass from ambient conditions to reaction temperature (500°C), has been experimentally calculated as 0.8 MJ/kg to 1.6 MJ/kg, depending on the feedstock [8]. A theoretical calculation using thermodynamic data determined the enthalpy for pyrolysis to be 1.1-1.6 MJ/kg, nearly identical to experimental data [9]. This enthalpy for pyrolysis represents just 10% of the energy contained in biomass; thus, is a relatively small portion of energy. While this enthalpy for pyrolysis is often not considered an issue at the laboratory scale, providing this thermal energy at large commercial scale is more difficult requiring ancillary heat conveyance equipment [10]. As a result, at the commercial scale the secondary combustor, and auxiliary heat transfer equipment, are on the order of 30% of the total capital costs [11]. Consequently, the potential to eliminate this large capital cost will improve the economics of these commercial pyrolysis plants.

### **Overview of Autothermal Pyrolysis**

Traditionally pyrolyzers operate under inert conditions, so only a few researchers have explored the effects of oxygen. Nevertheless, researchers have admitted mixtures of nitrogen and oxygen into fluidized bed reactors to explore the feasibility of autothermal pyrolysis [12,13]. The goal of this autothermal pyrolysis is to balance the endothermic pyrolysis with exothermic oxidation reactions. Though innovative to biomass fast pyrolysis, the concept of autothermal operation is not novel and has been previously explored for hydrocarbon cracking [14,15]. Li et. al.[13] performed autothermal fast pyrolysis with birch bark using a fluidized bed reactor at

equivalences ratios as low as 0.05. Here the equivalence ratio is defined as the air (oxygen) used over the stoichiometric requirement for full combustion. While autothermal operation was achieved, there was a 22% relative decrease in bio-oil. Other researchers used a fixed bed reactor to pyrolyze wood chips in autothermal and allothermal operation to measure the effect of oxygen [16]. Again, under the autothermal operation large quantities of bio-oil were consumed, approximately 22 wt. %, and the fixed bed caused a flame front with wide variation ( $>100^{\circ}\text{C}$ ) in bed temperature. While these groups demonstrated that autothermal pyrolysis is possible, further research was needed to prevent unacceptable bio-oil losses.

Though autothermal operation was not the goal, admittance of oxygen into pyrolyzers does not necessarily result in large losses of bio-oil. Using a fluid bed reactor, Kim et. al.[17,18] pyrolyzed red oak, and admitted a small amount of oxygen in the nitrogen sweep gas at 0.525% to 8.40% (v/v) to determine the effect of oxygen. The calculated equivalence ratios for these experiments, ranged from 0.034 to 0.539. At equivalence ratios below 0.136, representing 2.10%  $\text{O}_2$  in the fluidizing gas, select characterized bio-oil products decreased from 12.7 wt. %, on a biomass basis, to just 11.1 wt.%. In particular, acetic acid and acetol decreased by 25% and 45%, respectively comparing the inert condition to an equivalence ratio of 0.136. Consequently, while there was a decrease in bio-oil products, the overall yield of bio-oil was minimally impacted with the addition of small amounts of oxygen.

### **Autothermal Processing at Iowa State University**

While other attempts at autothermal operation had large losses in bio-oil, recent research at Iowa State University (ISU) demonstrated certain reactor conditions can minimize bio-oil consumption. Using a 3.5 inch bubbling fluidized bed reactor operating at  $500^{\circ}\text{C}$ , Polin et al.[19] conducted experiments under inert and autothermal conditions, at equivalence ratio of 0.107,

pyrolyzing red oak. Comparison of the carbon yield between autothermal and conventional, non-oxidative, pyrolysis (Figure 1) indicated large losses of carbon in the bio-char (4.9%). A similar decrease (5.1%) was measured for the aqueous fraction, here called the bio-oil light ends containing water and light oxygenated compounds. However, the carbon yield of the valuable bio-oil heavy ends, containing the lignin derived phenolic oil and anhydrosugars, had a relatively small (3%) decrease. As a result, this demonstrated that under proper operating conditions, valuable carbon can be retained in the bio-oil. Likewise, the large decrease in carbon for biochar indicated char oxidation was providing substantial amounts of the thermal energy.

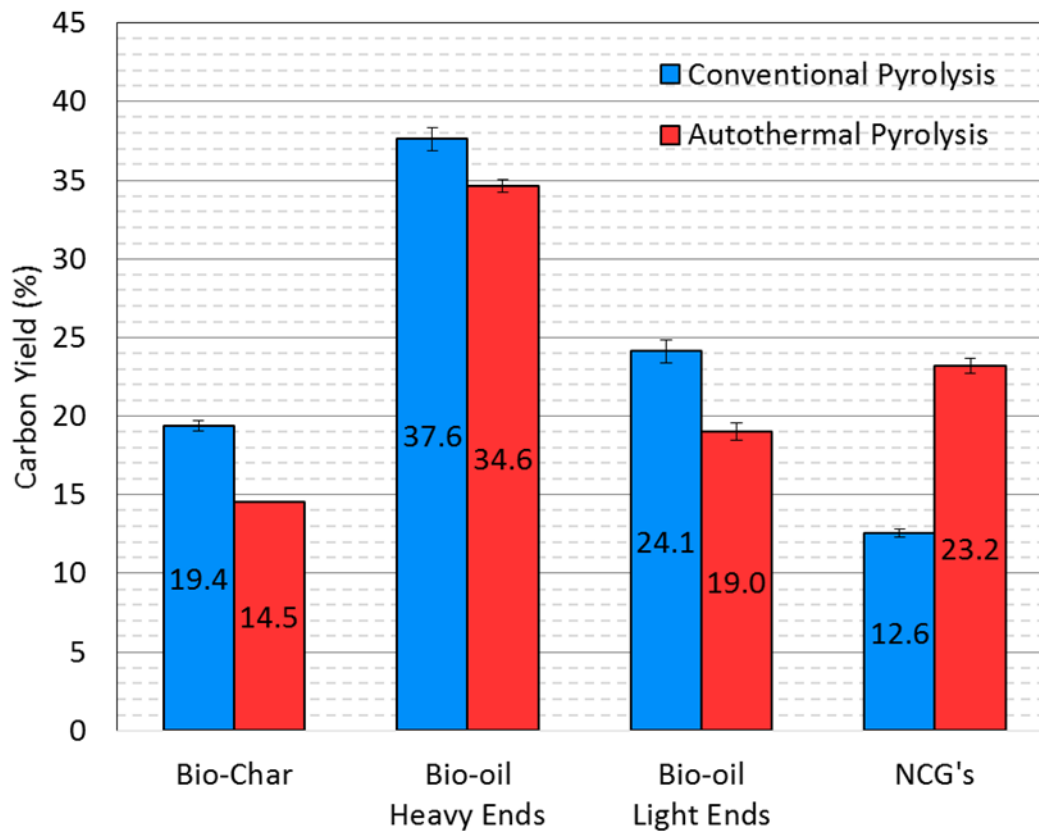


Figure 1 Carbon balance of autothermal pyrolysis of red oak performed on a fluidized bed reactor at 500 °C. Figure adapted from Polin et al.[19].

Similar experiments conducted by Polin et al. [20] with corn stover as a feedstock found that again biochar and bio-oil light end carbon was consumed (Figure 2). Even more favorable,

bio-oil heavy ends had no measurable decrease in carbon content (27.1 vs 27.3%). Of note, the calculated equivalence ratio for corn stover was only 0.067, lower than that required for red oak. While the enthalpy for pyrolysis is lower for corn stover as compared to red oak [8] (1.35 MJ/kg vs. 1.46 MJ/kg) these two instances of autothermal pyrolysis suggest that differences in product consumption likely contributed to the different equivalence ratios.

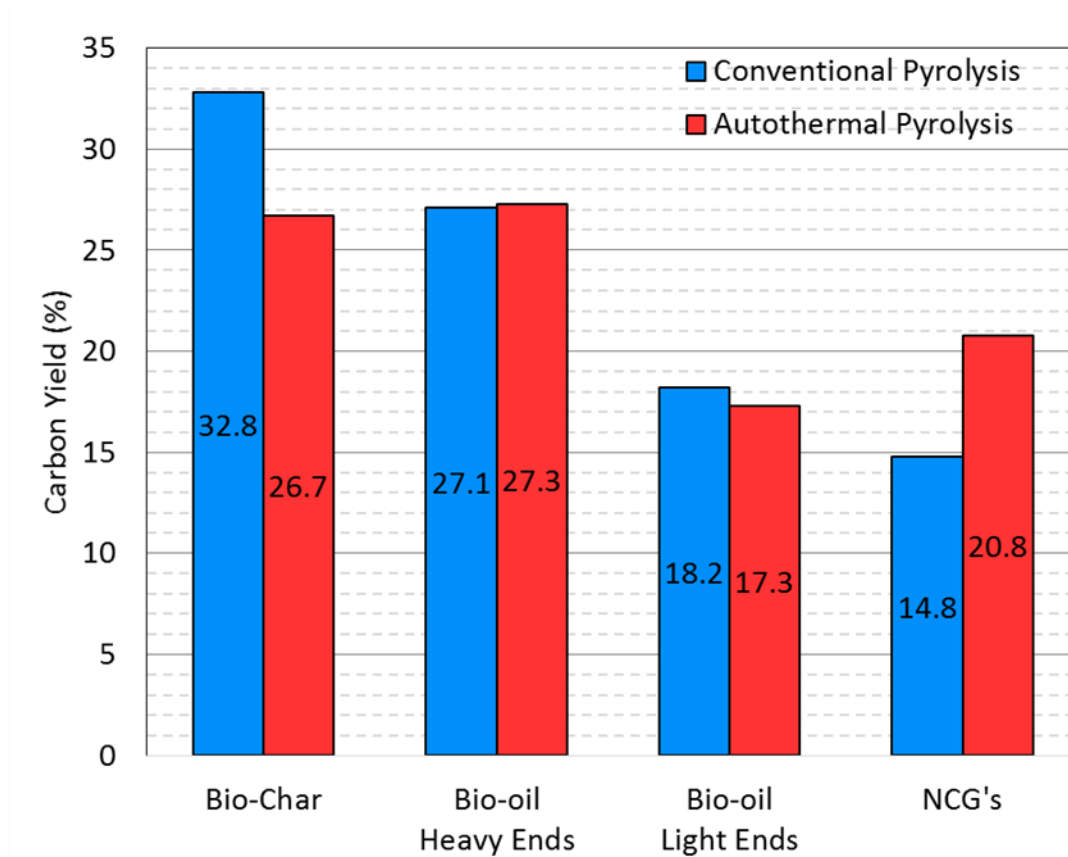


Figure 2 Carbon balance of corn stover autothermal and conventional pyrolysis. Figure adapted from Polin et al. [20].

The success of these two cases is from the retention of biochar in fluidized bed, allowing for a large concentration of biochar to oxidize providing energy towards the enthalpy for pyrolysis. Likewise, by minimizing a flame front, as seen with the autothermal pyrolysis in a fixed bed, oxidation of the bio-oil vapors was minimized. Consequently, these two instances of autothermal pyrolysis demonstrate that under proper operating conditions oxidation reactions can

be tailored to consume the least valuable products (biochar) while still providing energy for pyrolysis.

### **Initial Modeling of Autothermal Pyrolysis**

With the recent research at ISU demonstrating autothermal operation of fast pyrolysis is possible, modeling these reactions would assist with process scale-up and operability. Given the recent advances in autothermal pyrolysis operation, few attempts have been made to model this process. Mellin[21] used Ansys Fluent, a computational fluid dynamics software, to model the effects of oxygen in the fluidizing sweep gas of a fluidized bed pyrolyzer at low equivalence ratios (0.00-0.026). The model consisted of biomass first converting to an active volatile state and then further decomposing to char, non-condensable gas, or tar (bio-oil). The tar could then either oxidize or further decompose to a secondary tar, a gaseous product, or oxidize. Overall, the model predicted a large quantity of the tar (bio-oil), the upwards of 30%, would oxidize providing heat for pyrolysis. While the oxidation of the bio-oil is consistent with earlier attempts at autothermal pyrolysis, this large loss of bio-oil was not seen with the work at ISU. Furthermore, important gas-solid phase reactions with biochar (e.g. char oxidation) were not included. This highlights the importance of the gas solid phase reactions to support autothermal pyrolysis.

Given the value of bio-oil as compared to biochar and NCG, minimizing its oxidation is critical. While the goal is quite simple, initial modeling attempts determined there was a lack of relevant kinetic data. High temperature combustion is well known for select gaseous fuels at elevated temperatures ( $>1000^{\circ}\text{C}$ ) [22,23], however this information does not apply to the lower temperatures ( $\sim 500^{\circ}\text{C}$ ) of pyrolysis. Progress in autothermal pyrolysis will require a better understanding of the oxidation reactions that both drive the process and affect product

composition and distribution. Consequently, efforts to understand these partial oxidation reactions were undertaken.

### **Dissertation Organization**

To build an accurate model of autothermal pyrolysis, low temperature oxidation reactions of pyrolysis products needed to be explored. In particular, gas-solid phase reactions (e.g. char oxidation) and the oxidation of pyrolysis vapors were identified as the most important. Additionally, the effect of oxidation on the lignin derived phenolic oil was investigated using analytical analyses and model compound studies. Thus, the work of this dissertation is to bridge the gap between experimental operation of autothermal processing and computational models that fail to explain the reactions adequately.

Chapter 2 involved the derivation of char oxidation rates. Given differences in carbon consumption between the red oak and corn stover ISU autothermal experiments, it was hypothesized the alkali and alkaline earth metal (AAEM) content was partially responsible for these differences. Therefore, to determine the role of AAEM content, six fast pyrolysis produced biochars were subjected to kinetic studies. Using combined thermogravimetric analysis (TGA) and fluidized bed experiments reaction rates and correlations based on ash content were proposed. Additional experiments were conducted on acid washed biochars to passivate the catalytically active metals, further bolstering proposed relationship correlations. Fluidized bed experiments also explored the role of AAEM content on the production of CO and CO<sub>2</sub>.

Chapter 3 focused on the derivation of global oxidation rates using a fluidized bed reactor. Using the two-phase theory and modeling the fluid bed as ideal reactors, reaction rates were derived from experimental data. Given bio-oil contains hundreds of compounds, it was impossible to derive reaction rates for all the major bio-oil products [24]. Therefore, three

compounds: acetic acid, levoglucosan, and xylose were used representing the major bio-oil components of light acids and sugars. The rates derived are the first of their kind for the two sugar products (xylose and levoglucosan) offering valuable kinetic data to model autothermal pyrolysis.

Chapter 4 involved an in-depth analysis of the bio-oil heavy ends from the autothermal pyrolysis experiments of Polin et al [19]. The study explored the partial oxidation of lignin-derived compounds, which generates both carbon oxides and carbonyl compounds. By using several analytical techniques, it was found that partial oxidation reactions, those not producing CO<sub>2</sub> and H<sub>2</sub>O, was occurring with the lignin derived phenolic fraction. Oxidation of these phenolic compounds influences their subsequent polymerization and condensation to form phenolic oligomers. Additionally, model phenolic compounds were pyrolyzed to help understand the mechanisms of partial oxidation during autothermal pyrolysis of lignocellulose.

Finally, Chapter 5, examined the effect of temperature on autothermal pyrolysis of ferrous sulfate treated corn stover. The project analyzed the products from ferrous sulfate pretreated corn stover pyrolyzed at 400, 450, 500, and 550°C to determine the effect of temperature of this feedstock. With the four different temperatures, analysis of the bio-oil was also used to elucidate the role of temperature on the oxidation reactions. Using the kinetic data derived in this work, the goal was to optimize sugar yield by varying the reactor temperature.

## References

- [1] C. Ostle, R.C. Thompson, D. Broughton, L. Gregory, M. Wootton, D.G. Johns, The rise in ocean plastics evidenced from a 60-year time series, *Nat. Commun.* 10 (2019) 1622. <https://doi.org/10.1038/s41467-019-09506-1>.
- [2] B.M.H.J. Langholtz, L.M. Stokes, Eaton, 2016 BILLION-TON REPORT Advancing Domestic Resources for a Thriving Bioeconomy, Oak Ridge Natl. Lab. 1160 (2016) 448–2172. <https://doi.org/ORNL/TM-2016/160>.



- [3] R.C. Brown, T.R. Brown, *Biorenewable Resources: Engineering New Products from Agriculture: Second Edition*, John Wiley & Sons, Inc., Hoboken, NJ, USA, 2014. <https://doi.org/10.1002/9781118524985>.
- [4] F.H. Isikgor, C.R. Becer, Lignocellulosic biomass: a sustainable platform for the production of bio-based chemicals and polymers, *Polym. Chem.* 6 (2015) 4497–4559. <https://doi.org/10.1039/c5py00263j>.
- [5] R.C. Brown, *Thermochemical Processing of Biomass: Conversion into Fuels, Chemicals and Power*, John Wiley & Sons, Ltd, Chichester, UK, 2011. <https://doi.org/10.1002/9781119990840>.
- [6] A. V. Bridgwater, Review of fast pyrolysis of biomass and product upgrading, *Biomass and Bioenergy*. 38 (2012) 68–94. <https://doi.org/10.1016/j.biombioe.2011.01.048>.
- [7] S. Czernik, A. V. Bridgwater, Overview of applications of biomass fast pyrolysis oil, *Energy and Fuels*. 18 (2004) 590–598. <https://doi.org/10.1021/ef034067u>.
- [8] D.E. Dugaard, R.C. Brown, Enthalpy for pyrolysis for several types of biomass, *Energy and Fuels*. 17 (2003) 934–939. <https://doi.org/10.1021/ef020260x>.
- [9] H. Yang, S. Kudo, H.P. Kuo, K. Norinaga, A. Mori, O. Mašek, J.I. Hayashi, Estimation of enthalpy of bio-oil vapor and heat required for pyrolysis of biomass, *Energy and Fuels*. 27 (2013) 2675–2686. <https://doi.org/10.1021/ef400199z>.
- [10] L. Rosendahl, *Biomass combustion, technology and engineering*, n.d. <https://www.oreilly.com/library/view/biomass-combustion-science/9780857091314/> (accessed September 6, 2019).
- [11] M.M. Wright, D.E. Dugaard, J.A. Satrio, R.C. Brown, Techno-economic analysis of biomass fast pyrolysis to transportation fuels, *Fuel*. 89 (2010) S2–S10. <https://doi.org/10.1016/J.FUEL.2010.07.029>.
- [12] J.M. Mesa-Pérez, J.D. Rocha, L.A. Barbosa-Cortez, M. Penedo-Medina, C.A. Luengo, E. Cascarosa, Fast oxidative pyrolysis of sugar cane straw in a fluidized bed reactor, *Appl. Therm. Eng.* 56 (2013) 167–175. <https://doi.org/10.1016/j.applthermaleng.2013.03.017>.
- [13] D. Li, F. Berruti, C. Briens, Autothermal fast pyrolysis of birch bark with partial oxidation in a fluidized bed reactor, *Fuel*. 121 (2014) 27–38. <https://doi.org/10.1016/j.fuel.2013.12.042>.
- [14] H. Sun, C. Rosenthal, L.D. Schmidt, Oxidative pyrolysis of polystyrene into styrene monomers in an autothermal fixed-bed catalytic reactor, *ChemSusChem*. 5 (2012) 1883–1887. <https://doi.org/10.1002/cssc.201200412>.
- [15] C. Boyadjian, L. Lefferts, K. Seshan, Catalytic oxidative cracking of hexane as a route to olefins, *Appl. Catal. A Gen.* 372 (2010) 167–174. <https://doi.org/10.1016/j.apcata.2009.10.030>.

- [16] M. Milhé, L. van de Steene, M. Haube, J.-M. Commandré, W.-F. Fassinou, G. Flamant, Autothermal and allothermal pyrolysis in a continuous fixed bed reactor, *J. Anal. Appl. Pyrolysis*. 103 (2013) 102–111. <https://doi.org/10.1016/J.JAAP.2013.03.011>.
- [17] K.H. Kim, X. Bai, M. Rover, R.C. Brown, The effect of low-concentration oxygen in sweep gas during pyrolysis of red oak using a fluidized bed reactor, *Fuel*. 124 (2014) 49–56. <https://doi.org/10.1016/j.fuel.2014.01.086>.
- [18] K.H. Kim, R.C. Brown, X. Bai, Partial oxidative pyrolysis of acid infused red oak using a fluidized bed reactor to produce sugar rich bio-oil, *Fuel*. 130 (2014) 135–141. <https://doi.org/10.1016/j.fuel.2014.04.044>.
- [19] J.P. Polin, C.A. Peterson, L.E. Whitmer, R.G. Smith, R.C. Brown, Process intensification of biomass fast pyrolysis through autothermal operation of a fluidized bed reactor, *Appl. Energy*. 249 (2019) 276–285. <https://doi.org/10.1016/J.APENERGY.2019.04.154>.
- [20] J.P. Polin, H.D. Carr, L.E. Whitmer, R.G. Smith, R.C. Brown, Conventional and autothermal pyrolysis of corn stover: Overcoming the processing challenges of high-ash agricultural residues, *J. Anal. Appl. Pyrolysis*. 143 (2019) 104679. <https://doi.org/10.1016/j.jaap.2019.104679>.
- [21] P. Mellin, Y. Wu, E. Kantarelis, W. Yang, CFD Modelling of Heat Supply in Fluidized Bed Fast Pyrolysis of Biomass. CFD MODELLING OF HEAT SUPPLY IN FLUIDIZED BED FAST PYROLYSIS OF BIOMASS, in: *Proc. 10th Int. Conf. Comput. Fluid Dyn. Oil Gas, Metall. Process Ind. (CFD 2014)*, Trondheim , Norway, 2014.
- [22] W. Tsang, R.F. Hampson, Chemical Kinetic Data Base for Combustion Chemistry. Part I. Methane and Related Compounds, *J. Phys. Chem. Ref. Data*. 15 (1986) 1087–1279. <https://doi.org/10.1063/1.555759>.
- [23] N.M. Marinov, A detailed chemical kinetic model for high temperature ethanol oxidation, *Int. J. Chem. Kinet*. 31 (1999) 183–220. [https://doi.org/10.1002/\(SICI\)1097-4601\(1999\)31:3<183::AID-KIN3>3.0.CO;2-X](https://doi.org/10.1002/(SICI)1097-4601(1999)31:3<183::AID-KIN3>3.0.CO;2-X).
- [24] Y.S. Choi, P.A. Johnston, R.C. Brown, B.H. Shanks, K.H. Lee, Detailed characterization of red oak-derived pyrolysis oil: Integrated use of GC, HPLC, IC, GPC and Karl-Fischer, *J. Anal. Appl. Pyrolysis*. 110 (2014) 147–154. <https://doi.org/10.1016/j.jaap.2014.08.016>.

## CHAPTER 2. OXIDATION KINETICS OF BIOCHAR FROM WOODY AND HERBACEOUS BIOMASS

Chad A. Peterson<sup>1</sup>, Robert C. Brown<sup>1,2</sup>

<sup>1</sup>*Department of Mechanical Engineering, Iowa State University, Ames, IA 50011, United States*

<sup>2</sup>*Bioeconomy Institute, Iowa State University, Ames, IA 50011, United States*

Modified from a manuscript published in Chemical Engineering Journal

### Abstract

The goal of this study was to determine oxidation kinetics for biochar produced from fast pyrolysis of various biomass feedstocks. In particular, the role of inherent ash content on the oxidation rate was evaluated. Thermogravimetric analysis (TGA) and fluidized bed combustion experiments were used to explore oxidation kinetics of six fast pyrolysis produced biochars with diverse ash content. Reaction rates varied by a factor of three under chemical kinetic-limited conditions, demonstrating inorganic content impacts oxidation rate. Chemical kinetic rate coefficients were proposed as a function of compositional parameters to determine overall fit and impact. Potassium content was found to have a positive correlation, best describing the differences in the oxidation kinetic rate coefficients. Additionally, feedstocks were subjected to a 1M HCl acid wash mitigating the catalytic activity of the metals. Acid washed biochars had lower oxidation kinetic rates compared to their unwashed counterparts, indicating the removal of catalytically active metals reduced oxidation rate. Gas composition (CO/CO<sub>2</sub>) was measured during fluidized bed experiments for both acid-washed and unwashed biochars, which varied between the six biochars. Formation of CO<sub>2</sub> was greatly affected by catalytic metals, finding potassium content to correlate well with a higher percentage of CO<sub>2</sub> formation as compared to

CO. Comparison of oxidation rates were made between the two experimental apparatuses to measure the effect of attrition on biochar oxidation.

### **Introduction**

Lignocellulosic biomass has gained attention as feedstock for producing renewable chemicals and biofuels [1]. Thermochemical processing of biomass, including fast pyrolysis, is a promising route to convert biomass into bio-oil, biochar, and non-condensable gases [2]. Because pyrolysis is an endothermic process [3], an external energy source is required to drive the process. Providing this energy through heat transfer is readily achieved at laboratory scale, but it becomes increasingly difficult as the reactor is scaled due to the decreasing surface area-to-volume ratio [4]. To provide thermal energy at large scale, the biochar product is commonly directed to a solid-fuel combustor where refractory particles are heated and then conveyed to the pyrolyzer. This system is commonly manifested as bubbling or circulating fluidized beds [5] or auger reactors [6] in combination with an external combustor and appropriate solids conveyance systems. The need to convey solid heat carriers between a char combustor and pyrolysis reactor adds complexity and cost to the system.

Polin et al. [7,8] has recently demonstrated autothermal pyrolysis as an alternative to heat transfer to provide the enthalpy for pyrolysis. Small amounts of oxygen, approximately 10% of that required for full combustion, is admitted to the reactor, which partially oxidizes products of pyrolysis and releases thermal energy to the process. Recent studies indicate that biochar is preferentially oxidized during autothermal pyrolysis, substantially preserving the more valuable bio-oil [7,8]. Differences among feedstocks (e.g. herbaceous vs woody) appear to influence biochar oxidation and the total oxygen required for autothermal operation. For example, red oak required processing at an equivalence ratio 40% higher than corn stover to achieve autothermal

operation. Thus, a better understanding of the oxidation kinetics for biochar at pyrolysis temperatures (400-600°C) will improve the design and operability of autothermal pyrolysis reactors.

Char oxidation kinetics have been extensively studied in the past fifty years [9]. These early reports revealed three distinct regimes of gas-solid phase reactions (combustion) based on temperature [10]. Regime I is controlled by chemical kinetics, with internal and external mass transfer playing no role. In Regime I, using sufficiently small particles, the intrinsic activation energy can be determined. The second regime is at slightly elevated temperatures where mass transfer limitations can no longer be ignored and is partially rate limiting. In Regime II, the apparent activation energy is approximately half that of Regime I, assuming first order kinetics. Regime III occurs at elevated temperatures where chemical kinetics are sufficiently fast; thus, the rate is determined by the external mass transfer rate. Here the apparent activation energy is very small. In order to derive accurate reaction kinetics, it is important to delineate these combustion regimes. In addition to the external mass transfer rate, oxygen partial pressure and internal mass transfer can impact the oxidation rate. Typically, sufficiently small particles (<300  $\mu\text{m}$ ) are required to minimize internal mass transfer effects [11]. Likewise, decreasing oxygen partial pressure reduces the overall combustion rate [12]. Consequently, controlling these two is important to derive true reaction kinetics.

Naturally occurring metals in biomass, in particular alkali and alkaline earth metals (AAEM), can catalyze char oxidation [13–15]. Zhang et al. [13] found that chars impregnated with metals shortened the total burnout time. All the metals evaluated reduced the burnout time; however, potassium had a higher reactivity than sodium, calcium, or magnesium [13]. Yi et al. [14] studied combustion characteristics of cattle manure with varying metal content finding

sodium, calcium, and potassium increased combustion rates, while magnesium had a negligible impact. These two studies indicate both the quantity and the type of AAEM can modify the overall combustion rate.

While the presence of inorganic content in chars appears to play a significant role in combustion kinetics, studies with coal chars suggest the fraction of carbon in the char could be a significant factor. Miura et al. [16] determined that when carbon content was greater than 80 wt. %, gasification reactivity was determined by the char matrix (i.e. structure). However, Várhegyi et al. [15] used a hot citric acid wash to remove AAEM from corncob biochar and found combustion reactivity decreased despite a substantial increase in surface area. This indicates inorganic content rather than structure is the driving factor behind combustion reactivity of biochar. Given operational differences observed in autothermal pyrolysis between a low ash feedstock (red oak) and high ash (corn stover), the biochar oxidation rate is hypothesized to be primarily determined by its inherent ash content.

Inorganic content also influences the relative rates of CO and CO<sub>2</sub> formation during char oxidation. Traditionally, it is assumed that oxygen first adsorbs onto the particle, reacts with the carbonaceous char forming CO, and then is released into the gas phase. After this desorption step, CO is further oxidized in the gas phase to CO<sub>2</sub>. However, Cheng et al. [17] found that char combustion with varying metal content (Na, Fe, Ca, and Al) had different rates of char consumption and relative rates of CO and CO<sub>2</sub> formation. Specifically, it was found that the metals appeared to enhance gas-solid reactions between char and oxygen to form CO<sub>2</sub> by facilitating the transport of oxygen to the char surface. Metals shuttle oxygen to the char surface through a reduction-oxidation cycle to directly form CO<sub>2</sub>. Du et al. [18] reached a similar conclusion, finding CO<sub>2</sub> formation for pure carbon was catalyzed by the addition of calcium.

Thus, inorganic content appears to affect both the oxidation rate and formation of the gases, demonstrating its importance for biochar oxidation.

Under kinetically limited oxidation, biochar diameter must be sufficiently small, usually less than 100  $\mu\text{m}$ , to mitigate internal mass transfer limitations [9]. However, in practice pyrolyzers process biomass particles that are an order of magnitude larger [8]. Therefore, bridging the gap between pure kinetic measurements (i.e. TGA) and actual systems (such as fluidized bed reactors) is an important aspect for developing accurate models. In fluidized beds, attrition of the biochar to a sufficiently small size will improve mass transfer rates increasing the overall oxidation rate. Similarly, the char attrition rate under oxidative (combustion) conditions is enhanced; thus, biochar fragmentation would occur more rapidly in an oxidative environment [19]. The increased attrition under oxidative conditions would generate biochar fines with a faster oxidation rate (from greater surface area vs. volume and improved mass transfer) as compared to the original biochar particle [20]. Enhanced attrition improves the overall char combustion rate, with the upwards of 40% of the carbon oxidized in the form of fines [20]. Scala et al. [20] found the fines produced through attrition at typical fluidized bed combustion temperatures (850°C) increased the oxidation rates, but this may not be representative of attrition at the lower temperatures of pyrolysis (400-600°C). Morin et al. [21] compared biochar oxidation rates at 370°C for experiments performed in an isothermal TGA and a fluidized bed reactor determining rates were indeed higher in the fluidized bed. While this result is consistent with accelerated oxidation of fine particles produced through attrition in the fluidized bed, the authors argued that oxidation was suppressed in the TGA due to formation of a stagnation zone that limited oxygen diffusion [21].

The overall goal of the present study is to determine biochar oxidation kinetics related to biomass autothermal fast pyrolysis. Given the low temperature of autothermal pyrolysis (400-600°C) and various feedstocks used (woody and herbaceous) relevant biochar oxidation kinetics to these conditions will aid in the scale-up and development of these autothermal pyrolyzers. Hence, one of the goals of the present study is to compare char oxidation rates under a purely chemical kinetic regime in a TGA with a fluidized bed reactor to elucidate the role of attrition on biochar oxidation at pyrolysis temperatures. Another objective is to determine the effect of ash content on rates of biochar oxidation. Biochar was produced from fast pyrolysis of six kinds of biomass with varying ash content including herbaceous and woody feedstocks. Further investigations on the effect of inorganic content on biochar oxidation were performed using biochars prepared by washing with 1M HCl acid with the goal of substantially removing metals from the biochar.

## **Materials and methods**

### **Biochar production**

Six feedstocks were selected for production of biochar: Douglas fir, pine, red oak, willow, switchgrass, and corn stover. All biomass samples were knife milled to under 1.60 mm particle size and dried to under 10 wt. % moisture. The experimental apparatus consisted of a 3.81 cm diameter, 316 stainless steel fluidized bed reactor loaded with 400 g of sand sieved to 300-600 micron. The reactor was fluidized at 500°C with 20 standard liters per minute (SLPM) of nitrogen gas. Biomass feed rate was 0.5-1.0 kg/hr. Bed temperature was  $\pm 10^\circ\text{C}$  of reactor set-point for all experiments, allowing for consistent heating of the biomass for biochar production. Biochar was collected in two cyclones, at ambient temperature, immediately following the reactor. Total sand bed loss was typically under 1%, with minimal sand collected in the biochar.



The produced pyrolysis vapors subsequently entered a staged bio-oil condenser train after the cyclones. A detailed description of reactor construction and operation can be found in previous work [22].

### **Acid washing of biochar**

Select chars were washed with hydrochloric acid (HCl) to remove metals or passivate their catalytic activity. HCl was selected as it preserves the biochar structure, while still removing some of the catalytic metals [23,24]. For this procedure, approximately 350 mg of biochar was placed in a beaker, then 300 mL of 1M HCl was added. The mixture was stirred using a magnetic stir bar for 25 minutes at room temperature. After stirring, the water was decanted, and the biochar was extensively washed with de-ionized water to remove any residual acid. Finally, the biochar was dried for sixteen hours at 85°C to drive off any remaining moisture.

### **Biochar characterization**

The moisture, volatile, and total inorganic (ash) content of the biochar was determined using proximate analysis procedures in a TGA. Total volatile content was determined as the weight lost from 105-900°C (excludes moisture) under inert conditions. Ash content was then calculated as the residual material left after oxidation at 900°C. Ultimate analysis to determine carbon, hydrogen, nitrogen, and sulfur content was performed using an Elementar Analyzer (Vario MICRO cube). The values for carbon, hydrogen, nitrogen, and sulfur content were reported on a dry basis. Oxygen content was not calculated due to the high inorganic oxygen content of the ash, consistent with previous work [25]. All samples were analyzed in duplicate.

Inductively coupled plasma (ICP)-Optical Emission Spectrometry (OES) was used to provide partial elemental analysis. The biochar was first combusted in a muffle furnace for two hours at 550°C followed by an acid digestion. The samples were digested in nitric acid via

microwave heating. The digested samples were then diluted 10,000-fold with 18.2 $\Omega$  water before analysis. Quantification followed standard acid digestion method ASTM D6349.

## **Experiments to determine chemical kinetics of biochar oxidation**

### **Thermogravimetric analysis**

A Mettler Toledo TGA/DSC1 (Columbus, OH, USA) was used for isothermal experiments. For the oxidation studies, approximately 1 mg of sieved 150-250  $\mu\text{m}$  biochar was weighed into a 150 mL alumina pan. Sample size was determined to limit the temperature rise ( $\sim 10^\circ\text{C}$ ) associated with the exothermic oxidation reactions. Likewise, preliminary experiments indicated sieving to 150-250  $\mu\text{m}$  particle size avoided internal mass transfer limitations. To derive reaction kinetics, seven temperature set points at  $33^\circ\text{C}$  intervals were used from  $333^\circ\text{C}$ - $566^\circ\text{C}$ . Selecting a particular sieve size may have resulted in a biochar reactivity bias, as particle size is known to impact fast pyrolysis yields [26]. However, given particle size was consistent between feedstocks for the biochar oxidation experiments, this represents a direct comparison of the derived rates.

For isothermal combustion, experiments were initiated by increasing temperature at  $35^\circ\text{C}/\text{min}$  with biochar samples exposed to a nitrogen flow of 100 mL/min. After ten minutes of temperature stabilization, the gas was switched from nitrogen to air at a flow rate of 250 mL/min. Mass loss due to biochar devolatilization in the nitrogen environment ranged from 5 wt. % at the lowest temperature to 25 wt. % at the hottest. This mass loss from biochar illustrates that residence times of biochar in a fast pyrolysis is often not long enough for it to fully devolatilize [27]. Exposure of the samples to oxygen, ranging from 120 minutes at  $333^\circ\text{C}$  to just 10 minutes at  $566^\circ\text{C}$ , was long enough in all cases to achieve complete combustion. Gas turnover, defined as the gas volumetric flow rate over reactor volume, was on the order of six changes per minute. The high gas turnover helped to alleviate the effect of oxygen partial pressure on combustion

experiments when switching from nitrogen to air [28]. Samples were performed in duplicates at each temperature.

The use of a volumetric model and first order kinetics are consistent with previous studies of biochar oxidation kinetic studies [29,30]. The volumetric model assumes combustion takes place uniformly in the particle and has an overall reaction order of one. More complex models accounting for changing particles (e.g. surface area, shrinking diameter, etc.) have been developed [31], but were deemed unwarranted as the volumetric model can accurately model biochar combustion kinetics while simplifying calculations [30]. For the isothermal combustion of biochar, weight loss versus time was used to derive kinetic rate coefficients. The extent of reaction was defined as the total mass loss at a certain time over the total mass loss after complete oxidation at that temperature:

$$\alpha = \frac{W_t}{W_o} \quad (1)$$

Where  $W_t$  is the weight loss at time “t”,  $W_o$  is the total weight loss (excluding mass loss from initial devolatilization), and  $\alpha$  is the extent of the reaction. From the mass loss, the rate equation is set up in the form of an ordinary differential equation assuming first order kinetics:

$$\frac{d\alpha}{dt} = k * (1 - \alpha) \quad (2)$$

Where  $k$  is the reaction rate coefficient (1/s). The differential equation and its solution are used to determine the kinetic rate coefficient based on the slope of mass loss versus time:

$$\ln(1 - \alpha) = -k * t = -\left(A * \exp\left(-\frac{E}{R*T}\right)\right) * t \quad (3)$$

Where  $A$  is the pre-exponential factor (1/s),  $E$  is the activation energy (kJ/mol),  $R$  is the universal gas constant (kJ/mol-K), and  $T$  is the temperature (K). From equation 3, the kinetic rate coefficient can be found at each temperature by measuring the mass loss of  $\ln(1 - \alpha)$  against time with a straight line, where the slope equals the kinetic rate coefficient. Then, the activation

energy and pre-exponential factor can be calculated from the slope and the intercept, respectively.

The reaction rate coefficient was calculated for the biochar oxidation rate up to 50% conversion and subsequently plotted on an Arrhenius plot. The average sample temperature, as measured with an internal thermocouple, for the same conversion frame was used for plotting the X-axis.

### **Fluidized bed experiments**

The fluidized bed reactor used for the combustion studies was a 3.81-cm diameter, 316 stainless steel reactor loaded with 400 g of 250-300  $\mu\text{m}$  diameter sand. Gas flow controllers allowed mixing of nitrogen gas and air to any desired oxygen concentration up to 21 vol. %. For the combustion experiments, air was used at a flow rate of 3.5 SLPM. Six temperature set points were used to develop reaction kinetics: 420, 445, 466, 500, 533, and 566°C. The fluidization velocity over the minimum fluidization velocity ( $U_m/U_{mf}$ ) was calculated as 2.3 to 3, increasing with reactor temperature and gas expansion. Gas turnover for the fluidized bed was calculated at 3.5 seconds, indicating a rapid change from inert to oxidative conditions. This airflow quantity was also found to minimize partial oxygen pressure effects. All experiments were performed in triplicate. A block diagram of the reactor is shown in Fig. 1.

The biochar particle size used was 600-850  $\mu\text{m}$ , which as determined from the TGA experiments, introduced internal mass transfer limitations. The larger particle size was necessary to avoid immediate elutriation from the fluidized bed reactor and to measure the impact of attrition on biochar oxidation. If biochar attrition is sufficiently fast (i.e. immediately reducing the biochar diameter to <200  $\mu\text{m}$ ) the kinetic rate coefficients from the TGA and fluidized bed should be identical as the internal mass transfer limitation is mitigated. However, if the biochar particle is primarily oxidized at its original size, the overall reaction rate will be slower than that

of the TGA experiments. Note, two temperatures for corn stover oxidation experiments (420 and 440°C) used a slightly smaller sieve size of 450-600  $\mu\text{m}$ , though the impact of attrition will remain the same.

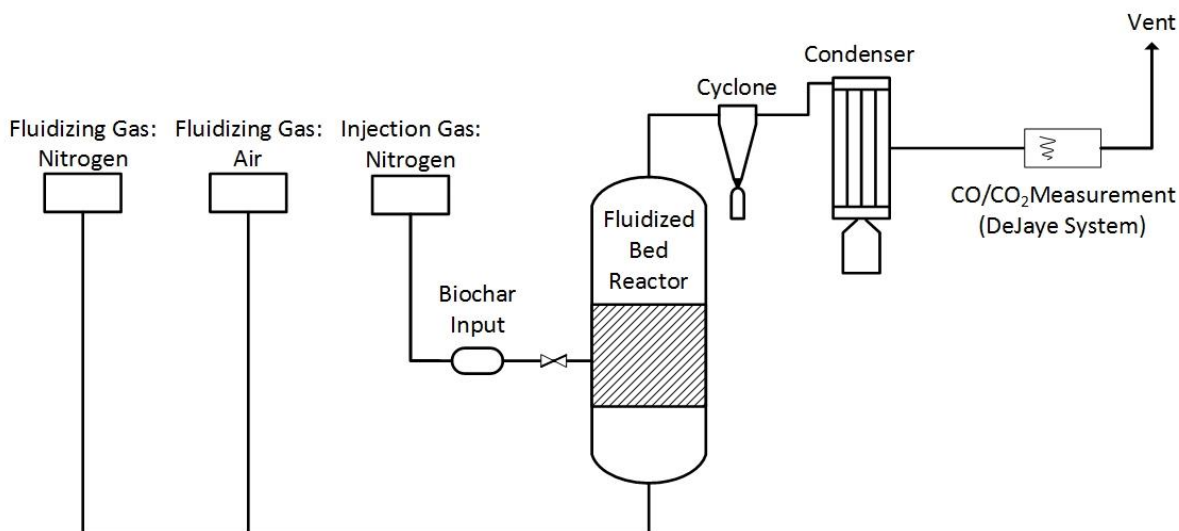


Fig. 1. Block flow diagram of the fluidized bed used for char oxidation tests.

For isothermal combustion experiments, the reactor was fluidized with nitrogen and heated to the desired oxidation temperature at which point 100 mg of 600-850  $\mu\text{m}$  biochar was pneumatically injected into the reactor with a stream of nitrogen. After the biochar injection, the fluidizing conditions were kept as nitrogen for approximately two minutes to drive off any remaining volatiles before the fluidizing gas was switched to air. With the introduction of air, the carbon in the biochar oxidized producing CO/CO<sub>2</sub>. The gas concentration was measured downstream on the DeJaye System (infrared five gas analyzer), with a one second sampling rate. From the produced carbon oxides, reaction kinetics could again be derived based on the concentration of carbon oxides and gas flow rate assumed constant at 3.5 SLPM. Total biochar carbon closure ranged from 60-102% with an average carbon closure of ~75%. This lower mass closure was the result of unmeasured carbon associated with the initial devolatilization, given

TGA results showed 25 wt. % of the biochar can volatilize, and unreacted biochar exiting the reactor due to elutriation.

The kinetic rate for the biochar was determined by measuring the flow of carbon monoxide and carbon dioxide exiting the reactor using the DeJaye system (five gas analyzer). By measuring the concentration of the produced gases, the instantaneous and total carbon content could be determined. From the measured carbon oxides, the reaction rate coefficient was derived similar to previous work [21]. The total carbon flow was determined by measuring both carbon monoxide and carbon dioxide:

$$\dot{n}_c = \dot{n}_{CO} + \dot{n}_{CO_2} \quad (4)$$

Where  $\dot{n}_c$  is the instantaneous mass flow rate of carbon oxides (g/s),  $\dot{n}_{co}$  is the mass flow rate of carbon monoxide (g/s) and  $\dot{n}_{co2}$  is the mass flow rate of carbon dioxide (g/s). From the mass flow of carbon, the instantaneous conversion is determined from the total carbon measured by the gas analyzer and the instantaneous mass flow of carbon:

$$\frac{dX_c}{dt} = \frac{\dot{n}_{CO}(t) + \dot{n}_{CO_2}(t)}{n_{tc}} \quad (5)$$

Where  $X_c$  is the conversion of carbon at time “t” (seconds) and  $n_{tc}$  is the total mass of carbon oxides measured for the duration of the experiment (g). Then, based on the total carbon flow measured, the reaction rate can be written as a function of the total carbon measured and the kinetic rate coefficient:

$$\frac{dn_c}{dt} = k * n_{tc} * (1 - X_c) \quad (6)$$

Where  $k$  is the reaction rate coefficient (1/s). The solution (equation 6) for the ordinary differential equation has an identical answer to the TGA rate equation, with the rate determined from the slope of carbon oxide production versus time:

$$\ln(1 - X_c) = -k * t = -\left(A * \exp\left(-\frac{E}{R*T}\right)\right) * t \quad (7)$$

Where A is the pre-exponential factor (1/s), E is the activation energy (kJ/mol), R is the universal gas constant (kJ/mol-K), and T is the temperature (K). With the solved equations, the kinetic rate coefficient can be found at each temperature by measuring the carbon flow of  $\ln(1 - X_c)$  against time with a straight line, and slope equal to the kinetic rate coefficient. Then, the activation energy and pre-exponential factor can be calculated from the slope and the intercept, respectively.

First order kinetics and the volumetric model were again assumed for these experiments. The kinetic rate coefficient for the fluidized bed was determined to a conversion of 50%. These experiments could be essentially treated as isothermal since the large mass of sand held temperature increases to less than 5°C.

## Results

### Biochar elemental and compositional analysis

The total ash content (Table 1) was much higher for the herbaceous materials (switchgrass and corn stover) as compared to the four woody feedstocks. This trend is expected as woody biomass feedstocks have lower total ash content than herbaceous material [32]. The willow, which was not debarked before comminution, had ash content intermediate between the herbaceous biomass and other woody biomass samples. Bark is well known to contain high levels of inorganic compounds relative to heart wood [33], accounting for this difference with other wood samples.

As shown in Table 2, the metals content, as determined through ICP, also varied between feedstocks. The two most prevalent metals were calcium and potassium, together accounting for greater than 70% of the total metals content in the samples. Very similar to total ash content,

total metals content for the herbaceous materials (>4.6 wt. %) was much greater than the debarked woody biomass (<1.4 wt. %). Willow had a much higher metal content due to the inclusion of bark. While not explicitly measured, the mass difference between the metals content and ash content is expected to be primarily silica oxides [25].

Table 1 Ultimate and proximate analysis of fast pyrolysis produced biochars.

<b>Feedstock</b>	<b>Douglas fir</b>	<b>Pine</b>	<b>Red oak</b>	<b>Willow</b>	<b>Switchgrass</b>	<b>Corn stover</b>
<b>Proximate Analysis</b>						
	wt. % (as received)					
Moisture	3.5	3.2	2.2	3.3	4.1	4.6
Volatile Matter	30.6	28.9	35.2	34.7	29.0	29.0
Fixed Carbon	62.0	62.0	56.2	48.7	42.4	35.9
Ash	3.9	5.9	6.4	13.3	24.4	30.6
<b>Ultimate Analysis</b>						
	wt. % (dry basis)					
Carbon	74.3	75.6	72.0	70.7	56.0	51.2
Hydrogen	2.5	3.5	3.1	3.4	2.9	2.5
Nitrogen	0.3	0.3	0.4	1.1	1.2	0.6
Sulfur	0.1	0.1	0.1	0.1	0.1	0.1

Table 2 Minor elemental analysis of biochars on a char weight basis as determined through ICP measurement.

	<b>Douglas fir</b>	<b>Pine</b>	<b>Red oak</b>	<b>Willow</b>	<b>Switchgrass</b>	<b>Corn stover</b>
Aluminum	0.01	0.02	0.00	0.02	0.13	0.40
Calcium	0.48	0.53	0.49	3.93	1.32	1.46
Copper	0.00	0.00	0.00	0.00	0.00	0.00
Iron	0.03	0.04	0.01	0.23	0.18	0.48
Magnesium	0.06	0.15	0.03	0.47	0.79	0.74
Manganese	0.02	0.04	0.02	0.00	0.05	0.02
Zinc	0.00	0.00	0.00	0.01	0.00	0.00
Sodium	0.00	0.00	0.00	0.00	0.04	0.01
Potassium	0.30	0.57	0.44	1.22	2.11	2.28
<b>Total (wt. %)</b>	<b>0.90</b>	<b>1.36</b>	<b>1.00</b>	<b>5.89</b>	<b>4.64</b>	<b>5.39</b>

## Oxidation rates from TGA experiments

### TGA Modeling Results

The oxidation rate versus conversion was plotted for red oak to validate the accuracy of the volumetric model (Fig. 2). At temperatures below 400°C, the maximum rate occurred at near



zero conversion, indicating the volumetric model accurately describes the biochar oxidation. However, with increasing temperature the maximum rate started to occur after zero conversion in contradiction of the volumetric model. While this could be attributed to a structural change, instead this increased rate is better explained by the initial switch from nitrogen (inert) to air (oxidative) [28,34]. Given biochar oxidation is dependent on oxygen partial pressure, the transient gas turnover likely impacted this initial conversion rate.

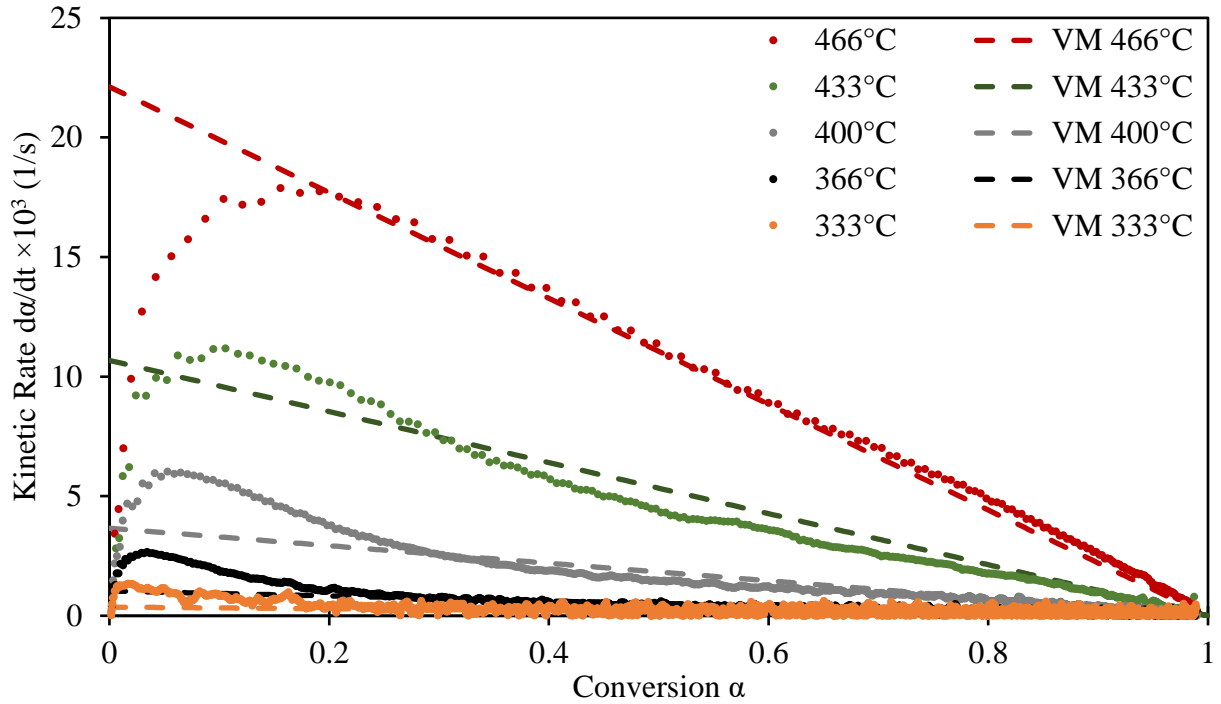


Fig. 2 Red oak conversion versus oxidation rate for validation of the volumetric model. At kinetically limited temperatures, the volumetric model (VM) accurately modeled the biochar oxidation rate.

From Fig. 2, the volumetric model accurately captures the combustion reactivity of the biochars at temperatures below 466°C. The linear decrease in reaction rate is indicative that the volumetric model is sufficient for modeling biochar kinetics. Above these temperatures, accuracy was diminished as the biochar rate switches from being kinetically limited to mass transfer controlled. This effect is discussed in the following section (3.2.2).

### Oxidation reaction rates from isothermal TGA experiments

Rate coefficients from these oxidation experiments were plotted as a semi-log plot against reciprocal absolute temperature to determine activation energy. As the standard deviations indicate, excellent repeatability was obtained.

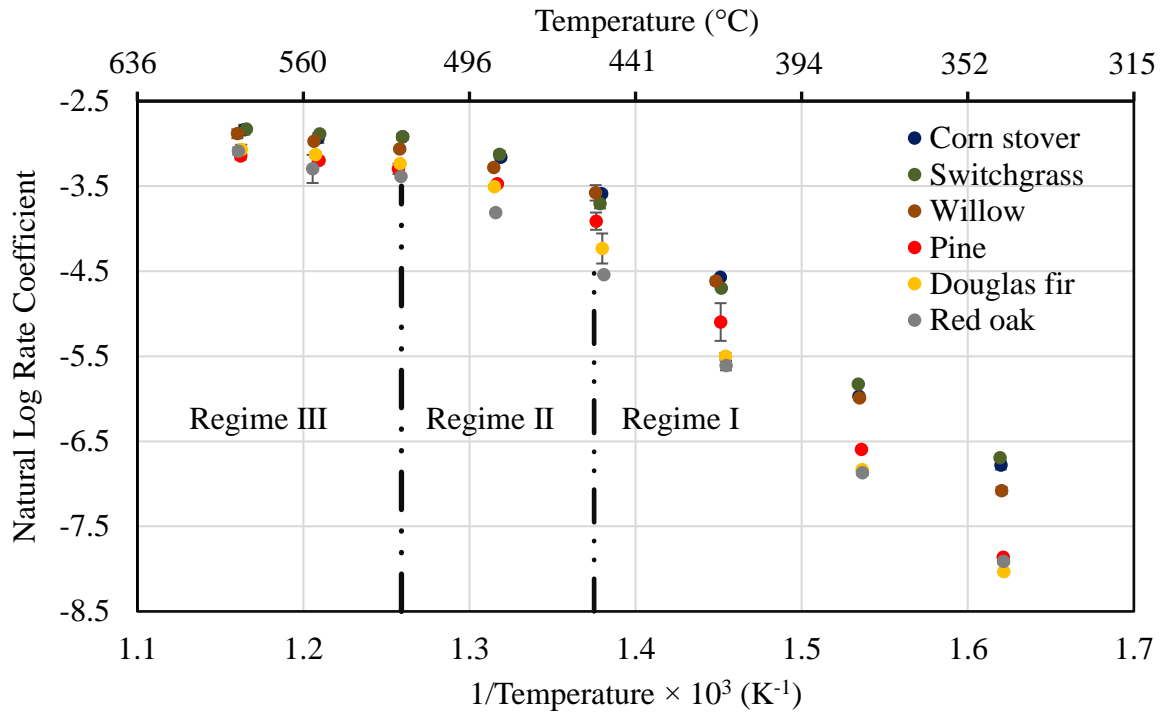


Fig. 3. Arrhenius plot of the TGA derived reaction rates indicates ash content affect oxidation rate of the biochars. Convergence in the rates at elevated temperatures suggest mass transfer limitations are now driving the observed rate. Error bars represent sample standard deviation. Vertical dashed lines indicate the combustion regime.

Analysis of the Arrhenius plot (Fig. 3) suggests biochar oxidation is kinetically limited at lower temperatures (333-433 $^{\circ}\text{C}$ ) while rates are mass transfer limited at higher temperatures (466-566  $^{\circ}\text{C}$ ). This observation is based on the change of slope between temperature points, as the slope progresses to a horizontal line at higher temperatures. As previously discussed, gas solid phase reactions have three combustion regimes. Therefore, it was important to distinguish the temperature range of these regimes for accurate reaction kinetics. One way of determining the regimes is calculating the apparent activation energies over different temperature ranges [10].

However, it is important to note these ranges are not absolute as there are additional transition zones between regimes and are dependent on the external mass transfer rate. As detailed in Table 3, the kinetically limited regime was determined from 333-433°C based on linear fit. The second regime was then calculated up to 500°C, assuming the activation energy is half that of the first regime. Finally, the highest three temperatures (Regime III) indicate the start of a purely mass transfer limited regime with apparent activation energy averaging only 14 kJ/mol among the six biomass samples.

Table 3 Apparent activation energies calculated based on the difference combustion regimes. Regime I is the true activation energy whereas the second and third regimes have mass transfer limitations.

<b>Feedstock</b>	<b>Apparent Activation Energy (kJ/mol)</b>		
	<b>Regime I (333-433°C)</b>	<b>Regime II (433-500°C)</b>	<b>Regime III (500-566°C)</b>
Douglas fir	126	60	18
Pine	129	41	15
Red oak	111	68	27
Willow	109	34	8
Switchgrass	94	44	9
Corn stover	100	41	10

These temperature ranges are similar to TGA experiments from Morin et al.[34] determining Regime I was up to 450°C, and Regime II was from 450-600°C. The biochar used in their study was produced at a much higher temperature (850°C) and is expected to have different reactivity [35]. These results indicate at the typical pyrolysis temperatures of 500°C, biochar oxidation kinetics are expected to be partially mass transfer limited.

Table 4 presents the kinetic data obtained from Regime I in terms of pre-exponential factor (A) and apparent activation energy ( $E_a$ ). The feedstocks offer distinct differences in both of these factors, with A varying by a factor of one hundred and  $E_a$  ranging from 94 to 129

kJ/mol. The activation energies are within the range of previous studies that assumed one-step models of biochar oxidation [36].

Table 4 Activation energy and pre-exponential factor from TGA biochar oxidation experiments. Arrhenius data is derived from temperature points of 333-433°C.

<b>Feedstock</b>	<b>Pre-Exponential Factor (1/s)</b>	<b>Activation Energy (kJ/mol)</b>
Douglas fir	$3.76 \times 10^7$	126
Pine	$1.08 \times 10^8$	129
Red oak	$3.12 \times 10^6$	111
Willow	$1.24 \times 10^7$	109
Switchgrass	$7.09 \times 10^5$	94
Corn stover	$3.75 \times 10^6$	100

### **Proposed relationships based on biochar composition**

Differences in reaction rates and activation energy were hypothesized to arise from variations in ash content. It is well known that metals can influence char oxidation rates [14,37,38]. Therefore, correlations for the kinetic rate coefficient at 366°C (in the kinetically limited regime) were performed and compared to the biochar's composition for total ash, potassium, calcium, and total metals content. Potassium and calcium were selected as they are the two largest individual quantified metals in the samples, together constituting over 70 wt. % of the quantified metals.

From Fig. 4, potassium ( $R^2=0.86$ ) had a strong relationship with the kinetic rate coefficient at 366°C. Whereas calcium, poorly explained the kinetic rate coefficient as the correlation was quite weak ( $R^2=0.38$ ). This would indicate calcium is a less reactive metal as compared to potassium during biochar oxidation. Fig. 5 compares the total metals content ( $R^2=0.88$ ) and total ash content ( $R^2=0.75$ ) both had strong relationships with the rate coefficient. However, silica is not expected to enhance the oxidation; thus, total ash content likely has a high degree of fit due to its positive covariance with potassium content. Likewise, while total metal

content also has high correlation ( $R^2=0.88$ ), the lack of fit with calcium indicates this is likely again due to its positive covariance with potassium.

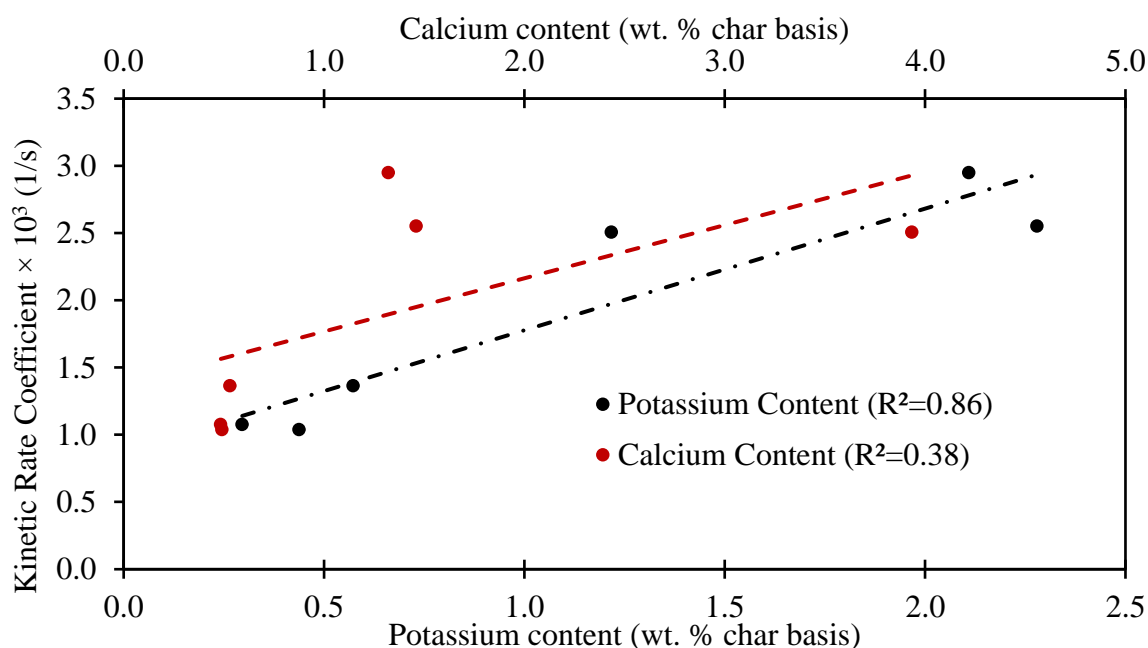


Fig. 4. Potassium and calcium content was plotted for linear regression versus the calculated kinetic rate coefficient at 366°C of the six biochars. Each point represents the kinetic rate. Error bars represent sample standard deviation.

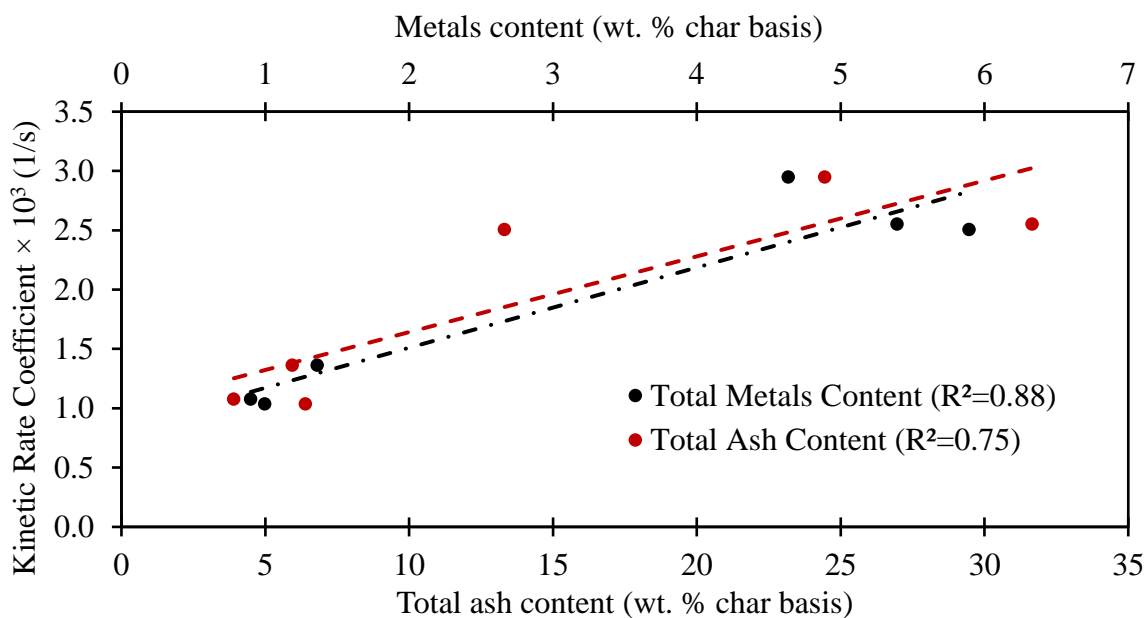


Fig. 5. Total metals content from ICP analysis and total ash content were plotted for linear regression versus the calculated kinetic rate coefficient at 366°C of the six biochars. Each point represents the kinetic rate. Error bars represent sample standard deviation.

Consequently, these results strongly suggest that potassium is the most catalytically active metal, which is consistent with previous work [13]. The reactivity of potassium coupled with its large concentration in the biochar means it is the most significant factor in determining the rate of oxidation.

As catalysts lower the activation energy of a given reaction, increasing potassium content can be expected to lower the activation energy (under Regime I). Specifically, lower activation energies for oxidation have been observed with chars impregnated with catalytically active metals [13].

As shown in Fig. 6, there is a modest relationship ( $R^2=0.62$ ) indicating that activation energy is likely not solely a function of catalytic metals content. Though, coupled with the previous correlations, potassium content does appear to greatly impact oxidation reactivity.

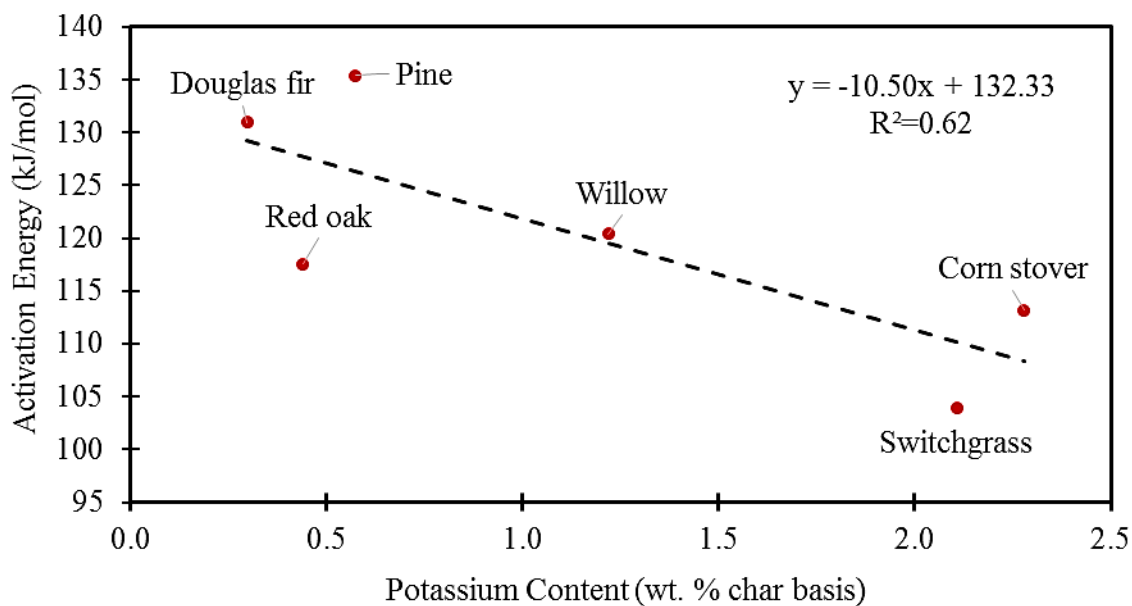


Fig. 6. Activation energy of biochar oxidation has a negative correlation with potassium content. This result indicates potassium is acting as a catalyst for biochar oxidation lowering activation energy.

### **Isothermal TGA kinetics of select washed biochars**

The previous correlations indicate that the presence of metals in biochar, particularly potassium, strongly influence oxidation kinetics. To bolster this theory, three biochars (switchgrass, corn stover, and red oak) were washed in 1M HCl solution to remove AAEM followed by oxidation in the TGA at temperatures ranging from 366°C to 566°C.

As shown in Table 5, washing reduced the oxidation rates for all three biochar samples at the four temperatures shown. Although, the effect was more pronounced for the two biochars obtained from herbaceous biomass (switchgrass and corn stover). Under the previously defined kinetically limited regime (366 - 433°C), the rate decreased 69-83% for herbaceous biochars and 26-49% for the red oak. The dramatic decrease associated with the herbaceous material is from the larger fraction of material being passivated/removed as compared to the lower ash feedstock of red oak. At elevated temperatures (>500°C), the herbaceous biochars rate still had a relatively large decrease (37-69%), as compared to the red oak which had a relative decrease of only 36% and 8% at 500°C and 566°C, respectively. While the negligible decrease in kinetic rate for red oak at 566°C indicates it is mass transfer limited, the herbaceous materials still had a dramatic decrease. This would indicate the herbaceous biochars are no longer mass transfer limited at elevated temperature. Examining the kinetic rate of the acid washed corn stover at 566°C, it is now comparable to the unwashed rate at 433°C ( $3.0 \times 10^{-2}$  vs.  $2.8 \times 10^{-2}$  1/s). With the removal of the catalytically active metals, and subsequent reduced kinetic rate, the herbaceous biochar is now oxidizing slowly enough to be partially limited by kinetics again (Regime II). In the absence of catalytically active metals, biochar structure is likely the controlling reactivity factor. This notion is supported as the washed red oak now has a faster oxidation rate as compared to the washed corn stover and switchgrass. Consequently, these results indicate how strong of a catalyst the metals are on the oxidation rate.

Table 5 1M HCl washed biochars had a reduced oxidation kinetic rate as compared to unwashed samples. Herbaceous material (switchgrass and corn stover) had a larger reduction in rate as compared to a woody biochar (red oak). Parenthesis represent the sample deviation.

Feedstock	Kinetic rate coefficient (1/s)			
	366°C	433°C	500°C	566°C
Corn stover	$2.6 \times 10^{-3}$ ( $6.9 \times 10^{-5}$ )	$2.8 \times 10^{-2}$ ( $9.1 \times 10^{-4}$ )	$5.4 \times 10^{-2}$ ( $1.8 \times 10^{-3}$ )	$5.9 \times 10^{-2}$ ( $3.4 \times 10^{-3}$ )
HCl washed-Corn stover	$7.9 \times 10^{-4}$ ( $9.3 \times 10^{-6}$ )	$4.8 \times 10^{-3}$ ( $3.0 \times 10^{-4}$ )	$2.1 \times 10^{-2}$ ( $8.8 \times 10^{-4}$ )	$3.0 \times 10^{-2}$ ( $3.2 \times 10^{-4}$ )
<b>Relative Decrease</b>	69%	83%	62%	48%
Switchgrass	$2.9 \times 10^{-3}$ ( $2.2 \times 10^{-5}$ )	$2.5 \times 10^{-2}$ ( $1.4 \times 10^{-3}$ )	$5.4 \times 10^{-2}$ ( $1.4 \times 10^{-3}$ )	$5.9 \times 10^{-2}$ ( $9.2 \times 10^{-4}$ )
HCl washed-Switchgrass	$7.9 \times 10^{-4}$ ( $1.8 \times 10^{-5}$ )	$4.2 \times 10^{-3}$ ( $6.6 \times 10^{-5}$ )	$1.7 \times 10^{-2}$ ( $1.7 \times 10^{-4}$ )	$3.7 \times 10^{-2}$ ( $7.7 \times 10^{-4}$ )
<b>Relative Decrease</b>	73%	83%	69%	37%
Red oak	$1.0 \times 10^{-3}$ ( $2.6 \times 10^{-5}$ )	$1.1 \times 10^{-2}$ ( $1.1 \times 10^{-4}$ )	$3.4 \times 10^{-2}$ ( $6.3 \times 10^{-4}$ )	$4.6 \times 10^{-2}$ ( $2.1 \times 10^{-3}$ )
HCl washed-Red oak	$7.7 \times 10^{-4}$ ( $1.1 \times 10^{-5}$ )	$5.5 \times 10^{-3}$ ( $3.1 \times 10^{-4}$ )	$2.2 \times 10^{-2}$ ( $1.5 \times 10^{-3}$ )	$4.2 \times 10^{-2}$ ( $5.8 \times 10^{-4}$ )
<b>Relative Decrease</b>	26%	49%	36%	8%



With the acid washing results, this provides direct evidence that the catalytically active metals are responsible for the difference in reaction rates. Moreover, while total ash content provided a moderate fit with kinetic rate coefficient, the acid washing experiments verify that potassium content is a far better predictor, as silica cannot be readily removed nor is catalyst for oxidation.

### **Char oxidation rates from fluidized bed experiments**

#### **Oxidation reaction rates from isothermal fluidized bed experiments**

In addition to the TGA experiments, oxidation kinetic rates were derived using a fluidized bed reactor. While not explicitly measured, the use of a fluidized bed would account for the attrition effects on oxidation kinetics. Triplicates performed at each temperature showed excellent repeatability between trials.

Examination of the fluidized bed produced Arrhenius plot (Fig. 7) corroborates the previous TGA results demonstrating that different ash content causes the biochars to have different oxidation kinetic rate coefficients.

At temperatures lower than 450°C, the reaction rate varies by a factor of three between the biochars but appears to converge at greater temperatures. Taking a ratio of the slowest rate and fastest rate provides insight into this convergence. At 420°C this ratio is 0.38 (Douglas fir over switchgrass). At the highest temperature (566°C) this ratio is now only 0.74 (Douglas fir over switchgrass), confirming this convergence in rate. This increasing similarity again suggests the rates become externally mass transfer limited, and the intrinsic reactivity of the char is no longer as important when the external mass transfer rate begins to dominate the overall rate.

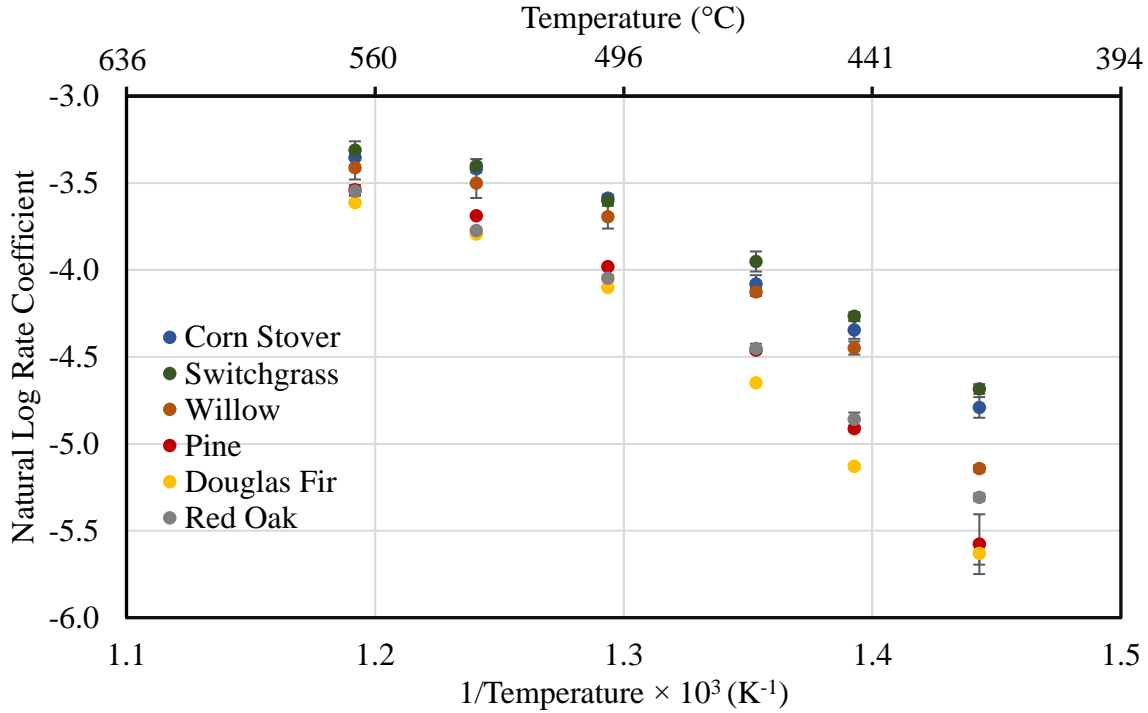


Fig. 7. Arrhenius plot suggests ash content increases biochar oxidation rate. Triplicates of each temperature was performed with error bars showing the sample standard deviation.

### Fluidized bed reaction rate correlations

The TGA results showed potassium to closely correlate with biochar oxidation rate.

Therefore, reaction rate coefficients from the fluidized bed experiments were tested for fit versus potassium at select temperatures.

Similar to the TGA experiments, potassium content and the kinetic rate coefficient had a strong correlation ( $R^2 > 0.91$ ) at the two temperatures shown in Fig. 8. This relationship again indicates that potassium content is likely responsible for the differences in oxidation reactivity. The correlation at 500°C suggests that the oxidation rate is still partially limited by chemical kinetics, as mass transfer would not be affected by potassium content.

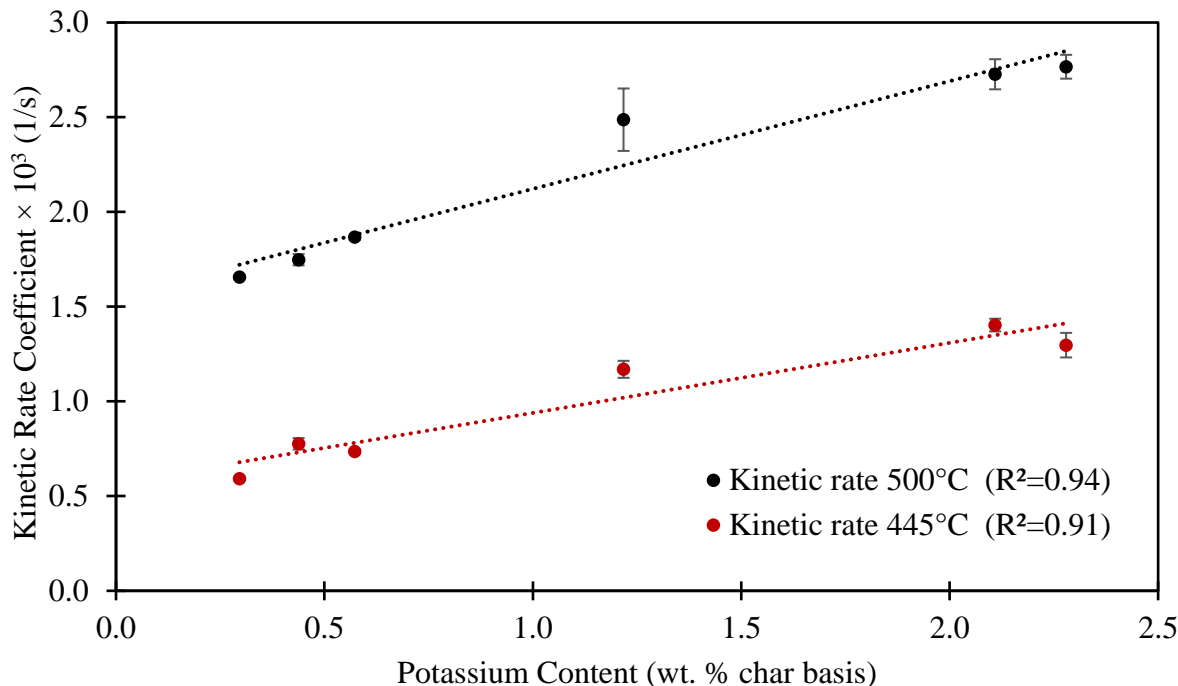


Fig. 8. The strong correlation between potassium content and kinetic rate coefficient for 445 and 500°C indicates that potassium content can be used to predict the kinetic rate. Each point represents a different biochar sample at two temperatures (445 and 500 °C) with error bars representing standard deviation.

### Carbon oxide formation in a fluidized bed reactor

The fluidized bed tests allowed carbon oxides gas production during biochar oxidation to be measured and correlated against the ash and metal content of the biochar. Table 6 illustrates the mole fraction of CO<sub>2</sub> with respect to total carbon oxide gases as a function of temperature and biochar.

Table 6 CO<sub>2</sub> production increased with increasing reactor temperatures for all biochars during oxidation in a fluidized bed. Parenthesis is the sample standard deviation of three trials.

Feedstock	Mole Ratio CO <sub>2</sub> /(CO + CO <sub>2</sub> )					
	420°C	445°C	466°C	500°C	533°C	566°C
Douglas fir	0.62 (0.01)	0.65 (0.02)	0.67 (0.01)	0.69 (0.01)	0.70 (0.01)	0.73 (0.01)
Pine	0.71 (0.04)	0.69 (0.02)	0.71 (0.01)	0.72 (0.01)	0.74 (0.01)	0.78 (0.01)
Red oak	0.66 (0.01)	0.68 (0.02)	0.69 (0.01)	0.70 (0.01)	0.72 (0.01)	0.76 (0.01)
Willow	0.69 (0.01)	0.70 (0.01)	0.72 (0.01)	0.73 (0.01)	0.75 (0.01)	0.80 (0.01)
Switchgrass	0.80 (0.01)	0.82 (0.01)	0.84 (0.01)	0.85 (0.01)	0.86 (0.01)	0.88 (0.01)
Corn stover	0.79 (0.01)	0.83 (0.01)	0.85 (0.01)	0.86 (0.01)	0.87 (0.01)	0.88 (0.01)

The effect of ash and metal content on carbon oxide production during biochar oxidation at 500°C is explored in Fig. 9 and Fig. 10. The same parameters from the kinetic rate correlations were used: potassium, calcium, total ash, and totals metals content.

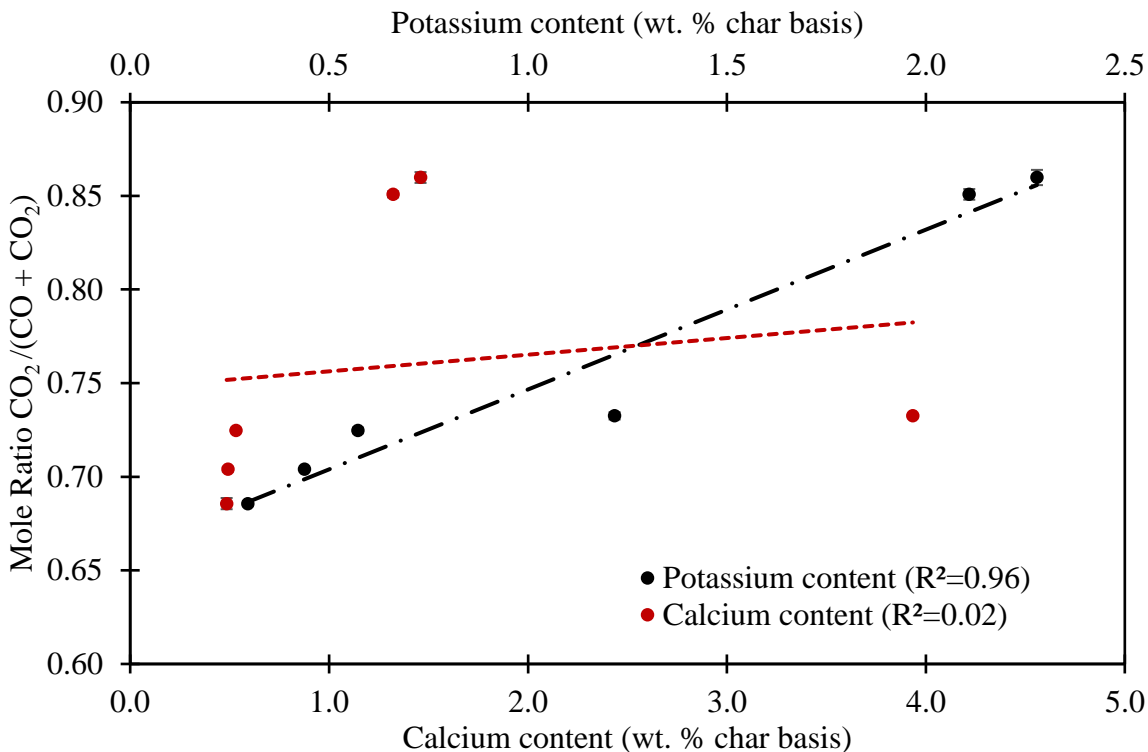


Fig. 9. Potassium and calcium content versus mole ratio of carbon oxides at 500°C. Potassium content had a strong correlation with  $\text{CO}_2$  production. Calcium content poorly correlated with carbon oxide ratio, despite its relatively large concentration in the biochar. Error bars represent sample standard deviation.

As shown in Fig. 9 and Fig. 10, the fraction of  $\text{CO}_2$  production relative to total carbon oxide gases increased with ash and metal content, being particularly well correlated with total ash ( $R^2=0.96$ ) and potassium ( $R^2=0.96$ ). Whereas calcium content ( $R^2=0.03$ ) and totals metals content ( $R^2=0.51$ ) poorly described the produced carbon oxide ratio. Given the positive covariance between potassium content and total ash content, the strong correlation with ash content could again be a false positive, similar to the previous TGA kinetic rate correlations.

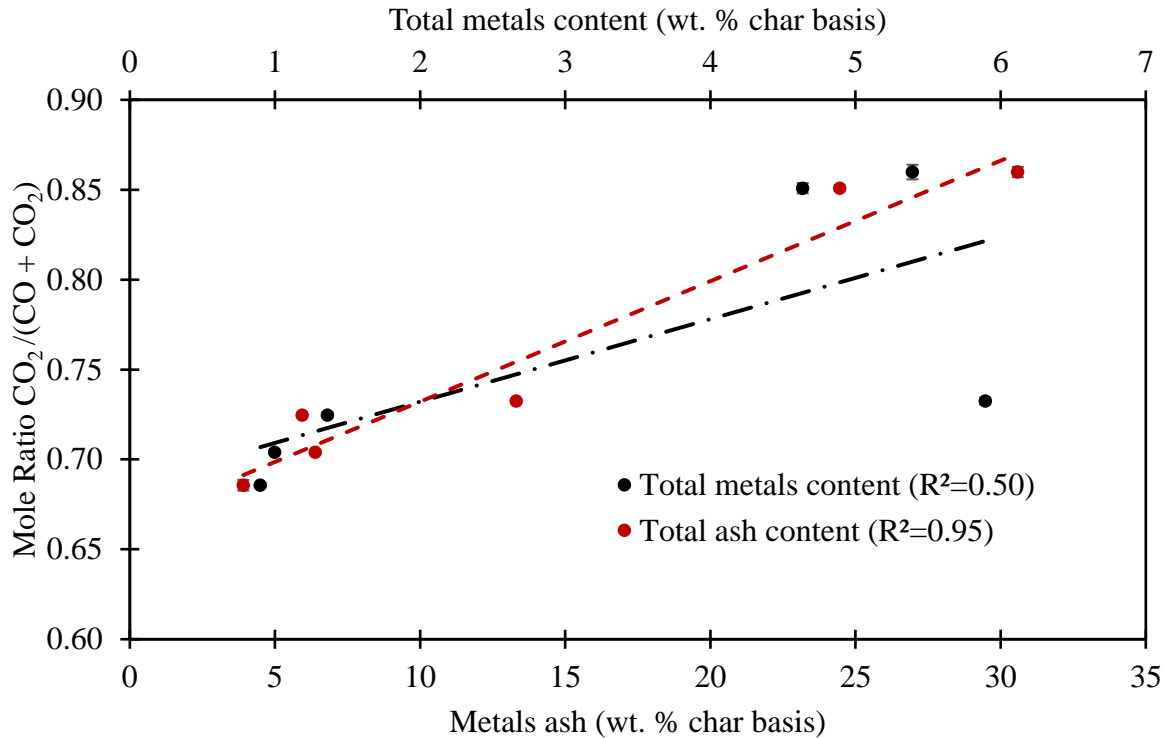


Fig. 10. Total ash and total metals content versus mole ratio of carbon oxides at 500°C. Total ash content had a strong correlation with CO<sub>2</sub> production, whereas total metals content poorly described oxide ratio. Error bars represent sample standard deviation.

The difference in carbon oxide ratio was initially somewhat surprising, considering that production of CO<sub>2</sub> during char oxidation is normally considered to be a purely gas-phase reaction. However, a similar phenomenon has been observed during coal combustion [14,39,40]. Metals in char are able to adsorb oxygen and participate in a reduction/oxidation cycle with the solid carbon resulting in solid-gas reactions directly producing CO<sub>2</sub> [17]. These results again indicate that potassium content is particularly important for modeling oxidation rates and the molar production of gases. For visual clarity, and future use, the mole ratio of carbon oxide production at 500°C compared to potassium content is shown in Fig. 11, with a proposed linear regression.

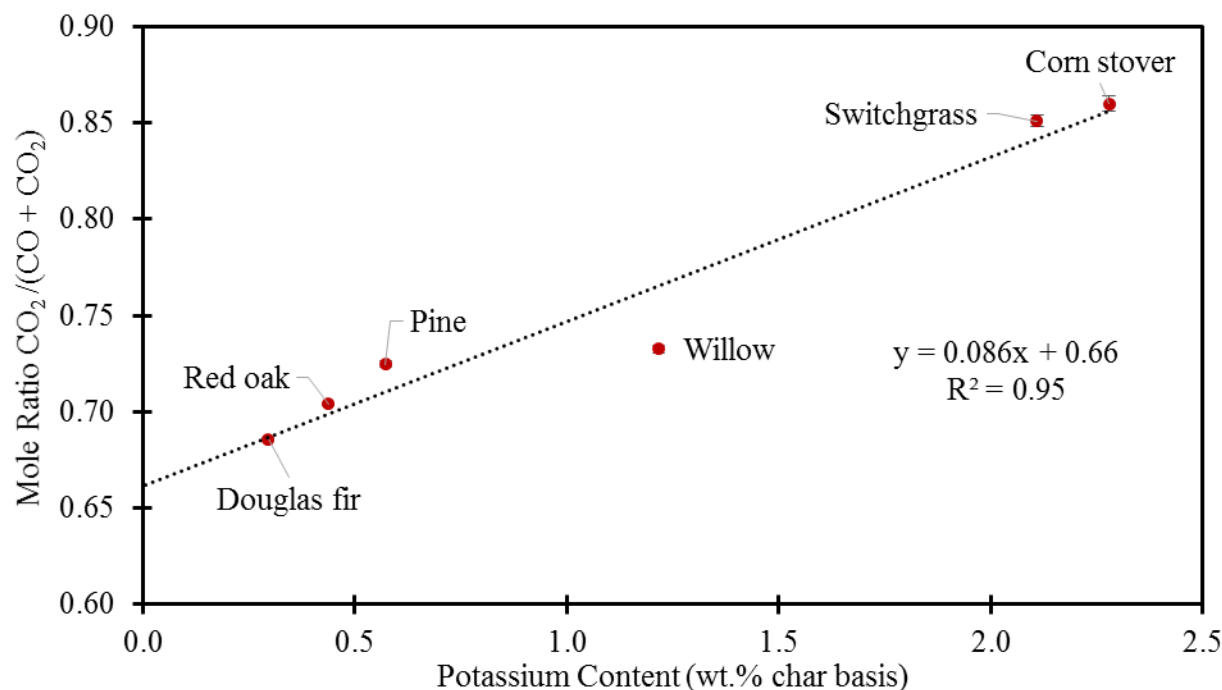


Fig. 11. CO<sub>2</sub> formation increases with ash content, indicating increased oxygen consumption efficiency. Values are from fluidized bed experiments at 500°C with error bars representing sample standard deviation of three trials.

The variation in CO<sub>2</sub> formation is important for modeling oxidation kinetics of biochar at pyrolysis temperatures. Given the temperatures are not hot enough to fully oxidize all the CO to CO<sub>2</sub>, this indicates an incomplete combustion and differences in energy released. The variation in molar production of CO vs CO<sub>2</sub> would release different quantities of energy based on the heat of formation. The enthalpy of formation for CO is only -110 kJ/mol versus -393 kJ/mol for CO<sub>2</sub>, varying by a factor of three. This means that per mole of oxygen, biochars containing higher amounts of ash (i.e. potassium) would release greater energy at pyrolysis temperatures (400-600°C). Consequently, under starved oxygen environments (such as autothermal pyrolysis) oxygen would be used more efficiently with higher ash feedstocks, requiring a lower equivalence ratio for autothermal pyrolysis operation, consistent with experimental works [7,8].

### Fluidized bed experiments of washed biochars

The fluidized bed experiments with unmodified biochar indicate that the presence of metals (i.e. potassium) strongly influence oxidation kinetics and preferential production of CO<sub>2</sub>. To confirm this effect, three biochars (switchgrass, corn stover, and red oak) were washed in 1M HCl solution to remove AAEM followed by oxidation in the fluidized bed at 500°C. This experiment isolates catalytic ash content as the sole independent variable. Any other relevant differences between the biochars should be evident.

As shown in Table 7, acid washing the biochars reduced oxidation rates for all three biomass types, although the effect was more pronounced for the two biochars obtained from herbaceous biomass (switchgrass and corn stover), similar to the TGA experiments. The acid washed herbaceous biochars reduced the kinetic rate to levels comparable to the acid washed red oak biochar, indicating that washing was effective in removing most of the catalytic metals.

Table 7 Acid washing of biochars reduced the kinetic rate coefficient of herbaceous chars. Oxidation kinetic rate coefficient determined with fluidized bed reactor at 500°C. Parenthesis represent sample standard deviation. Acid washed samples were tested in duplicate.

Feedstock	Kinetic Rate Coefficient (1/s)		Relative Decrease
	Unwashed	HCl Washed	
Corn stover	$2.8 \times 10^{-2}$ ( $6.3 \times 10^{-4}$ )	$1.2 \times 10^{-2}$ ( $6.0 \times 10^{-4}$ )	58%
Switchgrass	$2.7 \times 10^{-2}$ ( $7.9 \times 10^{-4}$ )	$1.6 \times 10^{-2}$ ( $3.5 \times 10^{-4}$ )	41%
Red oak	$1.7 \times 10^{-2}$ ( $3.0 \times 10^{-4}$ )	$1.4 \times 10^{-2}$ ( $3.7 \times 10^{-5}$ )	19%

Similarly, as illustrated in Table 8, acid washing of biochars prior to oxidation at 500°C reduced the mole fraction of CO<sub>2</sub> relative to total carbon oxide gases, bringing it to comparable levels for all three biochars (average of 0.65). This mole ratio for acid washed biochar is close to the mole fraction extrapolated from Fig. 11 for a potassium concentration of zero.

Table 8 Mole fraction of CO<sub>2</sub> relative to total carbon oxide gases was reduced by acid washing of biochars prior to oxidation at 500°C. Parenthesis represent sample standard deviation. Acid wash samples were only performed in duplicates.

<b>Feedstock</b>	<b>Mole Ratio CO<sub>2</sub>/CO+CO<sub>2</sub></b>		<b>Relative Decrease</b>
	<b>Unwashed</b>	<b>HCl Washed</b>	
Corn stover	0.86 (0.01)	0.67 (0.01)	22%
Switchgrass	0.85 (0.01)	0.64 (0.01)	25%
Red oak	0.70 (0.01)	0.63 (0.01)	10%

These results indicate that the strong correlation of CO<sub>2</sub> ratio and ash content was likely due to positive covariance with potassium. Given silica is not removed in this acid washing step, this indicates that potassium is responsible for the difference in CO<sub>2</sub> production.

### **Estimating the effect of particle attrition on biochar oxidation kinetics**

In principle, comparing the results obtained from TGA and fluidized bed experiments should allow the role of particle attrition during oxidation to be estimated. In the absence of attrition, the TGA experiments would have a faster reaction rate as the particle size used (150-250 µm) was sufficiently small to minimize internal mass transfer. In comparison, the particle size (600-850 µm) for the fluidized bed experiments would introduce internal mass transfer limitations. However, if particle attrition was instantaneous in the fluidized bed experiments, the calculated rates would be identical as the particle size would no longer have these mass transfer limitations. Switchgrass and Douglas fir were selected given the fastest and slowest kinetic rate coefficient for comparison of rates (Table 9) between the two experimental conditions. The kinetic rate coefficient was calculated from the TGA experiments by using linear interpolation of the nearest two data points. This allows for a direct temperature comparison with the fluidized bed results.



Table 9 Comparison between kinetic rate coefficients from isothermal TGA and fluidized bed kinetic studies. TGA kinetic rates were calculated using linear interpolation between two closest data points corresponding to fluidized bed temperature.

Feedstock	Reactor	Kinetic Rate Coefficient (1/s)					
		420°C	445°C	466°C	500°C	533°C	566°C
Switchgrass	Fluidized bed	$9.2 \times 10^{-3}$	$1.4 \times 10^{-2}$	$1.9 \times 10^{-2}$	$2.7 \times 10^{-2}$	$3.3 \times 10^{-2}$	$3.6 \times 10^{-2}$
	TGA (calculated)	$1.1 \times 10^{-2}$	$2.1 \times 10^{-2}$	$3.2 \times 10^{-2}$	$4.8 \times 10^{-2}$	$5.5 \times 10^{-2}$	$5.7 \times 10^{-2}$
Ratio fluidized bed over TGA rate coefficient		0.85	0.65	0.59	0.57	0.61	0.64
Douglas fir	Fluidized bed	$3.6 \times 10^{-3}$	$5.9 \times 10^{-3}$	$9.6 \times 10^{-3}$	$1.7 \times 10^{-2}$	$2.3 \times 10^{-2}$	$2.7 \times 10^{-2}$
	TGA (calculated)	$5.6 \times 10^{-3}$	$1.3 \times 10^{-2}$	$2.1 \times 10^{-2}$	$3.3 \times 10^{-2}$	$4.1 \times 10^{-2}$	$4.5 \times 10^{-2}$
Ratio fluidized bed over TGA rate coefficient		0.64	0.47	0.46	0.50	0.55	0.60

At lower temperatures ( $< 466^{\circ}\text{C}$ ) the fluidized bed rate was approximately 50% and 70% of the TGA rate, for Douglas fir and switchgrass, respectively. As previously discussed, in the absence of attrition, the TGA should have a faster rate due to the smaller particle size, minimizing internal mass transfer limitations. Given the slower oxidation rate measured with the fluidized bed experiments under a kinetically limited regime, particle attrition does not appear to significantly enhance biochar oxidation under these conditions. While this may contradict the work of Scala et al.[20], the hotter temperatures used ( $850^{\circ}\text{C}$ ) and faster superficial gas velocity ( $0.8\text{ m/s}$ ) likely increased the rate of attrition and rates of oxidation. Given the low gas velocity used for these experiments ( $\sim 0.2\text{ m/s}$ ), the attrition rate is much slower than typically used in fluidized bed combustors with high superficial gas velocity ( $> 4\text{ m/s}$ ) [19]. Biochar fines were collected in the cyclone after oxidation experiments, indicating the overall combustion rate was not sufficient to completely oxidize the particles before elutriation. Consequently, for these experimental conditions, most of the biochar appears to be oxidized as its original size, reducing the reaction rate due to internal mass transfer limitations. Though particle attrition does not affect oxidation rate, the overall trends between the two conditions are consistent (e.g. potassium vs. kinetic rate) bridging the gap between pure kinetic studies and actual systems.

### **Conclusions**

Oxidation kinetic data was calculated for six different biochars using combined TGA and fluidized bed experiments. Correlations were proposed for compositional parameters versus the isothermal TGA kinetic rate coefficient, finding potassium offers the most likely explanation for the difference in reactivity. Furthermore, all three regimes of biochar combustion apply at pyrolysis temperatures, providing valuable information for modeling efforts and pyrolysis operation. Additional biochar oxidation experiments conducted using a fluidized bed reactor

confirmed the TGA results, finding potassium content correlated very well increasing the reaction rate. Measurements of CO<sub>2</sub> and CO formation found that inorganic content was an important parameter for modeling biochar oxidation. Analogous to the kinetic rate, as potassium content increased, there was an enhanced CO<sub>2</sub> formation as compared to CO. This demonstrates that oxygen with higher ash feedstocks is used more efficiently during combustion (with subsequent greater energy release). Additional acid washed biochars indicate when the catalytically active metals were removed, CO<sub>2</sub> formation was reduced, providing additional evidence inorganic content is an important parameter. Reaction kinetics were compared between the TGA and fluidized bed experiments finding a faster overall rate with the TGA derived rates. The faster rate associated with the TGA experiments is the result of using a sufficiently small particle size, minimizing internal mass transfer limitations. The comparison of experimental methods indicate that biochar attrition does not significantly impact the oxidation rate at the conditions used.

### **Acknowledgements**

This paper is based upon work supported by the Department of Energy under Award Number EE0008326. It was prepared as an account of work sponsored by an agency of the United States Government. Neither the United States Government nor any agency thereof, nor any of their employees, makes any warranty, express or implied, or assumes any legal liability or responsibility for the accuracy, completeness, or usefulness of any information, apparatus, product, or process disclosed, or represents that its use would not infringe privately owned rights. Reference herein to any specific commercial product, process, or service by trade name, trademark, manufacturer, or otherwise does not necessarily constitute or imply its endorsement, recommendation, or favoring by the United States Government or any agency thereof. The views

and opinions of authors expressed herein do not necessarily state or reflect those of the United States Government or any agency thereof.

### **Declaration of Competing Interest**

The authors declare that they have no known competing financial interests or personal relationships that could have appeared to influence the work reported in this paper.

### **References**

- [1] R.C. Brown, T.R. Brown, *Biorenewable Resources: Engineering New Products from Agriculture: Second Edition*, John Wiley & Sons, Inc., Hoboken, NJ, USA, 2014. <https://doi.org/10.1002/9781118524985>.
- [2] R.C. Brown, *Thermochemical Processing of Biomass: Conversion into Fuels, Chemicals and Power*, John Wiley & Sons, Ltd, Chichester, UK, 2011. <https://doi.org/10.1002/9781119990840>.
- [3] D.E. Daugaard, R.C. Brown, Enthalpy for pyrolysis for several types of biomass, *Energy and Fuels*. 17 (2003) 934–939. <https://doi.org/10.1021/ef020260x>.
- [4] L. Rosendahl, *Biomass combustion, technology and engineering*, n.d. <https://www.oreilly.com/library/view/biomass-combustion-science/9780857091314/> (accessed September 6, 2019).
- [5] D. Meier, O. Faix, State of the art of applied fast pyrolysis of lignocellulosic materials — a review, *Bioresour. Technol.* 68 (1999) 71–77. [https://doi.org/10.1016/S0960-8524\(98\)00086-8](https://doi.org/10.1016/S0960-8524(98)00086-8).
- [6] F. Campuzano, R.C.R.C. Brown, J.D. Martinez, J.D. Martínez, Auger reactors for pyrolysis of biomass and wastes, *Renew. Sustain. Energy Rev.* 102 (2019) 372–409. <https://doi.org/10.1016/j.rser.2018.12.014>.
- [7] J.P. Polin, H.D. Carr, L.E. Whitmer, R.G. Smith, R.C. Brown, Conventional and autothermal pyrolysis of corn stover: Overcoming the processing challenges of high-ash agricultural residues, *J. Anal. Appl. Pyrolysis*. 143 (2019) 104679. <https://doi.org/10.1016/j.jaap.2019.104679>.
- [8] J.P. Polin, C.A. Peterson, L.E. Whitmer, R.G. Smith, R.C. Brown, Process intensification of biomass fast pyrolysis through autothermal operation of a fluidized bed reactor, *Appl. Energy*. 249 (2019) 276–285. <https://doi.org/10.1016/J.APENERGY.2019.04.154>.
- [9] M.A. Field, Rate of combustion of size-graded fractions of char from a low-rank coal between 1200°K and 2000°K, *Combust. Flame*. 13 (1969) 237–252. [https://doi.org/10.1016/0010-2180\(69\)90002-9](https://doi.org/10.1016/0010-2180(69)90002-9).

- [10] J. Szekely, J. Evans, H.Y. Sohn, *Gas-Solid Reactions*, Academic Press, 1976.
- [11] Y. Zhang, P. Geng, Y. Zheng, Exploration and practice to improve the kinetic analysis of char-CO<sub>2</sub> gasification via thermogravimetric analysis, *Chem. Eng. J.* 359 (2019) 298–304. <https://doi.org/10.1016/j.cej.2018.11.122>.
- [12] W. Wang, C. Bu, A. Gómez-Barea, B. Leckner, X. Wang, J. Zhang, G. Piao, O<sub>2</sub>/CO<sub>2</sub> and O<sub>2</sub>/N<sub>2</sub> combustion of bituminous char particles in a bubbling fluidized bed under simulated combustor conditions, *Chem. Eng. J.* 336 (2018) 74–81. <https://doi.org/10.1016/j.cej.2017.11.027>.
- [13] R. Zhang, K. Lei, B.Q. Ye, J. Cao, D. Liu, Effects of alkali and alkaline earth metal species on the combustion characteristics of single particles from pine sawdust and bituminous coal, *Bioresour. Technol.* 268 (2018) 278–285. <https://doi.org/10.1016/J.BIORTECH.2018.07.145>.
- [14] B. Yi, Q. Yuan, H. Cao, W. Niu, M. Wang, Y. Zhu, S. Yan, Effect of alkali and alkaline earth metal species on the combustion characteristics of cattle manures, *RSC Adv.* 8 (2018) 11705–11713. <https://doi.org/10.1039/C8RA00965A>.
- [15] G. Várhegyi, E. Mészáros, M.J. Antal, J. Bourke, E. Jakab, Combustion kinetics of corncob charcoal and partially demineralized corncob charcoal in the kinetic regime, *Ind. Eng. Chem. Res.* 45 (2006) 4962–4970. <https://doi.org/10.1021/ie0602411>.
- [16] K. Miura, K. Hashimoto, P.L. Silveston, Factors affecting the reactivity of coal chars during gasification, and indices representing reactivity, *Fuel.* 68 (1989) 1461–1475. [https://doi.org/10.1016/0016-2361\(89\)90046-X](https://doi.org/10.1016/0016-2361(89)90046-X).
- [17] J. Cheng, F. Zhou, X. Xuan, J. Liu, J. Zhou, K. Cen, Comparison of the catalytic effects of eight industrial wastes rich in Na, Fe, Ca and Al on anthracite coal combustion, *Fuel.* 187 (2017) 398–402. <https://doi.org/10.1016/j.fuel.2016.09.083>.
- [18] Z. Du, A.F. Sarofim, J.P. Longwell, C.A. Mims, Kinetic Measurement and Modeling of Carbon Oxidation, *Energy and Fuels.* 5 (1991) 214–221. <https://doi.org/10.1021/ef00025a035>.
- [19] U. Arena, A. Cammarota, L. Massimilla, L. Siciliano, P. Basu, Carbon attrition during the combustion of a char in a circulating fluidized bed, *Combust. Sci. Technol.* 73 (1990) 383–394. <https://doi.org/10.1080/00102209008951658>.
- [20] F. Scala, R. Chirone, P. Salatino, Combustion and Attrition of Biomass Chars in a Fluidized Bed, *Energy & Fuels.* 20 (2006) 91–102. <https://doi.org/10.1021/ef050102g>.
- [21] M. Morin, S. Pécate, M. Hémati, Kinetic study of biomass char combustion in a low temperature fluidized bed reactor, *Chem. Eng. J.* 331 (2018) 265–277. <https://doi.org/10.1016/j.cej.2017.08.063>.

- [22] S.A. Rollag, J.K. Lindstrom, R.C. Brown, Pretreatments for the continuous production of pyrolytic sugar from lignocellulosic biomass, *Chem. Eng. J.* 385 (2020) 123889. <https://doi.org/10.1016/j.cej.2019.123889>.
- [23] M. Shakirullah, I. Ahmad, M.A. Khan, M. Ishaq, H. ur Rehman, U. Khan, Leaching of Minerals in Degari Coal, *J. Miner. Mater. Charact. Eng.* 05 (2006) 131–142. <https://doi.org/10.4236/jmmce.2006.52009>.
- [24] R. Zhang, Y. Chen, K. Lei, D. Liu, The effects of specific surface area and ash on char gasification mechanisms in the mixture of H<sub>2</sub>O, CO<sub>2</sub>, H<sub>2</sub> and CO, *Fuel*. 209 (2017) 109–116. <https://doi.org/10.1016/j.fuel.2017.07.085>.
- [25] C.E. Brewer, K. Schmidt-Rohr, J.A. Satrio, R.C. Brown, Characterization of biochar from fast pyrolysis and gasification systems, *Environ. Prog. Sustain. Energy*. 28 (2009) 386–396. <https://doi.org/10.1002/ep.10378>.
- [26] J. Shen, X.S. Wang, M. Garcia-Perez, D. Maurant, M.J. Rhodes, C.Z. Li, Effects of particle size on the fast pyrolysis of oil mallee woody biomass, *Fuel*. 88 (2009) 1810–1817. <https://doi.org/10.1016/j.fuel.2009.05.001>.
- [27] P. Gable, R.C. Brown, Effect of biomass heating time on bio-oil yields in a free fall fast pyrolysis reactor, *Fuel*. 166 (2016) 361–366. <https://doi.org/10.1016/J.FUEL.2015.10.073>.
- [28] A. Gomez, R. Silbermann, N. Mahinpey, A comprehensive experimental procedure for CO<sub>2</sub> coal gasification: Is there really a maximum reaction rate?, *Appl. Energy*. 124 (2014) 73–81. <https://doi.org/10.1016/J.APENERGY.2014.02.077>.
- [29] C. Di Blasi, F. Buonanno, C. Branca, Reactivities of some biomass chars in air, *Carbon N. Y.* 37 (1999) 1227–1238. [https://doi.org/10.1016/S0008-6223\(98\)00319-4](https://doi.org/10.1016/S0008-6223(98)00319-4).
- [30] A.M.C. Janse, H.G. de Jonge, W. Prins, W.P.M. van Swaaij, Combustion Kinetics of Char Obtained by Flash Pyrolysis of Pine Wood, *Ind. Eng. Chem. Res.* 37 (1998) 3909–3918. <https://doi.org/10.1021/ie970705i>.
- [31] S.K. Bhatia, B.J. Vartak, Reaction of microporous solids: The discrete random pore model, *Carbon N. Y.* 34 (1996) 1383–1391. [https://doi.org/10.1016/S0008-6223\(96\)00080-2](https://doi.org/10.1016/S0008-6223(96)00080-2).
- [32] P. Thy, C. Yu, B.M.M. Jenkins, C.E.E. Lesher, Inorganic composition and environmental impact of biomass feedstock, *Energy and Fuels*. 27 (2013) 3969–3987. <https://doi.org/10.1021/ef400660u>.
- [33] B. Klasnja, S. Kopitovic, S. Orlovic, Wood and bark of some poplar and willow clones as fuelwood, *Biomass and Bioenergy*. 23 (2002) 427–432. [https://doi.org/10.1016/S0961-9534\(02\)00069-7](https://doi.org/10.1016/S0961-9534(02)00069-7).

- [34] M. Morin, S. Pécate, E. Masi, M. Hémati, Kinetic study and modelling of char combustion in TGA in isothermal conditions, *Fuel*. 203 (2017) 522–536. <https://doi.org/10.1016/j.fuel.2017.04.134>.
- [35] M. Morin, S. Pécate, M. Hémati, Y. Kara, Pyrolysis of biomass in a batch fluidized bed reactor: Effect of the pyrolysis conditions and the nature of the biomass on the physicochemical properties and the reactivity of char, *J. Anal. Appl. Pyrolysis*. 122 (2016) 511–523. <https://doi.org/10.1016/j.jaap.2016.10.002>.
- [36] C. Di Blasi, Combustion and gasification rates of lignocellulosic chars, *Prog. Energy Combust. Sci.* 35 (2009) 121–140. <https://doi.org/10.1016/j.pecs.2008.08.001>.
- [37] G. Mul, F. Kapteijn, J.A. Moulijn, A DRIFTS study of the interaction of alkali metal oxides with carbonaceous surfaces, *Carbon N. Y.* 37 (1999) 401–410. [https://doi.org/10.1016/S0008-6223\(98\)00202-4](https://doi.org/10.1016/S0008-6223(98)00202-4).
- [38] R. Jiménez, X. García, T. López, A.L. Gordon, Catalytic combustion of soot. Effects of added alkali metals on CaO–MgO physical mixtures, *Fuel Process. Technol.* 89 (2008) 1160–1168. <https://doi.org/10.1016/J.FUPROC.2008.05.013>.
- [39] M.L. Hobbs, P.T. Radulovic, L.D. Smoot, Combustion and gasification of coals in fixed-beds, *Prog. Energy Combust. Sci.* 19 (1993) 505–586. [https://doi.org/10.1016/0360-1285\(93\)90003-W](https://doi.org/10.1016/0360-1285(93)90003-W).
- [40] C. Dupont, S. Jacob, K.O. Marrakchy, C. Hognon, M. Grateau, F. Labalette, D. Da Silva Perez, How inorganic elements of biomass influence char steam gasification kinetics, *Energy*. 109 (2016) 430–435. <https://doi.org/10.1016/J.ENERGY.2016.04.094>.

### CHAPTER 3. LOW TEMPERATURE OXIDATION KINETICS OF THE PRODUCTS OF BIOMASS PYROLYSIS

Chad A. Peterson<sup>1</sup>, Robert C. Brown<sup>1,2</sup>

<sup>1</sup>*Department of Mechanical Engineering, Iowa State University, Ames, IA 50011, United States*

<sup>2</sup>*Bioeconomy Institute, Iowa State University, Ames, IA 50011, United States*

Modified from a manuscript to be submitted to Energy and Fuels.

#### Abstract

Oxidation kinetics relevant to fast pyrolysis products at low temperatures (<600°C) are not well known. With the recent advancement of biomass autothermal processing, oxidation kinetics are necessary to aid in the development of these autothermal reactors. As a result, this work derives oxidation kinetics of fast pyrolysis products at low temperatures (400-600°C) using a fluidized bed reactor. Application of the two-phase theory of fluidization models the bubbling fluid bed reactor as a series of CSTRs and PFRs, simplifying rate derivation. The decomposition rate for levoglucosan was first determined finding agreement with previous published values. The comparable decomposition rate for levoglucosan offered validation of the two-phase theory and its novel application to derive oxidation kinetics. First order global oxidation rates were subsequently derived for three bio-oil pyrolysis products: xylose, levoglucosan, and acetic acid. The oxidation rate varied by a factor of ten at 500°C, indicating large differences in reactivity for these compounds. Analysis of the combustion products was used to calculate the enthalpy of combustion under conditions of low temperature oxidation.

#### Introduction

Fast pyrolysis is an endothermic process requiring a source of energy, conventionally provided through external heat transfer [1]. Polin et al. [2] recently demonstrated that addition of



small amounts of oxygen into a pyrolyzer can provide the enthalpy for pyrolysis by partially oxidizing products of pyrolysis. Oxygen added in an amount equal to as little as one-tenth that required for complete combustion provides enough energy for autothermal operation, eliminating the need for external heat transfer. Significantly, biochar is preferentially oxidized compared to bio-oil vapor products, although small losses in bio-oil were measured during autothermal operation [2,3]. Since bio-oil is the most valuable product of pyrolysis, autothermal pyrolysis should be contrived to selectively oxidize the other products. While kinetic data is well known for oxidation of gaseous fuels at elevated (combustion) temperatures ( $>1000^{\circ}\text{C}$ ) [4,5], it is unlikely that this information applies to the much lower temperatures ( $\sim 500^{\circ}\text{C}$ ) of pyrolysis. Progress in autothermal pyrolysis will require better understanding of the oxidation reactions that both drive the process and affect product composition and distribution.

In contrast, secondary decomposition reactions of vapors produced during biomass pyrolysis have been well studied, although calculated rates vary greatly [6–10]. Fukutome et al. [6] determined that gas phase degradation of levoglucosan followed first order kinetics distinguished by two different temperature regimes. Shin et al. [7] studied the decomposition of various carbohydrate-derived products, including levoglucosan, again finding first order kinetics accurately described the decomposition rate. However, despite similarities in experimental methods employed by these two research teams, reaction coefficients for levoglucosan decomposition varied by up to an order of magnitude (Table 1). Fukutome et al. [6] suggested this difference might have been impacted by mass transfer limitations arising from molten levoglucosan in the work of Shin et al. [7].

Table 1 Calculated kinetic rate coefficient of levoglucosan decomposition. Below 600°C there is an order of magnitude difference in the decomposition rate. Note: Fukutome has a low temperature regime (550-600°C) and elevated temperature (>600°C) regime.

<b>Source</b>	<b>Calculated Kinetic Rate Coefficient (1/s)</b>			
	<b>550°C</b>	<b>600°C</b>	<b>650°C</b>	<b>700°C</b>
Fukutome et al. [6]	0.956	3.271	5.335	8.520
Shin et al. [7]	0.059	0.280	1.116	3.865

Given the prominence of levoglucosan among the products of fast pyrolysis [11], global rates for decomposition of whole pyrolysis vapors might be expected to resemble those for levoglucosan. Liden et al. [8] derived the secondary vapor decomposition of tar (bio-oil) using a fluidized bed reactor at a temperature range of 400-600°C by varying gas residence time. Similar work by Morf et al. [9] pyrolyzed fir and spruce wood chips, followed by a heated tubular reactor for additional gas phase decomposition. Baumlin et al. [10] similarly used a heated tube reactor to measure the homogeneous decomposition of bio-oil vapors to non-condensable gases. The three decomposition rates of bio-oil vapors (Table 2) indicate agreement between the models.

Table 2 Decomposition kinetic rate coefficient calculated for bio-oil vapors. Reaction rates were determined to follow first order kinetics.

<b>Source</b>	<b>Calculated Kinetic Rate Coefficient (1/s)</b>		
	<b>500°C</b>	<b>600°C</b>	<b>700°C</b>
Liden et al. [8]	0.233	1.582	7.248
Morf et al. [9]	0.267	1.044	3.088
Baumlin et al. [10]	0.317	0.861	1.902

An average of the three rates at 500°C (0.271 1/s) is nearly identical to the decomposition rate of levoglucosan extrapolated from Fukutome et al. [6] at 500°C (0.238 1/s). The comparable rates of the global models and Fukutome et al. [6] provide additional evidence that the decomposition rate of Shin et al. [7] suffered from experimental bias.

Comprehensive reaction mechanisms that include decomposition and oxidation reactions have been proposed for pyrolysis of biomass. Ranzi et al. [12] recently published an updated

mechanism, containing thousands of elementary reactions and hundreds of intermediate species, related to biomass vapor decomposition and oxidation. In an earlier work, Debiagi et al. [13] described the development of the mechanism, comparing a favorable levoglucosan decomposition rate to experimental work [7]. While the model contains relevant species to autothermal pyrolysis, it was originally developed for biomass combustion, which is at greater temperatures ( $>700^{\circ}\text{C}$ ) than autothermal pyrolysis. Likewise, the basis of the reaction mechanism was hydrocarbons and subsequently expanded to oxygenated compounds (e.g. ethanol and propanol), with minimal validation for biomass pyrolysis products [14–16]. Dhahak et al. [17] employed the Ranzi mechanism in combination with several other mechanisms to achieve an updated model with favorable decomposition rates (levoglucosan, anisole, and hydroxyacetaldehyde) to experimental work. This model was also shown to depict the accurate oxidation rate predictions of guaiacol, a lignin pyrolysis product, and several hydrocarbon products. While the model was regarded as an improvement, relevant oxidation kinetics of cellulose (levoglucosan) and hemicellulose (xylose) products was not addressed. Importantly, the Ranzi mechanism originally validated levoglucosan decomposition to the work of Shin et al. [7], which as previously discussed, is the outlier for decomposition rates. Consequently, these elementary reaction mechanisms still lack accuracy at temperatures relevant to autothermal pyrolysis.

Given the complexity of developing elementary reactions, simple one step combustion models have been developed for single particle combustion. These models include devolatilization (pyrolysis), char oxidation, and tar (bio-oil vapors) oxidation steps to describe the particle combustion process [18,19]. While a simplification, the tar vapors were grouped together and approximated as a single chemical entity. The elemental composition, which was

originally developed for coal tars, was approximated as  $C_1H_{1.65}O_{0.91}$ , similar to that of biomass bio-oil ( $C_1H_{0.99}O_{0.88}$ ) [2]. The global tar oxidation rate used in these particle models is a modified Arrhenius equation from the work of Smoot and Smith [20]:

$$\text{rate} = A * T^{0.3} * \exp\left(-\frac{E}{R*T}\right) * C_{O_2} * C_{CHO}^{0.5} \quad (1)$$

where A the pre-exponential factor (20,700 1/s), E the activation energy (80.2 kJ/mol), T the gas temperature, and R the universal gas constant (0.008314 kJ/mol-K). The reaction order was determined to be first order with oxygen and fuel at 0.5.

Dryer and Westbrook [21] developed another one step hydrocarbon combustion model that was subsequently adapted to ethanol [22]. The rate equation of this model is a conventional Arrhenius equation:

$$\text{rate} = A * \exp\left(-\frac{E}{R*T}\right) * C_F^{0.15} * C_{O_2}^{1.6} \quad (2)$$

where A equal to the pre-exponential factor ( $1.55 \times 10^{10}$  1/s), E the activation energy (125.6 kJ/mol), T the gas temperature, and R the universal gas constant (0.008314 kJ/mol-K). The reaction order is 1.6 regarding oxygen and 0.15 for the fuel. The kinetic rate coefficient for the models is calculated in Table 3 at pyrolysis temperatures, demonstrating orders of magnitude difference in rates.

Table 3 Calculated kinetic rate coefficients for two global oxidation models.

Source	Calculated Kinetic Rate Coefficient (1/s)		
	400°C	500°C	600°C
Smoot and Smith [20]	0.09	0.58	2.50
Dryer and Westbrook [21]	2.76	50.44	473.12

The large uncertainty in decomposition and oxidation rates complicates the modeling of autothermal reaction chemistry. As a result, the main objective of this study was to determine oxidation kinetics relevant to autothermal pyrolysis. To represent pyrolytic vapors, three model

products were selected: xylose, acetic acid, and levoglucosan. Subsequently, the oxidation rate was derived at multiple temperatures ( $<600^{\circ}\text{C}$ ) producing Arrhenius expressions for each of the products. Additional experiments were conducted on the gas phase degradation of levoglucosan. Analysis of the combustion products was used to calculate the enthalpy released at these low temperatures. The derived results can subsequently be used in modeling of autothermal pyrolysis, aiding in its scale-up and operability.

## **Methods**

### **Continuous reactor system**

Oxidation and decomposition studies were conducted in a fluidized bed by continuously feeding a model bio-oil product into an isothermal fluidized bed reactor at ambient pressure. The reactor was a 3.81 cm diameter bubbling fluid bed loaded with 400 grams of 500-600  $\mu\text{m}$  diameter sand for oxidation studies or 250-300  $\mu\text{m}$  diameter sand for levoglucosan decomposition. Reactor height was 42 cm from plenum to the transfer line, with the liquid injection located 5 cm above the plenum. The transfer line was 0.95 cm internal diameter with a length of 76 cm. The fluidized bed reactor and transfer line (including cyclone) were independently controlled at the same temperature preventing unwanted condensation. A single Exergy shell and tube condenser collected the condensed liquid product into a 250mL bottle. Gas temperature at condenser outlet was  $<10^{\circ}\text{C}$ . Following the condenser, a glass wool packed bed collected any aerosols formed. Finally, a Varian 4800 MicroGC measured non-condensable gases at the reactor exit.

For the experiments, two gas flow controllers were used allowing for independent control of air and nitrogen. Given differences in the stoichiometric air required for combustion, the two controllers allowed for accurate control of the equivalence ratio. A peristaltic pump continuously

fed a liquid reactant into the reactor at rates of 2-5 ml/min. Instantaneous mass balance was measured with the liquid container atop an analytical balance.

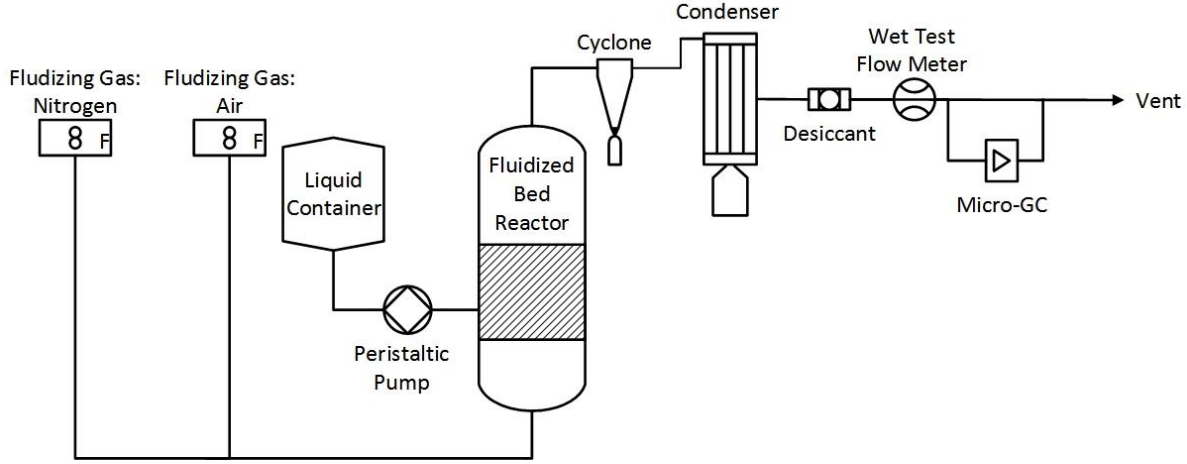


Figure 1 Reactor block flow diagram used for kinetic studies.

### Hydrodynamic model

A fluidized bed reactor is a non-ideal reactor comprising an emulsion and bubble phase corresponding to the sand and bypassing gas, respectively. By utilizing the two-phase theory of fluidization (Figure 2), the reactor can be modeled as a series of continuously stirred reactors (CSTR) and plug flow reactors (PFR) [23]. These ideal reactors have analytical solutions, simplifying rate derivation.

Table 4 Correlations used for two phase theory of fluidization calculations.

Parameter	Correlation	Ref
Archimedes Number	$Ar = \rho_g * d_s^3 * \frac{(\rho_s - \rho_g) * g}{\mu_g^2}$	[27]
minimum fluidization velocity ( $U_{umf}$ )	$U_{umf} = \frac{(\sqrt{27.2^2 + 0.0408 * Ar} - 27.2) * \mu_g}{\rho_g * d_{sand}}$	[27]
bubble diameter	$d_{b,i} = 0.00376 * (U_o - U_{umf})$	[26]
max diameter	$b_m = 0.652 * (A * (U_o - U_{umf}))^{0.4}$	[26]
bubble size	$d_b = -[(exp(-0.3 * (\frac{H_r}{(d_{Bed})})) * (d_m - d_{b,i}))] + d_m$	[26]
velocity bubble	$U_b = U_o - U_{umf} + 0.711 * [(9.81 * d_b)^{0.5}]$	[28]
volume PFR	$V_b = (U_o - U_{umf}) / (U_b)$	[29]

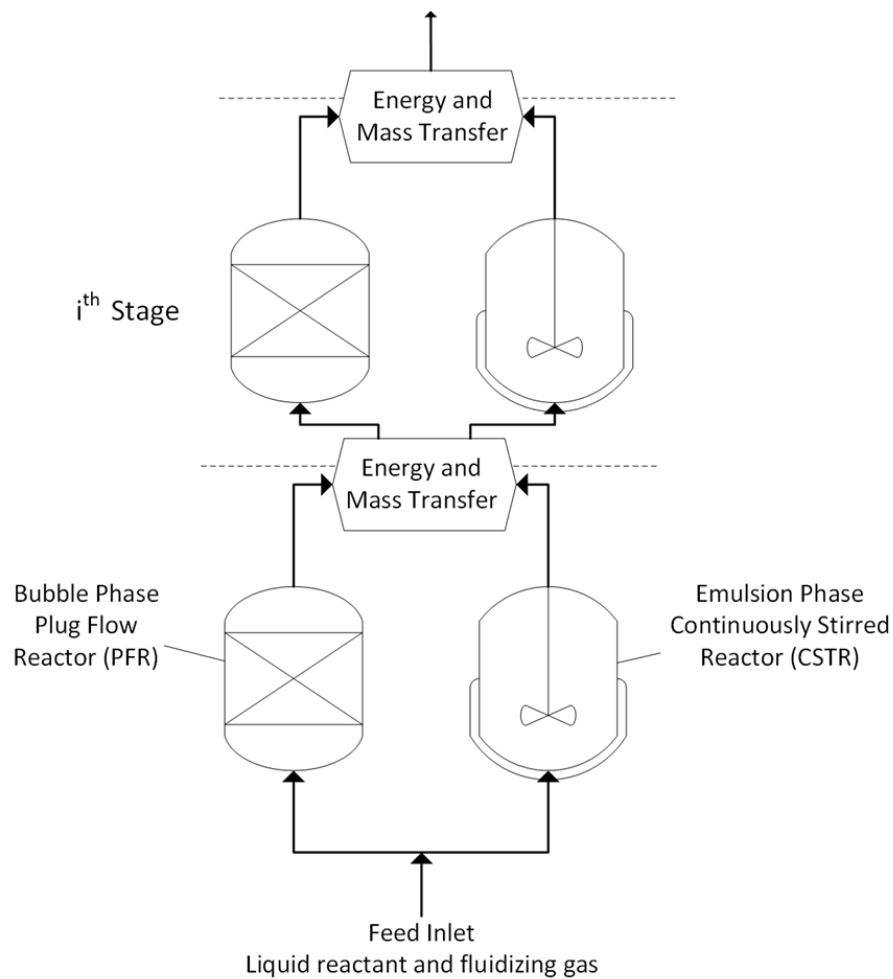


Figure 2 Two phase theory can be applied to model a fluidized bed reactor as a set of CSTRs and PFRs.

To calculate the gas percentage partitioned to each reactor, several correlations from fluidized bed studies were used (Table 4). These correlations have been used in previous works to accurately model fluidized bed processes [24,25]. From the correlations, the percent of gas in the PFR is calculated as a function of height in the reactor. The gas percentage changes with reactor height due to the growth and coalescence of bubbles as they rise in the reactor [26]. The gas not partitioned to the PFR is allocated to the CSTR.

### **Derivation of decomposition rates**

For the decomposition experiments, levoglucosan was continuously fed into the reactor under inert conditions. With levoglucosan a solid at ambient conditions, a solution of 20 wt. % (in water) was prepared and fed into the reactor at ~3.5 g/min. Fluidization gas was 3.5 SLPM of nitrogen, with gas residence time of approximately one second. The reactor and transfer line were kept at identical temperatures to avoid any unwanted vapor condensation before reaching the condenser. Following the transfer line, the vapor products were cooled to 10°C in the condenser, with the condensed liquid product collected in a 250 ml bottle. Any aerosols formed were subsequently collected in glass wool following the condenser. Total feed time was sixty minutes, ensuring a steady state was achieved.

Analysis of the collected liquid product, in particular levoglucosan, was accomplished using high performance liquid chromatography (HPLC). Details on this sugar method analysis are discussed elsewhere [30]. In addition to liquid product collected in the bottle, it was discovered levoglucosan aerosols were formed and trapped in the glass wool following the condenser. However, direct analysis of the glass wool was not feasible, as the captured aerosols were not easily separated. Therefore, to analyze the collected aerosols, 1.5 grams of wool was placed into a 10 ml solution of water. After thorough mixing, a portion of the liquid phase was extracted and subsequently analyzed on GC-MS/FID identifying and quantifying the largest compounds. Quantification of the compounds was performed using the PolyARC system, with phenanthrene as an internal standard. Then, the remaining glass wool not used for GC-MS/FID analysis, was dried at 105°C to drive off any moisture. The moisture content of the wool was calculated by this mass loss from drying.



First order kinetics were assumed with the decomposition rate of levoglucosan, consistent with previous works [31]. The conversion was calculated as the mass of levoglucosan recovered over mass fed. From the calculated conversion, the decomposition rate could be derived using the analytical solutions of the PFR and CSTR.

While previous works have used the two-phase theory to model fluidized bed processes [24,32] deriving reaction rates is not as well studied [25]. As a result, the decomposition rate of levoglucosan was first determined to validate the novel use of the two-phase theory. With subsequent validation, oxidation kinetics were derived of previously underexplored pyrolysis products at low temperatures ( $>600^{\circ}\text{C}$ ).

### **Oxidation rate derivation**

For the oxidation experiments, the ideal pyrolysis product was continuously fed into the reactor under oxidative conditions. The fluidizing gas for each experiment was consistent between species at 12 SLPM of nitrogen and air, with the dynamic sand bed expanding the reactor height. The oxygen required for stoichiometric combustion was adjusted based on the liquid feed rate, with a target equivalence ratio of 1.05. While one of the products was a liquid at ambient conditions (acetic acid) all the model compounds were prepared in a water solution. Analysis of the non-condensable gases was accomplished with a MicroGC.

The oxidation rate was determined from the consumption of oxygen. The oxygen flow rate into the reactor was calculated from the air flow controller set point and exit flow rate was measured with the MicroGC. From the oxygen consumption, first order kinetics were derived with first order to oxygen and zero order to the fuel. The order determination is a simplification; however, the low order (zero) in regard to the fuel source is consistent with previous works [20,21]:



$$r = k * [C_aH_bO_d]^0 * [O_2]^1 \quad (4)$$

$$X = (O_2^{inlet} - O_2^{exit}) / O_2^{inlet} \quad (5)$$

where  $C_aH_bO_d$  is the ideal pyrolysis product,  $\alpha$  the stoichiometric amount of oxygen required for combustion,  $r$  the oxidation rate,  $X$  the conversion of oxygen, and  $k$  the kinetic rate coefficient (1/s). The conversion  $X$  was calculated based on the consumption of oxygen from reactor inlet to the measured value at the MicroGC. Then, the kinetic rate coefficient was calculated from the PFR and CSTR analytical solutions. Subsequently, an Arrhenius plot was used to determine the activation energy and pre-exponential factor.

Each specie had combustion trials ran at three temperatures to determine Arrhenius behavior. Steady state combustion was conducted for 30 minutes, excluding a 20-minute stabilization period, gathering a minimum of seven MicroGC data points. Acetic acid and levoglucosan had identical temperatures run at 450, 500, and 550°C. However, xylose complicated these combustion experiments as its reactivity was not only greater, but lower temperatures were not possible given its high boiling point (415°C). For that reason, the lowest operable temperature was 430°C to prevent unwanted condensation in the transfer line and reactor. Likewise, given its instability, the concentration was kept at an 8 wt. % solution to avoid significant coking in the transfer line during liquid injection.

### **Reactor repeatability**

Triplicate trials were run for the acetic acid oxidation rate to determine reactor error. From the triplicate trials at 500°C, the average calculated kinetic rate (0.27 1/s) had a standard sample deviation of  $\pm 0.006$  (1/s), with a confidence interval (95%) of  $\pm 0.015$  (1/s). This

excellent repeatability indicates single trials are sufficient to measure accurate reaction kinetics. Consequently, all oxidation experiments were single trials.

## Results

From the two-phase theory calculations, a single PFR and CSTR in parallel were found to model the fluid bed reactor. An additional PFR was subsequently used to model the heated transfer line. Consequently, the gas percentage was calculated for each reactor and residence time calculated from volumetric flow rates. Detailed calculations on the hydrodynamic model for the experimental trials can be found in the supplemental information.

### Two phase theory validation

Starting with previously published decomposition rate for levoglucosan, this application of the two-phase theory was tested. While validation with a global combustion model would confirm this application of the two-phase theory, such data at low temperature and atmospheric pressure is not readily available.

Table 5 shows the allocation of gas flow to the emulsion (CSTR) and bubble (PFR) phases of the fluidized bed. Not surprisingly, with increasing temperature, the residence time decreased as the volumetric expansion of gases was greater.

Table 5 Gas distribution based on two phase theory for decomposition study of levoglucosan.

Temperature (°C)	PFR (%)	CSTR (%)	Residence time PFR (s)	Residence Time CSTR (s)	Residence Time Transfer Line (s)
500	42	58	0.68	1.32	0.17
550	46	54	0.60	1.10	0.14

From the levoglucosan mass recovered over the total mass fed, the conversion rate was calculated. Then, the kinetic rate was calculated based on this conversion value. From Table 6, the kinetic rate coefficient at 550°C was calculated as 0.68 (1/s) comparable to the value of Fukutome et al. [6] of 0.96 (1/s). Likewise, while not explicitly calculated, if the kinetic data of

Fukutome et al. [6] is extrapolated to 500°C, the kinetic rate coefficient is 0.24 1/s. This again shows a favorable comparison between their rate and the derived rate here 0.24 versus 0.37 1/s. Additional comparison with whole bio-oil decomposition rates indicated this work is again similar to those published values at 500°C (0.23-0.31 1/s) and 550°C (0.51-0.59 1/s) [8–10]. Consequently, the comparable decomposition rate of levoglucosan indicates that this use of the two-phase theory and ideal reactors can accurately calculate kinetic rates.

Table 6 Mass recovery of levoglucosan during inert decomposition studies.

Temperature (°C)	Fed (g)	Recovered (g)	Conversion (Recovered/Fed)	Kinetic Rate Coefficient (1/s)
500	38.9	26.3	0.68	0.37
550	48.2	27.0	0.56	0.68

### **Oxidation rate of select pyrolysis products**

#### **Acetic Acid**

The oxidation rate for acetic acid was determined at three temperatures: 450, 500, and 550°C. With a measured autoignition temperature of 464°C [33], it was expected that oxidation would be minimal at 450°C. For acetic acid, duplicate experimental trials were run at each temperature, and triplicates at 500°C. As previously discussed, the triplicate experiments determined reactor repeatability.

From Table 7, the oxygen consumption and calculated kinetic rate coefficients are reported for the temperature trials. As hypothesized, with an autoignition temperature of 464°C, acetic acid had minimal oxygen consumption at 450°C (5.4-6.0%). While the extent of reaction would be greater at longer residence times, this indicates that some pyrolysis products are relatively stable to oxidation at these temperatures and conditions (~0.5 second residence time). The duplicate trials at 450°C and 550°C indicated some variation in the calculated rate, though

repeatability was much worse at 550°C. However, the three trials at 500°C were nearly identical (0.26-0.28 1/s) suggesting excellent reactor repeatability.

Table 7 Calculated kinetic rate coefficient for acetic acid oxidation. Triplicates ran at 500°C indicate excellent reactor repeatability.

<b>Temperature (°C)</b>	<b>Oxygen Consumed (%)</b>	<b>Calculated Kinetic Rate (1/s)</b>
450-1	6.0	0.15
450-2	5.4	0.12
500-1	10.0	0.28
500-2	11.1	0.26
500-3	12.3	0.27
550-1	21.1	0.67
550-2	34.2	1.07

A subsequent Arrhenius plot (Figure 4) was used to calculate the activation energy at  $88.1 \pm 12.3$  kJ/mol and a pre-exponential factor of  $3.44 \times 10^5$  1/s. While unfair to directly compare, this activation energy is nearly identical to Smoot and Smith [20] (80.2 kJ/mol). The similar activation energy provides supplemental validation of these derived rates and the overall accuracy of the system. To calculate the heat of combustion, analysis of the products (i.e. carbon oxides) could indicate if complete oxidation occurred as CO<sub>2</sub> and H<sub>2</sub>O would be the only products. Given the low temperature operation, partial/incomplete oxidation may have occurred forming partial oxidative products (i.e. carbonyls or carbon monoxide). Likewise, additional analysis of CO<sub>2</sub> formation was used to calculate the conversion (i.e. oxidation) of the specie. From the stoichiometric amount of CO<sub>2</sub> produced, an additional conversion value was calculated from the measured CO<sub>2</sub> formation.

From Table 8, the CO<sub>2</sub> conversion was comparable to the oxygen conversion at 550°C (21.1-34.2 versus 21.1-32.1), indicating complete combustion. However, comparison at the lower temperatures indicated an under prediction of CO<sub>2</sub> formation versus O<sub>2</sub> consumption. With the low conversion at these temperatures, under 10%, the error is likely derived from

measurement bias with the MicroGC. Nevertheless, with no carbon monoxide formation, acetic acid appears to completely oxidize at these temperatures.

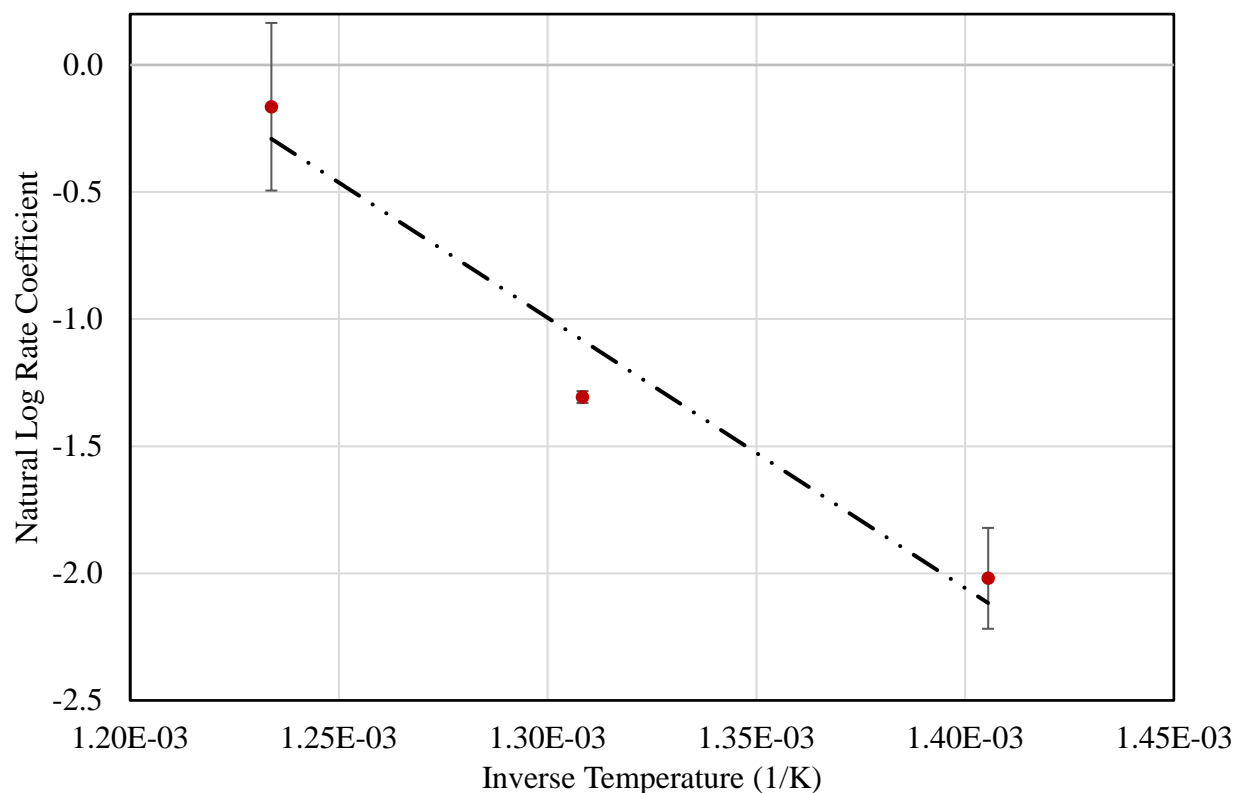


Figure 4 Arrhenius plot of acetic acid oxidation. Error bars are sample standard deviation from multiple experimental trials.

Table 8 Measurement of CO<sub>2</sub> formation from acetic acid combustion experiments indicated complete combustion occurred.

Temperature (°C)	Stoichiometric CO <sub>2</sub> Flowrate (g/min)	Measured CO <sub>2</sub> Flow (g/min)	Conversion (Measured/Stoichiometric) %
450-1	1.89	0.04	2.2
450-2	1.82	0.04	2.3
500-1	1.68	0.12	6.9
500-2	1.74	0.13	7.7
500-3	1.29	0.18	13.7
550-1	1.45	0.31	21.1
550-2	1.69	0.54	32.1

## Levoglucosan

Despite being included in biomass combustion mechanisms, the oxidation rate of levoglucosan is not studied. Likewise, even data such as the autoignition temperature is unknown, unlike common fuel sources [33]. Thus, the results determined here are the first of their kind regarding levoglucosan oxidation.

The kinetic rate was again calculated based on the consumption of oxygen in the reactor. From Table 9, the values of oxygen consumption and the calculated kinetic rate coefficient are shown. As compared to acetic acid, levoglucosan had a faster kinetic rate, indicating a greater reactivity at these temperatures.

Table 9 Calculated levoglucosan oxidation rate at pyrolysis temperatures.

Temperature (°C)	Oxygen Consumption (%)	Kinetic Rate Coefficient (1/s)
450	18.3	0.51
500	43.0	1.65
550	58.1	2.83

An Arrhenius plot was constructed from the kinetic rate coefficients (Figure 5). The calculated activation energy was 72.9 kJ/mol with a pre-exponential value of  $1.27 \times 10^5$  1/s. The activation energy is lower than the acetic acid but is still comparable to the Smoot and Smith [20] global oxidation model.

Analysis of the non-condensable gases indicated that partial oxidation of levoglucosan was occurring. At 500°C and 550°C, a significant fraction of carbon monoxide was detected (Table 10) indicating incomplete combustion.

When calculating the subsequent conversion based on the CO<sub>2</sub> measured (Table 11), it was no surprise that CO<sub>2</sub> conversion (11.7-45.5%) was lower than the oxygen conversion (18.3-58.1%). With incomplete combustion occurring, as evident with CO formation, this represents an

inefficient usage of oxygen. The impact of this incomplete combustion is discussed in a subsequent section regarding the enthalpy of combustion.

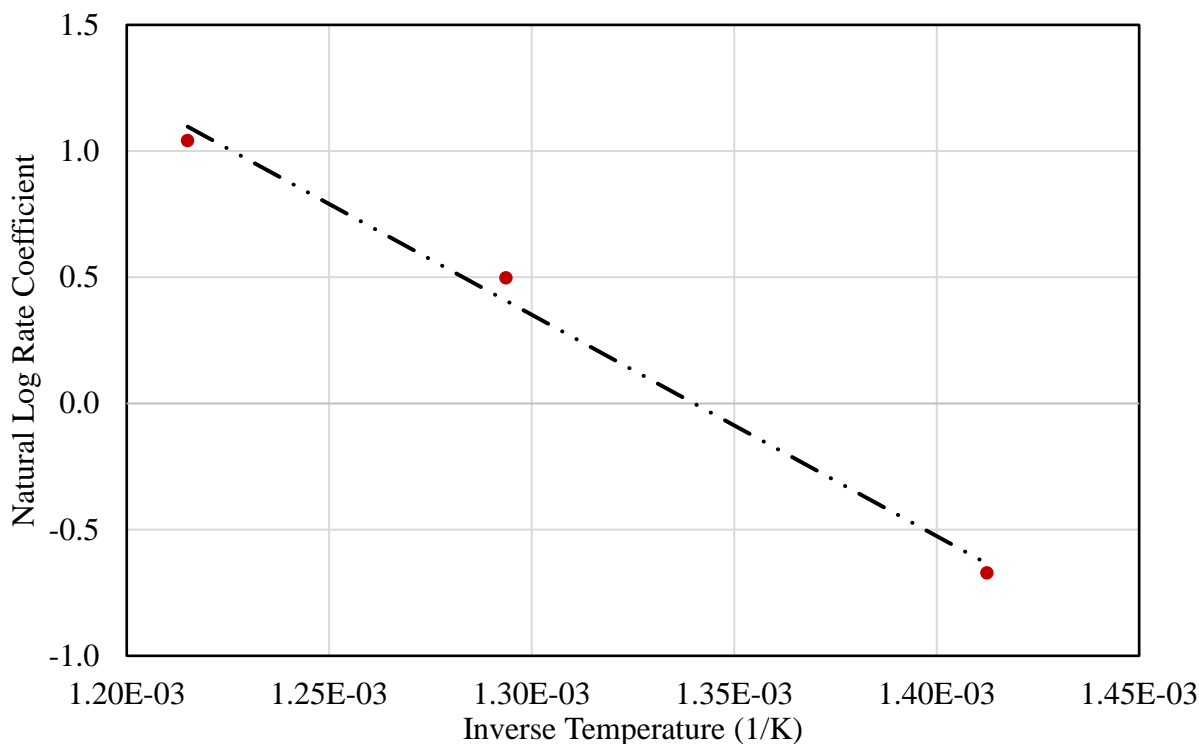


Figure 5 Arrhenius plot of levoglucosan oxidation.

Table 10 Detectable amounts of CO during oxidation of levoglucosan indicated incomplete combustion.

Temperature (°C)	CO Flowrate (g/min)	CO <sub>2</sub> Flow (g/min)
450	0.00	0.19
500	0.12	0.55
550	0.22	0.76

Table 11 The calculated CO<sub>2</sub> conversion was lower than the oxygen conversion value due to incomplete combustion occurring.

Temperature (°C)	Stoichiometric CO <sub>2</sub> Flowrate (g/min)	Measured CO <sub>2</sub> Flow (g/min)	Conversion (measured/Stoichiometric) %
450	1.66	0.19	11.3
500	1.75	0.55	31.3
550	1.75	0.76	43.5



## Xylose

In the same manner of levoglucosan, limited oxidation data is available for xylose. However, based on the decomposition rates of xylose, a faster oxidation rate was expected as compared to acetic acid and levoglucosan. While (inert) gas phase decomposition studies have not been performed for xylose, its liquid phase decomposition (caramelization) is often an order of magnitude greater than other sugars [34]. Likewise, pyrolysis of hemicellulose proxies (xylan) produce low yields of xylose (5 wt.%) [35], which could be attributed to the poor stability of xylose. Consequently, it was hypothesized that the instability of xylose would result in a faster oxidation rate.

The temperature range used for the xylose combustion experiments was narrower (430-500°C) than previous experiments. Likewise, elevated temperatures were not possible as complete oxygen consumption would occur in the reactor, skewing true residence times and the calculated rates. Consequently, a narrow temperature range was used to calculate and derive reaction kinetics.

Table 12 Calculated kinetic rate coefficient for xylose oxidation.

Temperature (°C)	Oxygen Consumption (%)	Kinetic Rate Coefficient (1/s)
430	49.2	1.56
465	53.5	1.89
500	60.1	2.42

From Table 12, the calculated kinetic rate coefficient at 500°C (2.42 1/s) demonstrates xylose is twice as reactive as levoglucosan and nearly ten times more reactive than acetic acid. This oxidation reactivity is likely attributed to its poor stability, allowing for rapid oxidation.

From the Arrhenius plot (Figure 6) the calculated activation energy was 28.2 kJ/mol with a pre-exponential factor of  $1.92 \times 10^2$ . Thus, the calculated activation energy is substantially lower

than the values of acetic acid and levoglucosan, indicating a difference in reactivity. On possible explanation for this low activation energy could be from variation in reactivity of the decomposition products. Typical xylose decomposition products include furfural and formic acid [36], which have measured auto-ignition temperatures of 315°C and 520°C, respectively. Given the instability of xylose, these two products could be readily produced with the furfural rapidly oxidized, while the formic acid is unaffected. Oxygen has been shown to increase decomposition rates, as compared to inert conditions, thus xylose may have undergone rapid decomposition [37]. Additionally, this hypothesis is supported from the minimal oxidation observed with acetic acid below its autoignition temperature. Consequently, the use of a global model may not accurately capture these competing parallel reactions, resulting in a low activation energy.

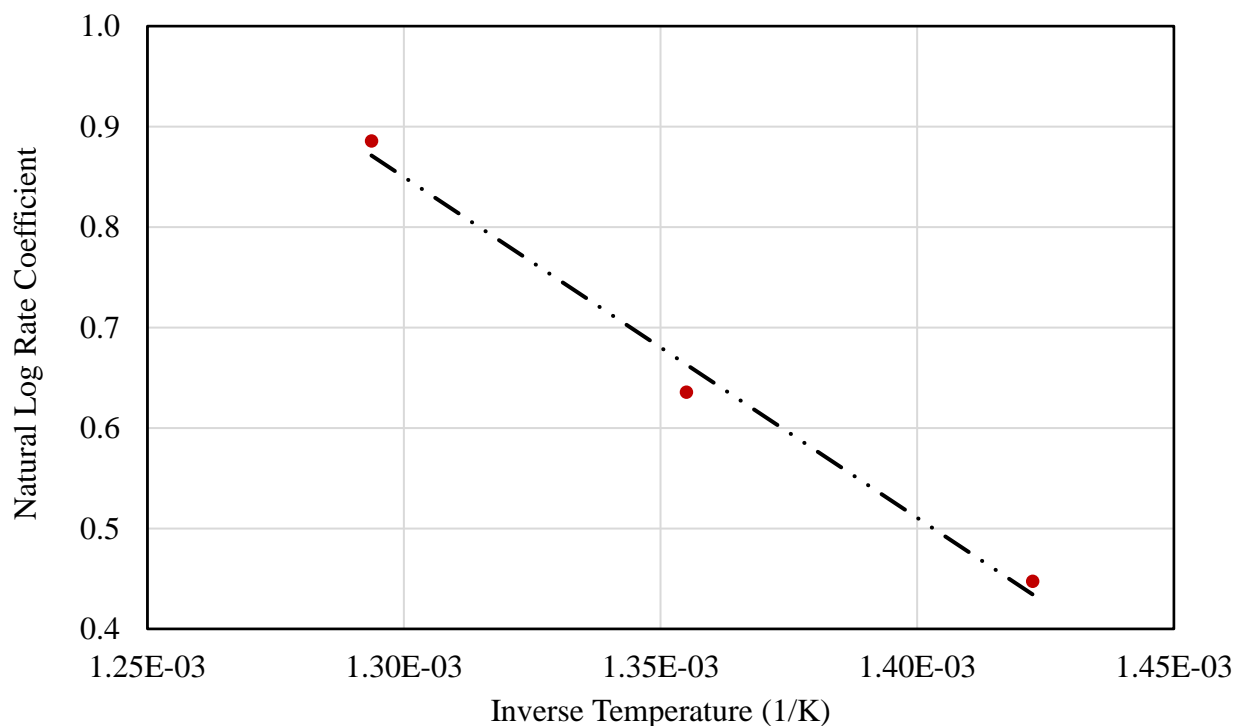


Figure 6 Arrhenius plot of xylose oxidation.

The non-condensable gases indicated that complete oxidation occurred at these temperatures as CO<sub>2</sub> was the only gas detected. Calculating a CO<sub>2</sub> conversion value, (Table 13) the CO<sub>2</sub> conversion (44-57%) was nearly identical to the oxygen conversion (49-60%). The

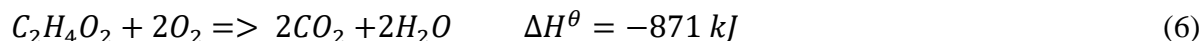
agreement between the two conversion values signifies that despite the low activation energy, complete oxidation was occurring.

Table 13 Calculated CO<sub>2</sub> conversion was nearly identical to the oxygen conversion value suggesting complete oxidation occurred.

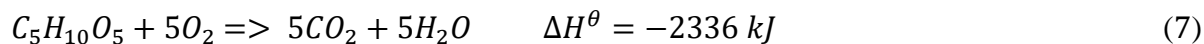
Temperature (°C)	Theoretical CO <sub>2</sub> Flowrate (g/min)	Measured CO <sub>2</sub> Flow (g/min)	Conversion (measured/theoretical) %
430	0.60	0.26	44.0
465	0.61	0.31	51.3
500	0.61	0.35	57.3

### Heat of combustion calculations

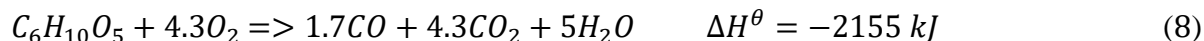
With the low temperature used for these experiments, incomplete oxidation occurred with one of the species (levoglucosan). This incomplete combustion would result in lower heat of combustion based on enthalpy of formations. For instance, the enthalpy release from the oxidation of carbon to CO<sub>2</sub> is nearly three times that of CO at -393 kJ/mol and -110 kJ/mol, respectively. Therefore, the heat of combustion, is calculated for the different species. The formula for this enthalpy release is based on the standard heat of formation at 298K. For acetic acid, complete combustion occurred, thus the stoichiometric combustion equation is calculated:



Likewise, xylose also had complete combustion, hence stoichiometric combustion:



However, based on the incomplete combustion of levoglucosan, the balanced molar equation must account for the formation of CO and CO<sub>2</sub>. The ratio of CO to CO<sub>2</sub> is the average mole ratio (0.40) from the 500°C (0.35 CO/CO<sub>2</sub>) and 550°C (0.45 CO/CO<sub>2</sub>) combustion trials:



Complete oxidation of levoglucosan would have a heat of combustion of -2824 kJ; thus, this incomplete combustion represents an inefficient usage of oxygen. Notably, even with this

small formation of CO, the energy released is just 75% of complete oxidation. With this underutilization of oxygen, during autothermal pyrolysis consumption of valuable bio-oil may increase as a higher equivalence ratio is required. Consequently, these results emphasize the significance of understanding the underlying oxidation kinetics to design a properly functioning autothermal pyrolyzer.

### **Conclusions**

The two-phase theory of fluidization was used to derive decomposition and oxidation kinetics of select pyrolysis products at low temperatures. Validation of the two-phase theory was performed with levoglucosan decomposition, with comparable rates to previous works. With the success of the decomposition rate, the subsequent oxidation rates derived are the first of their kind for individual biomass pyrolysis products. With the three species, the oxidation rate varied by an order of magnitude (0.26-2.42 1/s) highlighting varying reactivity of pyrolysis vapors. Likewise, enthalpy calculations indicated variation in combustion efficiency (i.e. CO vs CO<sub>2</sub> formation), representing an underutilization of oxygen. From the derived rates, this valuable kinetic data will aid in the development of autothermal pyrolysis reactors.

### **Acknowledgements**

This paper is based upon work supported by the Department of Energy under Award Number EE0008326. It was prepared as an account of work sponsored by an agency of the United States Government. Neither the United States Government nor any agency thereof, nor any of their employees, makes any warranty, express or implied, or assumes any legal liability or responsibility for the accuracy, completeness, or usefulness of any information, apparatus, product, or process disclosed, or represents that its use would not infringe privately owned rights. Reference herein to any specific commercial product, process, or service by trade name,

trademark, manufacturer, or otherwise does not necessarily constitute or imply its endorsement, recommendation, or favoring by the United States Government or any agency thereof. The views and opinions of authors expressed herein do not necessarily state or reflect those of the United States Government or any agency thereof.

### References:

- [1] Daugaard DE, Brown RC. Enthalpy for pyrolysis for several types of biomass. *Energy and Fuels* 2003;17:934–9. <https://doi.org/10.1021/ef020260x>.
- [2] Polin JP, Peterson CA, Whitmer LE, Smith RG, Brown RC. Process intensification of biomass fast pyrolysis through autothermal operation of a fluidized bed reactor. *Appl Energy* 2019;249:276–85. <https://doi.org/10.1016/J.APENERGY.2019.04.154>.
- [3] Polin JP, Carr HD, Whitmer LE, Smith RG, Brown RC. Conventional and autothermal pyrolysis of corn stover: Overcoming the processing challenges of high-ash agricultural residues. *J Anal Appl Pyrolysis* 2019;143:104679. <https://doi.org/10.1016/j.jaap.2019.104679>.
- [4] Tsang W, Hampson RF. Chemical Kinetic Data Base for Combustion Chemistry. Part I. Methane and Related Compounds. *J Phys Chem Ref Data* 1986;15:1087–279. <https://doi.org/10.1063/1.555759>.
- [5] Marinov NM. A detailed chemical kinetic model for high temperature ethanol oxidation. *Int J Chem Kinet* 1999;31:183–220. [https://doi.org/10.1002/\(SICI\)1097-4601\(1999\)31:3<183::AID-KIN3>3.0.CO;2-X](https://doi.org/10.1002/(SICI)1097-4601(1999)31:3<183::AID-KIN3>3.0.CO;2-X).
- [6] Fukutome A, Kawamoto H, Saka S. Kinetics and molecular mechanisms for the gas-phase degradation of levoglucosan as a cellulose gasification intermediate. *J Anal Appl Pyrolysis* 2017;124:666–76. <https://doi.org/10.1016/J.JAAP.2016.12.010>.
- [7] Shin E-J, Nimlos MR, Evans RJ. Kinetic analysis of the gas-phase pyrolysis of carbohydrates. *Fuel* 2001;80:1697–709. [https://doi.org/10.1016/S0016-2361\(01\)00056-4](https://doi.org/10.1016/S0016-2361(01)00056-4).
- [8] Liden AG, Berruti F, Scott DS. A kinetic model for the production of liquids from the flash pyrolysis of biomass. *Chem Eng Commun* 1988;65:207–21. <https://doi.org/10.1080/00986448808940254>.
- [9] Morf P, Hasler P, Nussbaumer T. Mechanisms and kinetics of homogeneous secondary reactions of tar from continuous pyrolysis of wood chips. *Fuel* 2002;81:843–53. [https://doi.org/10.1016/S0016-2361\(01\)00216-2](https://doi.org/10.1016/S0016-2361(01)00216-2).
- [10] Baumlin S, Broust F, Ferrer M, Meunier N, Marty E, Lédé J. The continuous self stirred tank reactor: Measurement of the cracking kinetics of biomass pyrolysis vapours. *Chem Eng Sci* 2005;60:41–55. <https://doi.org/10.1016/j.ces.2004.07.057>.

- [11] Lindstrom JK, Proano-Aviles J, Johnston PA, Peterson CA, Stansell JS, Brown RC. Competing reactions limit levoglucosan yield during fast pyrolysis of cellulose. *Green Chem* 2019;21:178–86. <https://doi.org/10.1039/C8GC03461C>.
- [12] Ranzi E, Debiagi PEA, Frassoldati A. Mathematical Modeling of Fast Biomass Pyrolysis and Bio-Oil Formation. Note II: Secondary Gas-Phase Reactions and Bio-Oil Formation. *ACS Sustain Chem Eng* 2017;5:2882–96. <https://doi.org/10.1021/acssuschemeng.6b03098>.
- [13] Debiagi PEA, Gentile G, Pelucchi M, Frassoldati A, Cuoci A, Faravelli T, et al. Detailed kinetic mechanism of gas-phase reactions of volatiles released from biomass pyrolysis. *Biomass and Bioenergy* 2016;93:60–71. <https://doi.org/10.1016/j.biombioe.2016.06.015>.
- [14] Frassoldati A, Cuoci A, Faravelli T, Niemann U, Ranzi E, Seiser R, et al. An experimental and kinetic modeling study of n-propanol and iso-propanol combustion. *Combust Flame* 2010;157:2–16. <https://doi.org/10.1016/j.combustflame.2009.09.002>.
- [15] Ranzi E, Frassoldati A, Stagni A, Pelucchi M, Cuoci A, Faravelli T. Reduced Kinetic Schemes of Complex Reaction Systems: Fossil and Biomass-Derived Transportation Fuels. *Int J Chem Kinet* 2014;46:512–42. <https://doi.org/10.1002/kin.20867>.
- [16] Ranzi E, Cavallotti C, Cuoci A, Frassoldati A, Pelucchi M, Faravelli T. New reaction classes in the kinetic modeling of low temperature oxidation of n-alkanes. *Combust Flame* 2015;162:1679–91. <https://doi.org/10.1016/J.COMBUSTFLAME.2014.11.030>.
- [17] Dhahak A, Bounaceur R, Le Dreff-Lorimier C, Schmidt G, Trouve G, Battin-Leclerc F. Development of a detailed kinetic model for the combustion of biomass. *Fuel* 2019;242:756–74. <https://doi.org/10.1016/J.FUEL.2019.01.093>.
- [18] Lu H, Robert W, Peirce G, Ripa B, Baxter LL. Comprehensive study of biomass particle combustion. *Energy and Fuels* 2008;22:2826–39. <https://doi.org/10.1021/ef800006z>.
- [19] Johansson R, Thunman H, Leckner B. Influence of intraparticle gradients in modeling of fixed bed combustion. *Combust Flame* 2007;149:49–62. <https://doi.org/10.1016/j.combustflame.2006.12.009>.
- [20] Smoot LD, Smith PJ. *Coal Combustion and Gasification*. Boston, MA: Springer US; 1985. <https://doi.org/10.1007/978-1-4757-9721-3>.
- [21] Dryer FL, Westbrook CK. Simplified Reaction Mechanisms for the Oxidation of Hydrocarbon Fuels in Flames. *Combust Sci Technol* 1981;27:31–43. <https://doi.org/10.1080/00102208108946970>.
- [22] Dubey R, Bhadraiah K, Raghavan V. On the estimation and validation of global single-step kinetics parameters of ethanol-air oxidation using diffusion flame extinction data. *Combust Sci Technol* 2011;183:43–50. <https://doi.org/10.1080/00102202.2010.497516>.
- [23] Grace JR, Clift R. On the two-phase theory of fluidization. *Chem Eng Sci* 1974;29:327–34. [https://doi.org/10.1016/0009-2509\(74\)80039-4](https://doi.org/10.1016/0009-2509(74)80039-4).

- [24] Eslami A, Hashemi Sohi A, Sheikhi A, Sotudeh-Gharebagh R. Sequential modeling of coal volatile combustion in fluidized bed reactors. *Energy and Fuels* 2012;26:5199–209. <https://doi.org/10.1021/ef300710j>.
- [25] Kopyscinski J, Schildhauer TJ, Biollaz SMA. Fluidized-bed methanation: Interaction between kinetics and mass transfer. *Ind Eng Chem Res* 2011;50:2781–90. <https://doi.org/10.1021/ie100629k>.
- [26] Mori S, Wen CY. Estimation of bubble diameter in gaseous fluidized beds. *AIChE J* 1975;21:109–15. <https://doi.org/10.1002/aic.690210114>.
- [27] Wen CY, Yu YH. A generalized method for predicting the minimum fluidization velocity. *AIChE J* 1966;12:610–2. <https://doi.org/10.1002/aic.690120343>.
- [28] Darton R, LaNauze R, Davidson J, Harrison D. Bubble growth due to coalescence in fluidised beds. *Trans Inst Chem Eng* 1977;55:274–80.
- [29] Kunii D, Levenspiel O. *Fluidization Engineering*. 2nd ed. Elsevier; 1991. <https://doi.org/10.1016/C2009-0-24190-0>.
- [30] Johnston PA, Brown RC. Quantitation of sugar content in pyrolysis liquids after acid hydrolysis using high-performance liquid chromatography without neutralization. *J Agric Food Chem* 2014;62:8129–33. <https://doi.org/10.1021/jf502250n>.
- [31] Fukutome A, Kawamoto H, Saka S. Processes forming Gas, Tar, and Coke in Cellulose Gasification from Gas-Phase Reactions of Levoglucosan as Intermediate. *ChemSusChem* 2015;8:2240–9. <https://doi.org/10.1002/cssc.201500275>.
- [32] Hashemi Sohi A, Eslami A, Sheikhi A, Sotudeh-Gharebagh R. Sequential-based process modeling of natural gas combustion in a fluidized bed reactor. *Energy and Fuels* 2012;26:2058–67. <https://doi.org/10.1021/ef300204j>.
- [33] Nicholas P. Setchkin. Self-Ignition Temperatures of Combustible Liquids. *J Res Natl Bur Stand (1934)* 1954;53:49–66.
- [34] Buera M Del P, Chirife J, Resnik SI, Lozano Rd. Nonenzymatic Browning in Liquid Model Systems of High Water Activity: Kinetics of Color Changes due to Caramelization of Various Single Sugars. *J Food Sci* 1987;52:1059–62. <https://doi.org/10.1111/j.1365-2621.1987.tb14275.x>.
- [35] Patwardhan PR, Brown RC, Shanks BH. Product distribution from the fast pyrolysis of hemicellulose. *ChemSusChem* 2011;4:636–43. <https://doi.org/10.1002/cssc.201000425>.
- [36] JING Q, LÜ X. Kinetics of Non-catalyzed Decomposition of D-xylose in High Temperature Liquid Water. *Chinese J Chem Eng* 2007;15:666–9. [https://doi.org/10.1016/S1004-9541\(07\)60143-8](https://doi.org/10.1016/S1004-9541(07)60143-8).
- [37] Boyadjian C, Lefferts L, Seshan K. Catalytic oxidative cracking of hexane as a route to olefins. *Appl Catal A Gen* 2010;372:167–74. <https://doi.org/10.1016/j.apcata.2009.10.030>.

## CHAPTER 4. OXIDATION OF PHENOLIC COMPOUNDS DURING AUTOTHERMAL PYROLYSIS OF LIGNOCELLULOSE

Chad A. Peterson<sup>1</sup>, Jake K. Lindstrom<sup>1</sup>, Joseph P. Polin<sup>1</sup>, Sarah D. Cady<sup>2</sup>, Robert C. Brown<sup>1,3</sup>

<sup>1</sup>*Department of Mechanical Engineering, Iowa State University, Ames, IA 50011, United States*

<sup>2</sup>*Department of Chemistry, Iowa State University, Ames, Iowa 50011, United States*

<sup>3</sup>*Bioeconomy Institute, Iowa State University, Ames, IA 50011, United States*

Modified from a manuscript published in Journal of Analytical and Applied Pyrolysis

### Abstract

Fast pyrolysis is traditionally defined as the rapid decomposition of organic material in the absence of oxygen to produce primarily a liquid product known as bio-oil. However, the introduction of small amounts of oxygen to the process holds prospects of internally generating the energy needed for pyrolysis. The present study investigates the partial oxidation of lignin-derived compounds during pyrolysis, which generates both carbon oxides and aromatic carbonyl compounds. Analysis of lignin derived phenolic compounds was performed to determine if the composition had changed under oxidative conditions. NMR analyses indicates aromatic carbonyls increased under oxidative conditions, with a corresponding decrease in phenolic hydroxyl groups. Model phenolic compounds were pyrolyzed to help understand the role of partial oxidation during autothermal pyrolysis of lignocellulosic biomass.

### Introduction

Lignocellulosic biomass has received considerable attention as feedstock for the production of advanced biofuels [1]. Fast pyrolysis, which is conventionally defined as the rapid decomposition of biomass in the absence of oxygen, has emerged as a promising approach, deconstructing plant biopolymers into bio-oil suitable for upgrading to transportation fuels [2].



Bio-oil consists of hundreds of carbohydrate-derived compounds, including ketones, aldehydes, and acids, as well as lignin-derived phenolic monomers and oligomers. The inherent complexity of lignin has hampered efforts to understand its thermal deconstruction into phenolic compounds [3,4].

Autothermal pyrolysis, which partially oxidizes some of the products of pyrolysis to provide the enthalpy for pyrolysis, has recently emerged as a new approach to bio-oil production. Because the enthalpy for pyrolysis is relatively small, the amount of oxygen required is only about one tenth that required for full combustion of lignocellulosic biomass [5,6]. Autothermal pyrolysis is a non-equilibrium process; thus, the final products are strongly dependent on poorly understood devolatilization and oxidation reaction kinetics. The high temperature (1000-2500°C) combustion of fuels such as methane [7] and ethanol [8] has been studied extensively and the oxidation kinetics are well known. However, this information is not necessarily relevant to autothermal pyrolysis, which occurs at only 400-500°C.

While pyrolysis of polysaccharides in lignocellulose generally yield monomers and other relatively small molecules, the products of lignin pyrolysis include both monomeric and oligomeric compounds [9]. The presence of non-volatile oligomers in bio-oil has been the subject of debate for many years. Dugaard and Brown [10] clearly established the significant presence of aerosol in the vapor stream leaving the pyrolysis reactor. An early suggestion was that liquid droplets of melted and partially depolymerized lignin were thermally ejected from pyrolyzing biomass [11]. Building on this thermal ejection premise, Marathe et al. [12] developed a mathematical model to describe the formation of these partially depolymerized lignin fragments. Droplet ejection undoubtedly occurs in some kinds of experimental apparatus as reported for both lignin [13] and cellulose [14], although these may be artifacts of the

experimental methodology. In recent comprehensive experiments with an optically accessible pyrolyzer, Tiarks et al. [15] did not observe significant thermal ejection of aerosols from lignocellulosic biomass, while thermal ejection from the pyrolysis of technical lignin was traced to melting and agglomeration phenomena not observed for lignocellulosic biomass. Thermal ejection from technical lignin essentially disappeared when the sample was dispersed in silica gel powder before pyrolysis. This study supported an alternative theory in which lignin effectively depolymerizes to monomers followed rapidly by their vaporization and entrainment into the gas stream leaving the pyrolyzer followed by chemical condensation to oligomers either in the vapor stream or after the monomers are physically condensed to liquid [16,17].

The effect of oxygen admission into the reactor on repolymerization is unknown. Oxidation of phenolic compounds may produce stable monomers that are less susceptible to condensation, as oxygen can inhibit polymerization [18]. Conversely, carbonyl content in bio-oil has been shown to increase the molecular weight of aged bio-oil [19]. Further research is required to understand the effect of partial oxidation on the molecular weight and chemical composition of phenolic compounds in bio-oil.

The transportation mode of phenolic compounds through the pyrolyzer is important in understanding their oxidation during autothermal pyrolysis. Aerosols of non-volatile phenolic oligomers would oxidize relatively slowly, in a manner similar to oxidation of non-porous, solid fuels, which have relatively limited surface area to support gas-solid reactions. On the other hand, vapors of phenolic monomers, well mixed with air or oxygen, would be expected to oxidize more rapidly than aerosols of phenolic oligomers. Since the study of Tiarks et al. [15] suggests that phenolic monomers are the primary products from the depolymerization of lignin, we hypothesize that phenolic compounds will significantly oxidize during autothermal pyrolysis.

Thus, we envision that lignin initially depolymerizes to monomers, then are oxidized in the gas phase before re-polymerizing to form larger oligomers.

In addition to generating gaseous carbon oxides, partial oxidation of lignin-derived phenolic monomers are likely to add oxygen to their molecular structure as aromatic aldehyde, ketone, and carboxylic acid functionalities [20]. Most lignin oxidation studies have focused on the production of vanillin and other high-value phenolic monomers [21–24]. Such experiments, conducted at pressures up to 20 bar and temperatures rarely exceeding 300°C, are of marginal utility to understanding the chemical kinetics of autothermal pyrolysis, which is conducted at atmospheric pressure and temperatures around 500°C. However, the impact of oxygen on lignin-derived compounds is still relevant for understanding chemical changes that may occur during autothermal pyrolysis.

The pulping industry has studied oxidation of Kraft lignin to valorize it beyond its usual application as boiler fuel. Villar et al. [25] oxidized hardwood Kraft lignin at moderate temperatures (140-190°C) and pressures (10-15 bar) using molecular oxygen, copper oxide, and nitrobenzene. Lignin conversion was low, less than 10%, but the major products were phenolic aldehydes (vanillin and syringic aldehyde) and carboxylic acids (vanillic and syringic acid). Likewise, Asgari et al. [26] used molecular oxygen at low temperatures (80-140°C) and pressure (7 bar) to quantify the rate of oxidation at different times and temperature. However, instead of measuring select monomer products (e.g. vanillin) the entire slate of products was analyzed using <sup>31</sup>P nuclear magnetic resonance (NMR) to quantify changes in hydroxyl groups. With increasing temperature and time, phenolic hydroxyl groups decreased, whereas carboxylic acids increased from 0.26 mmol g<sup>-1</sup> in the control lignin, to 1.5 mmol g<sup>-1</sup> under the most severe

processing conditions. Their results gives evidence that functional groups can be added without fully depolymerizing lignin.

Yields of desirable phenolic monomers are quite low from non-catalytic oxidation of lignin, which has encouraged the search for suitable catalysts to improve the process. Luo et al. [27] used a rhenium catalyst at 120°C and 2 bar of oxygen pressure in phenol to convert lignin to vanillin with high selectivity. Similar work by Schutyser et al.[28] used copper catalysts and NaOH under oxidative conditions to produce phenolic aldehydes and carboxylic acids, with monomer yield exceeding 30%. Demesa et al. [29] oxidized alkali-extracted lignin in a 0.1 M NaOH solution at temperatures and pressures up to 225°C and 15 bar, respectively. At these conditions, aromatic rings fractured to produce low molecular weight acids including acetic, succinic, and formic acids instead of phenolic formaldehydes and phenolic acids. More recent work has focused on oxidation of phenolic dimers as model compounds to deduce lignin oxidative reaction pathways [30]. However, theoretical yields have proved difficult to achieve even using model compounds, illustrating the complexity of the oxidation reactions and the instability of products in an oxidative environment.

Very few studies on the oxidation of phenolic compounds have been conducted at conditions relevant to autothermal pyrolysis. Kim et al. [31,32] pyrolyzed both untreated and acid pretreated red oak at 500°C under atmospheric conditions in a fluidized bed reactor using mixtures of nitrogen and oxygen as fluidization gas. The produced bio-oil was analyzed with gas chromatography (GC) with mass spectrometry (MS) and a flame ionization detector (FID). Select phenolic monomers were quantified and identified, finding the yield of vanillin increased over 100% in the presence of oxygen compared to non-oxidative conditions. Pyrolysis of mallee wood in a fluidized bed reactor with varying oxygen concentrations found an increase in

syringaldehyde through the addition of oxygen [33]. Kraft lignin pyrolyzed under partial oxidative conditions in a fluidized bed reactor produced bio-oil with increased oxygen content compared to bio-oil produced in the absence of oxygen [34]. Consequently, significant oxidation of lignin or its decomposition products can occur even for the very short residence time of vapors (less than a second) in the experiments.

Polin et al. [5] demonstrated that autothermal pyrolysis of red oak oxidizes only a small fraction of bio-oil products. Liquid extractions of the bio-oil indicated that the yield of water-soluble fraction (which includes pyrolytic sugars) was 6.6 wt. % for non-oxidative (nitrogen-blown) pyrolysis, decreasing to 5.3 wt. % for autothermal (air-blown) operation. Similarly, the yield of the toluene-soluble fraction of bio-oil, consisting primarily of phenolic monomers, was 4.2 wt. % for non-oxidative pyrolysis, decreasing to 2.5 wt. % for autothermal operation. The loss of phenolic monomers and pyrolytic sugars under autothermal operation suggests their complete oxidation to carbon dioxide and water. However, the remaining insoluble portion (predominantly phenolic oligomers) from these extractions appeared unaffected, as the yields were 19.8 wt. % and 20.3 wt. % for the non-oxidative and oxidative pyrolysis condition, respectively. Partially oxidized phenolic compounds in the reactor may have resulted in additional polymerization reactions, which would increase the yield of phenolic oligomers.

To further valorize pyrolysis, hydrotreating of the phenolic fraction could prove beneficial. Previous work has demonstrated that representative lignin pyrolysis products (guaiacol) can be efficiently converted to valuable hydrocarbons under catalytic hydrotreating [35]. Likewise, the prospect of turning whole bio-oil into hydrocarbons has been demonstrated as a viable process [36]. However, with increasing oxygen content, hydrogen consumption and total

costs are likely to rise. Thus, understanding the role of these partial oxidation reactions is first required.

The goal of this study is to investigate the effect of oxygen on the phenolic oligomers produced from the fast pyrolysis of red oak. Gel permeation chromatography (GPC) was used to analyze molecular weight distributions of phenolic compounds [37], coupled with quantitative  $^{31}\text{P}$  NMR and  $^{13}\text{C}$  NMR to identify changes in functional groups of phenolic compounds [25,26,34,38]. In addition, phenolic model compounds were pyrolyzed under inert conditions to evaluate differences in products that may be produced under oxidative conditions. This work helps elucidate the oxidative changes that occur to the lignin fraction of lignocellulosic biomass during fast pyrolysis.

## **Methods**

### **Pyrolysis of red oak and recovery of bio-oil fractions**

All experiments used *Quercus rubra* (red oak) wood chips reduced in particle size using a hammer mill with a 1/8th inch screen and dried to less than 10% moisture. The experimental apparatus consisted of a modified version [5] of Iowa State University's Pyrolysis Process Development Unit (PPDU) [39]. All bio-oil analysis performed in this work was produced from the modified reactor system. Briefly, a bubbling fluidized bed reactor operating at 500°C was fluidized with either 115 standard liters per minute (SLPM) nitrogen flow for conventional pyrolysis or air for oxidative (autothermal) pyrolysis. Two gas cyclones in series at the exit of the reactor removed biochar from the vapor stream. The hot pyrolysis vapors entered a bio-oil recovery system that collected bio-oil as multiple stage fractions. Stage fraction one (SF1) condenses pyrolysis vapors at 125°C with a spray of water [40]. Stage fraction two (SF2) collected aerosols from the stream using a wet electrostatic precipitator (ESP) operated at 40 kV

and 125°C. These two stage fractions are collectively referred to as heavy ends of bio-oil and consist primarily of anhydrosugars and phenolic compounds. Subsequent stages collected lower boiling point compounds (bio-oil light ends) including water. The typical yield of bio-oil heavy ends is 28.1-31.9 wt. % and light ends yield of 31.3-34.3 wt. % for red oak on a biomass basis [5,39]. This work focuses on the heavy ends of bio-oil collected in the first two stage fractions. For this work, the bio-oil was produced under two distinct operating conditions. The first was conventional fast pyrolysis using nitrogen as the fluidizing gas. Biomass feed rate for this conventional operation was 5 kg/hr. The second was partial oxidative pyrolysis using air as the fluidizing agent at equivalence ratio of 0.107 where equivalence ratio is defined as the fraction of air admitted to stoichiometric mass required for full combustion of the biomass. With improvements in autothermal processing, biomass feed rate was increased to 15 kg/hr. Vapor residence time in the reactor was calculated at 0.7 s and 1.0 s, for the oxidative and non-oxidative case, respectively. Polin et al. [5] provides additional details on the experimental apparatus and operation.

## **Bio-oil analysis**

### **Liquid-Liquid Extractions**

Phenolic compounds were recovered from the first two stage fractions of bio-oil through liquid-liquid extractions. Samples were analyzed in duplicates. Twenty milligrams of bio-oil were mixed with equal mass of water in 50 mL centrifuge tubes. These were heated to 75°C for 30 minutes and subsequently vortexed for four minutes followed by centrifugation (Fischer Scientific accuSpin 1) at 3000 RPM for 20 minutes to achieve phase separation. The aqueous phase, containing water-soluble carbohydrates from the heavy fraction, was decanted and discarded. The remaining heavy organic phase, consisting of water-insoluble phenolic compounds, was washed with an equal weight of toluene, which dissolved the lightest phenolic

compounds (mostly monomers but also some dimers). This toluene soluble portion was decanted and discarded. The toluene insoluble portion, consisting primarily of phenolic oligomers, was dried in a vacuum oven at 40°C at a pressure of 6 in-Hg for 65 hours to drive off any residual moisture and toluene before subsequent chemical analysis.

The extraction of phenolic oligomers between the two conditions was nearly identical at 19.8 wt. % and 20.3 wt. % (biomass basis), for the non-oxidative and oxidative condition, respectively. Additional discussion and analysis of the liquid extract is subsequently discussed elsewhere [5].

### **Gel permeation chromatography (GPC)**

Gel permeation chromatography (GPC) analysis was performed using a Dionex Ultimate 3000 High Performance Liquid Chromatograph. Two types of columns, MesoPore (3 mm inner diameter, 300x7.5 mm; 200–25000 Da) and PLgel (3 mm inner diameter; 300x7.5 mm; 100–4000 Da), were used in series at 25°C with tetrahydrofuran (THF) as the mobile phase (flow rate: 1 mL min<sup>-1</sup>). Phenolic oligomers extracted from the bio-oil (approximately 20 mg) were dissolved in 10 mL of THF. The phenolic oligomers recovered from the two stage fractions were combined and filtered through a 0.25 µm polytetrafluoroethylene (PTFE) filter prior to GPC analysis. Measurements were performed using a diode array detector. The GPC columns were calibrated with twelve polystyrene standards in the molecular weight range 162–38640 Da.

### **Ultimate Analysis**

Ultimate analysis was used to determine the carbon, hydrogen, sulfur, nitrogen, and oxygen (by difference) of the phenolic oligomers. Samples of phenolic oligomers weighing 5 mg were loaded into tin capsules and placed into an Elementar Analyzer (vario MICRO cube). The instrument measured mass fractions of carbon, hydrogen, sulfur, and nitrogen in a sample, with



oxygen content determined by difference on a dry, ash free basis. All samples were prepared in at least duplicates.

### **NMR Analyses**

An Avance NEO 400 MHz with narrow bore 9.4 Telsa shielded magnet coupled with a liquid nitrogen-cooled broadband Prodigy probe was used for NMR analyses. Both the analyses were based on previous work with lignin-derived phenolic bio-oil [41]. The  $^{31}\text{P}$  NMR spectra were acquired using an inverse gated decoupling pulse sequence,  $90^\circ$  pulse angle, 25 s pulse delay, and 128 scans. The  $^{13}\text{C}$  NMR spectra were acquired using an inverse gated decoupling pulse sequence,  $90^\circ$  pulse angle, 12 s pulse delay, and 4500 scans. The resulting NMR spectra were integrated and analyzed using Mestrenova software.

For  $^{13}\text{C}$  NMR preparation, 500 mg of liquid-liquid extracted phenolic oligomers was dissolved in 625 mg (0.61 mL) pyridine- $d_5$  and 1796 mg (1.51 mL) dimethylsulfoxide (DMSO)- $d_6$ . After thorough mixing, approximately 0.5 mL of the solution was pipetted into a borosilicate NMR tube.

For  $^{31}\text{P}$  NMR analyses, three stock solutions were made to allow for ease of preparation, following procedures described in a previous study [42]. The first solution (stock one) was 1.6 ml of deuterated pyridine and 1 ml of chloroform- $d$  ( $\text{CDCl}_3$ ) (1.6:1 v/v) pyridine/ $\text{CDCl}_3$ . The second solution (stock two) was the same 1.6:1 v/v pyridine/ $\text{CDCl}_3$  but with 13 mg of chromium (III) acetylacetonate added as a paramagnetic relaxation agent. The third solution (stock three) was 1.6:1 v/v pyridine/ $\text{CDCl}_3$  with 28.21 mg of endo-N-hydroxy-5-norbornene-2,3-dicarboximide (NHND) added as an internal standard. To ensure a representative sample, 75 mg of phenolic oligomers was first dissolved in a 3 mL of stock one. Then, 300 mg of 2-chloro-4,4,5, 5-tetramethyl-1,3,2-dioxaphospholane (TMDP) was added allowing for in situ derivation of the samples. Following this rapid reaction, 0.5 mL of this solution was pipetted into a 1 mL

volumetric flask, followed by 0.100 mL of the second and third stock solutions. Finally, stock one was used to fill the total volume to 1 mL. After the solution was further mixed, 0.5 mL of the solution was pipetted into an NMR tube.

NMR samples were prepared for each individual stage fraction, and results for SF1 and SF2 were analyzed separately. The results from each stage fraction were summarized into a single result for the two respective conditions.

### **Micropyrolysis experiments of model phenolic compounds**

We hypothesized that secondary reactions of phenolic monomers produced under oxidative conditions might depend on the extent of their oxidation. To test this hypothesis, we performed pyrolysis experiments on three model phenolic monomers of varying degrees of functional group oxidation: 4-hydroxybenzyl alcohol, 4-hydroxybenzaldehyde, and 4-hydroxybenzoic acid (structures illustrated in Fig. 1).

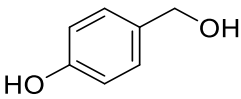
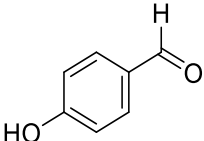
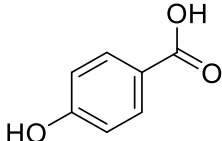

4-hydroxybenzyl alcohol	4-hydroxybenzaldehyde	4-hydroxybenzoic acid
		
Increasing Oxidation State 		

Fig. 1. Phenolic model compounds with an increasing oxidation state representative of possible oxidation that could be occurring during oxidative pyrolysis.

Experiments were performed in a modified Frontier micropyrolyzer using approximately 500 µg quantities of model compounds in an inert (helium) environment heated to 500°C. Two sets of experiments were performed. In some experiments the micropyrolyzer was attached directly to GC-MS/FID. Volatile compounds were analyzed with a 5975C GC/MSD coupled to an Agilent 7890 GC connected with a Polyarc® reactor (Activated Research Company) followed by a FID. The system was outfitted with Phenomenex DB-1701 fused silica capillary columns

(60m x 0.25mm ID, 0.25  $\mu\text{m}$  film thickness). The GC injector operated isothermally at 280°C with a split ratio of 10, with a constant helium (99.999%) flow rate of 2 mL min<sup>-1</sup>. The temperature program for the oven started at 35 °C with a 3-minute hold, then heated up to 280°C at 5°C min<sup>-1</sup> and held for 4 minutes. The MS operated with electron impact ionization operating at 280°C. Mass to charge ratio values ( $m/z$ ) were recorded over a range of 35 - 650  $m/z$  at a rate of 2 seconds per scan. Recorded peaks were identified using the 2008 NIST library. When examining the MS identified structures, judgement was applied with the identified structure based on the starting phenolic compound or produced products.

In other experiments, pyrolysis vapors from the micropyrolyzer were directed into a U-shaped steel tube immersed in liquid nitrogen, where the vapors were rapidly quenched for GPC analysis. To acquire enough mass for this purpose, twenty samples of model compounds were sequentially pyrolyzed and the product allowed to accumulate in the steel tube. After the completion of the twenty trials, the steel collection tube was rinsed with methanol and the collected liquid was vacuum dried at 40°C for twelve hours. The remaining residue was used for GPC analysis and prepared in the same manner as the phenolic oligomer samples. However, given the small quantity of the condensed product, only a single GPC trial was performed for each compound. Further details on this reactor technique are found in Lindstrom et al.[43].

## Results

### Effect of oxygen on the elemental composition of phenolic oligomers

Based on previous lignin oxidation work, it was expected that pyrolysis of lignin in an oxidative environment would decrease the carbon content and increase the oxygen content of phenolic oligomer products. However, as shown in Table 1, ultimate analysis found little difference in the phenolic oligomers produced under these two conditions. Application of the

Student t-test found no statistically significant difference ( $\alpha=0.05$ ) in the carbon, hydrogen, or oxygen content for oxidative and non-oxidative pyrolysis conditions.

Table 1 Ultimate analysis of phenolic oligomers produced during fluidized bed pyrolysis of lignocellulose indicates no statistically significant difference in carbon, hydrogen or oxygen for non-oxidative and oxidative pyrolysis conditions. Values in parentheses are sample standard deviations.

Condition	Compositional analysis (wt. %)				
	Nitrogen	Carbon	Hydrogen	Sulfur	Oxygen (Difference)
Non-Oxidative	0.41 (0.05)	58.12 (0.24)	5.53 (0.17)	0.01 (0.00)	35.93 (0.30)
Oxidative	0.47 (0.02)	59.59 (0.49)	5.23 (0.19)	0.02 (0.01)	34.69 (0.52)

Although these results indicate little uptake of oxygen by the phenolic oligomers, it is still possible that pyrolysis in the presence of oxygen produced changes in the relative distribution of functional groups or structure of these compounds. For example, Akim et al. [44] in studies on oxidative delignification of biomass, found significant changes in the distribution of lignin functional groups even though elemental composition was relatively unchanged. These possibilities are subsequently explored.

### Effect of oxygen on the molecular weight of phenolic oligomers

GPC was performed on the phenolic oligomers to measure their relative molecular weights. Given the reactivity of aromatic carbonyls towards condensation and repolymerization of phenolic compounds [19], it was expected that molecular weight would increase under oxidative conditions.

Both oxidative and non-oxidative conditions produced phenolic oligomers with significantly lower molecular weights than native lignin structures [45,46]. However, only minor differences in molecular weight distribution were observed for phenolic oligomers produced in oxidative environments compared to oligomers from non-oxidative environments. As shown in Fig. 2, the GPC spectra for phenolic oligomers from both conditions are similar, having minor

shoulders at approximately 270 Da, representative of monomers, and a major peak at 400 Da, representative of oligomers.

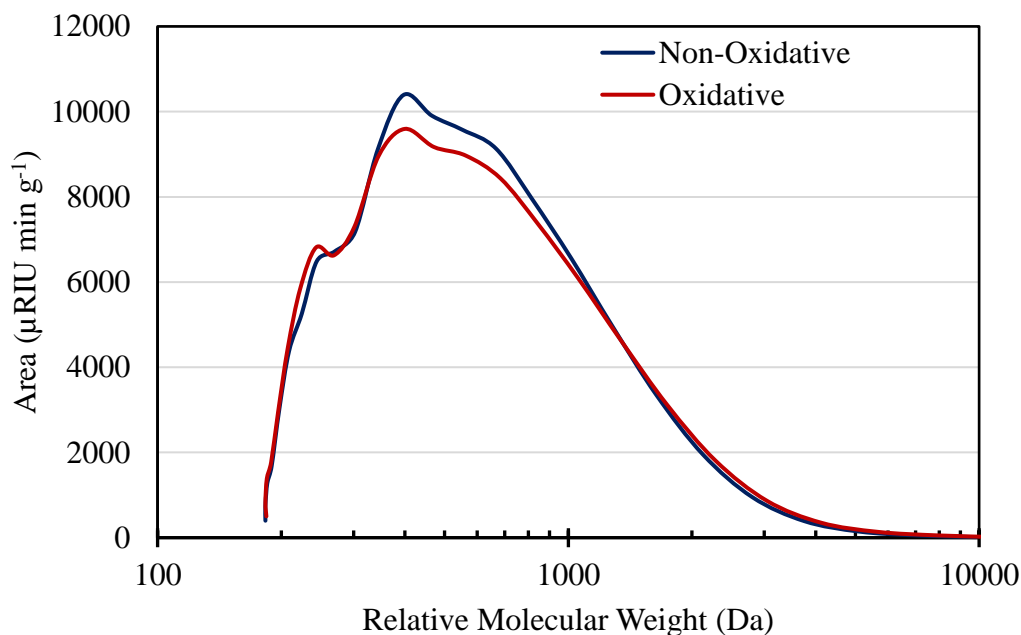


Fig. 2. GPC spectra of the phenolic oil shows minimal differences between operating conditions. (UV-VIS 254 nm)

As shown in Table 2, the weight-average molecular weight ( $M_w$ ) and number average molecular weight ( $M_n$ ) for phenolic oligomers produced under oxidative conditions are only slightly lower than the values for the non-oxidative case. Weight-average molecular weights are nearly identical, calculated at 595 and 591 Da for the non-oxidative and oxidative condition, respectively.

Table 2 Average molecular weight and dispersity was not significantly impacted under oxidative conditions.

Condition	$M_w$ (Da)	$M_n$ (Da)	Dispersity Index ( $M_w/M_n$ )
Non-Oxidative	595	390	1.52
Oxidative	591	378	1.56

Previous research has shown that partial oxidative pyrolysis of birch bark narrows the molecular weight distribution of whole bio-oil [47]. Similar results with Kraft lignin pyrolyzed

under oxidative conditions produced a lower molecular weight phenolic oil [34]. However, our work on the phenolic oligomer fraction of bio-oil indicates that under partial oxidation conditions, molecular weight was unaffected. The small quantity of oxygen admitted to the reactor was likely not enough to cause significant changes in molecular weight.

### **Effect of oxygen on phenolic oligomer functional groups**

$^{31}\text{P}$  NMR and  $^{13}\text{C}$  NMR were used to quantify changes in the relative concentrations of various functional groups associated with the phenolic oligomers. Oxidation was expected to decrease hydroxyl content of the phenolic oligomers, while producing a higher fraction of aromatic carbonyls.

Table 3 summarizes eight different phosphorylated hydroxyl groups that were identified and quantified using  $^{31}\text{P}$  NMR analysis. The chemical shifts of these groups were based on previous research analyzing bio-oil produced from lignin pyrolysis [41,48]. Each of the identified groups indicates the location of the hydroxyl group on the phenolic structure or proximity to other functionality (e.g. methoxy). Additionally, the three C-5 substituted groups are indicative of a phenolic oligomer structures, with the bonds ( $\beta$ -5, 4-O-5, 5-5) distinguishing the hydroxyl group.

Overall, phenolic hydroxyl groups mainly decreased under oxidative conditions compared to non-oxidative conditions, as would be expected if the hydroxyl groups were oxidized to aromatic carbonyl groups. Only aliphatic-OH groups increased for phenolic oligomers from oxidative pyrolysis, although the increase was small (1.28 vs 1.31 mmol g<sup>-1</sup>). Total hydroxyl functionality (excluding Acid-OH) was 5.60 mmol g<sup>-1</sup> and 4.98 mmol g<sup>-1</sup> for phenolic oligomers produced under non-oxidative and oxidative conditions, respectively, consistent with oxidation of phenolic hydroxyl groups.

Table 3  $^{31}\text{P}$  NMR measured phenolic hydroxyl content for non-oxidative and oxidative produced phenolic oligomers.

Phenolic Group	$\delta$ (ppm)	Phenolic -OH (mmol g $\text{PO}^{-1}$ )	
		Non-Oxidative	Oxidative
Aliphatic-OH	150.0-145.5	1.28	1.31
C5-substituted OH $\beta$ -5	144.7-142.8	1.20	1.04
C5-substituted OH 4-O-5	142.8-141.7	0.74	0.65
C5-substituted OH 5-5	141.7-140.2	0.33	0.30
Guaiacyl phenolic OH	140.2-139.0	1.02	0.88
Catechol type OH	139.0-138.2	0.73	0.57
P-hydroxyl-phenyl OH	138.2-137.3	0.30	0.23
Acid-OH	136.6-133.6	0.27	0.26

$^{13}\text{C}$  NMR measurement is semi-quantitative, with the identified functional group as a percentage of the total carbon bonds in a sample. For this calculation, the identified regions have the area summed and each region is then divided by the overall sum. The different integration regions were based on previous studies of lignin-derived bio-oil [41].

Table 4 Carbonyl bonds increased under oxidative conditions from the result of oxidation reactions.

Functional Group	$\delta$ (ppm)	% of Carbon Bonds	
		Non-Oxidative	Oxidative
Carbonyl	215.0-166.5	2.68	3.06
Aromatic C-O Bond	166.5-142.0	17.30	19.25
Aromatic C-C	142.0-125.0	39.49	36.20
Aromatic C-H	125.0-95.8	13.18	14.05
Aliphatic C-O	95.8-60.8	2.90	2.89
Methoxy-Aromatic	60.8-55.2	15.43	16.37
Aliphatic C-C	55.2-0.0	9.02	8.18

Examining the changes in carbon bonds shown in Table 4, aromatic carbonyls (including aromatic ketones, aldehydes, and carboxylic acids) increased from 2.68% to 3.06% for the oxidative case. The increase in carbonyl bonds is the result of oxidation reactions. Failure of  $^{31}\text{P}$  NMR analysis to detect an increase in aromatic carboxylic acids indicates that the aromatic carbonyls detected by  $^{13}\text{C}$  NMR analysis are either aldehydes or ketones or a combination of these two kinds of carbonyl compounds.

Along with the increase in carbonyl functionality, the phenolic oligomers showed other differences. By measuring the relative change between the two conditions, the most impacted functional groups are highlighted from the  $^{13}\text{C}$  NMR analysis. The relative change is defined as the difference in percentage for each functional group, between the non-oxidative and oxidative condition, over the area for the non-oxidative condition. The calculated relative change for each of the eight identified functional groups is shown in Fig. 3.

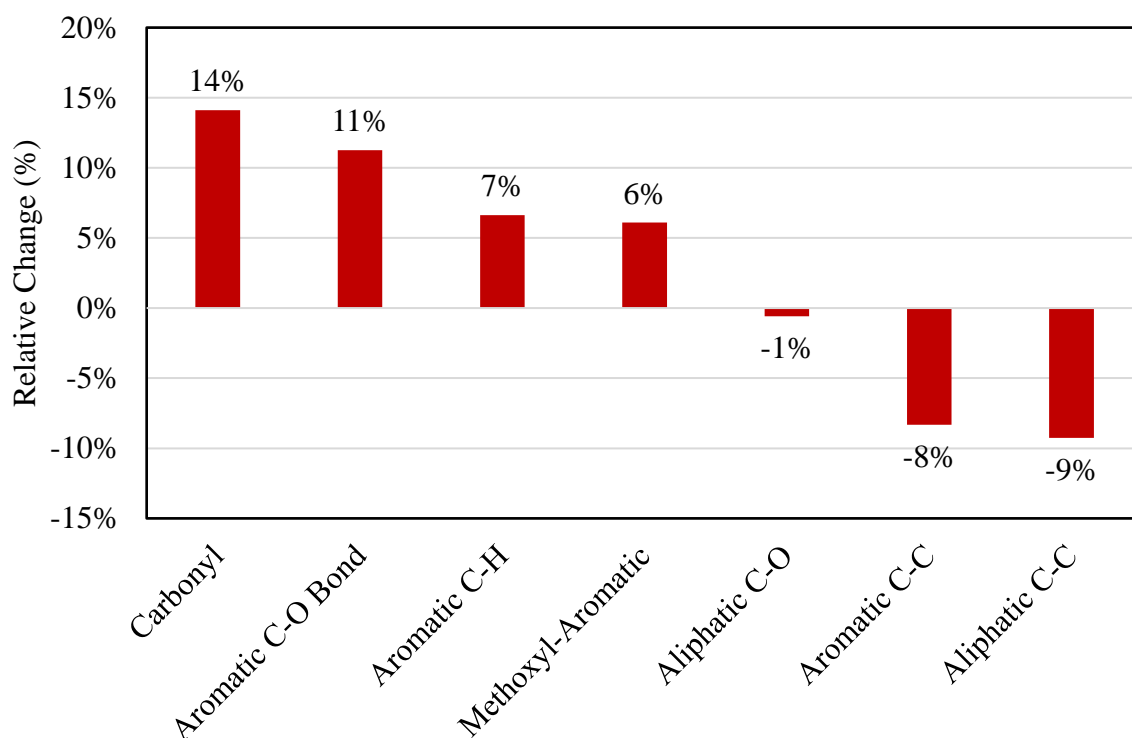


Fig. 3.  $^{13}\text{C}$  NMR results indicated carbonyls and aromatic C-O bonds had the largest relative increase comparing non-oxidative to oxidative conditions. This increase in aromatic carbonyl bonds is the result of partial oxidation reactions.

The two largest increases in carbon bonds were associated with aromatic carbonyls (14%) and aromatic C-O (11%). Conversely, aromatic C-C (8%) and aliphatic C-C (9%) decreased under oxidative conditions. As previously described, oxidation increased aromatic carbonyls. However, the other changes in functionality are not readily apparent. Hydrogenation of phenolic oil has been shown to decrease the quantity of methoxyl and carbonyls, while increasing



aliphatic C-C bonds [3]. Thus, an oxidative environment would be expected to do the opposite on the phenolic oligomers.

These results provide clear evidence that loss of hydroxyl groups arose from phenolic compounds being partially oxidized to aromatic carbonyl groups [25,26,44]. On the other hand, there is little evidence for increased phenolic carboxylic acid functionality, as typically occurs during oxidation of phenolic compounds.  $^{31}\text{P}$  NMR was unable to detect other aromatic carbonyl compounds (aldehydes and ketones) that are often associated with oxidation. Analysis with  $^{13}\text{C}$  NMR was used to (semi) quantify aromatic carbonyls, measuring their increase under oxidative conditions. This suggests that pyrolysis at an equivalence ratio of 10% and short vapor residence times can advance the oxidation of alcohols but not the oxidation of aldehydes. However, the possibility that carboxylic acids form under oxidative conditions cannot be completely dismissed since previous studies indicate they might further react with alcohols forming oligomers [49,50]. In the following section, pyrolysis of model phenolic monomers are used to further elucidate the kinds of reactions that occur under oxidation conditions.

### **Influence of oxygen functionality on polymerization of model compounds**

The NMR analysis on phenolic oligomers produced from pyrolysis of red oak indicates functional changes occurred in the presence of oxygen. Specifically, aromatic hydroxyl groups decreased and carbonyl groups increased, which are strong evidence of partial oxidation of phenolic compounds formed during lignocellulose pyrolysis. We hypothesize that these oxygenated phenolic compounds influence secondary reactions of pyrolysis, which was explored through micropyrolysis experiments on model phenolic compounds representative of phenolic monomers that might form under partial oxidative pyrolysis conditions (4-hydroxybenzyl alcohol, 4-hydroxybenzaldehyde, 4-hydroxybenzoic acid). 4-ethyl phenol was not employed as previous results indicate it is unreactive at pyrolysis conditions [17].

The first micropyrolysis experiments with model compounds condensed vapor products of multiple trials in a stainless steel U-shaped tube that was immersed in liquid nitrogen. The GPC spectra of the condensed liquid from these experiments is illustrated in Fig. 4. The peaks corresponding to the phenolic alcohol, aldehyde, and acid monomers occur approximately at 225 Da, 190 Da, and 240 Da, respectively. Despite the short residence times and rapid quenching achieved, there is clear evidence of condensation of some of the model compounds. The phenolic alcohol and acid indicate condensation to dimers and, for the alcohol, even trimers were formed. On the other hand, the phenolic aldehyde, which is between the alcohol and acid in its extent of oxidation, showed little evidence of condensation.

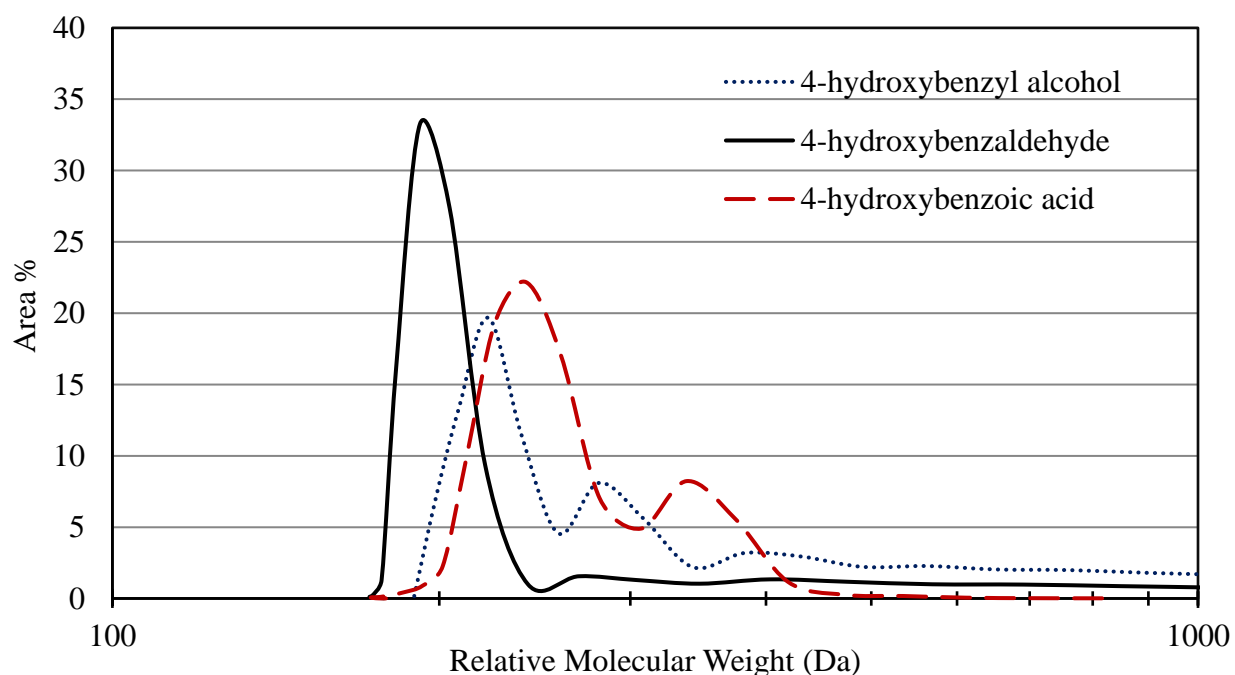


Fig. 4. GPC spectra for products of pyrolysis at 500°C for three model phenolic compounds. Phenolic dimers were detected as products from 4-hydroxybenzyl alcohol and 4-hydroxybenzoic acid indicating gas-phase condensation reactions. (UV-VIS 280nm)

The lack of condensation for the 4-hydroxybenzaldehyde is likely due to the radical intermediate being stabilized through the aldehyde group acting as an H-donor, stabilizing the

radical intermediate [51]. Accordingly, if phenolic compounds only oxidize to aldehydes, partial oxidative pyrolysis might discourage condensation of phenolic monomers to oligomers.

However, if the aldehyde was further oxidized, the resulting 4-hydroxybenzoic acid would readily polymerize. This suggests oxidation could both encourage and discourage polymerization of phenolic compounds, depending upon the extent of oxidation.

### **Effect of oxygen functionality on phenolic oligomer bonds**

In the next set of experiments, the micropyrolyzer was directly connected to a GC-MS/FID with each phenolic monomer separately pyrolyzed at 500°C. Gas residence time in the heated zone of the pyrolyzer was calculated at approximately one second.

Examining the mass spectrometry (MS) chromatographs suggest different reactivities among the three compounds. The chromatograph of the 4-hydroxybenzyl alcohol (Fig. 5) reveals multiple monomers and dimers as products. The monomeric products formed through various decomposition pathways of the starting phenolic compound. The formation of phenol was likely the result of cleavage of the aliphatic alcohol, leaving behind aromatic-OH (phenol). In a similar manner, dehydrogenation of aliphatic alcohol could yield benzaldehyde [52]. Finally, the formation of methyl phenolic compounds resulted from dehydration of the aliphatic alcohol. Dimethyl phenol likely formed from cleavage of the aliphatic alcohol, which then underwent dehydration and subsequent alkylation.

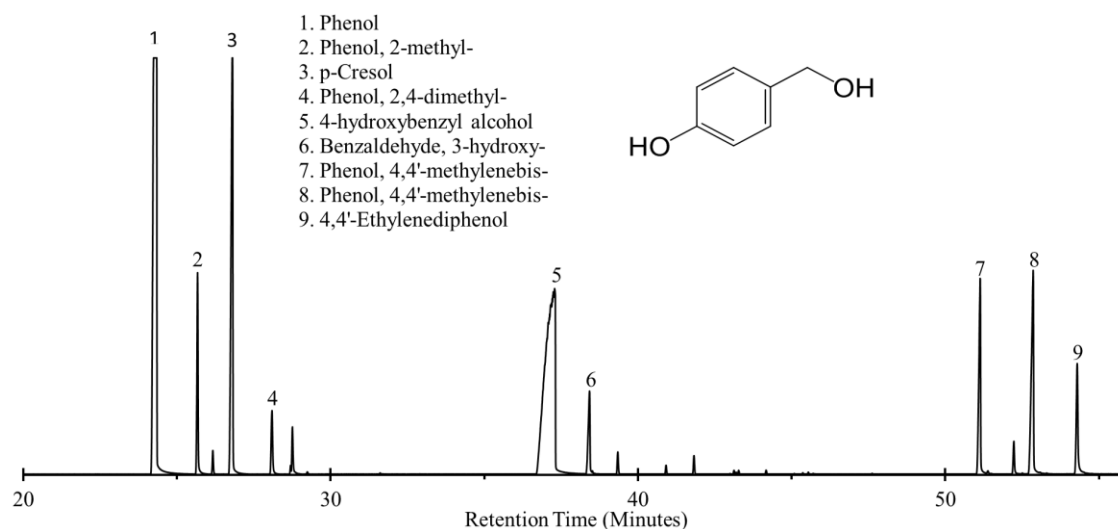


Fig. 5. Pyrolysis-GC/MS chromatograph of 4-hydroxybenzyl alcohol pyrolyzed at 500°C. Significant decomposition products were produced by the cleavage of the aliphatic alcohol.

On the other hand, 4-hydroxybenzaldehyde and 4-hydroxybenzoic acid were relatively stable, with phenol as the only monomeric product. The result for the 4-hydroxybenzaldehyde is consistent with the previous micropyrolysis experiments, indicating limited reactivity at these conditions. As illustrated in Fig. 7, 4-hydroxybenzoic acid also produced dimers (compounds detected above 50 minutes retention time), indicating condensation and polymerization of the phenolic carboxylic acid.

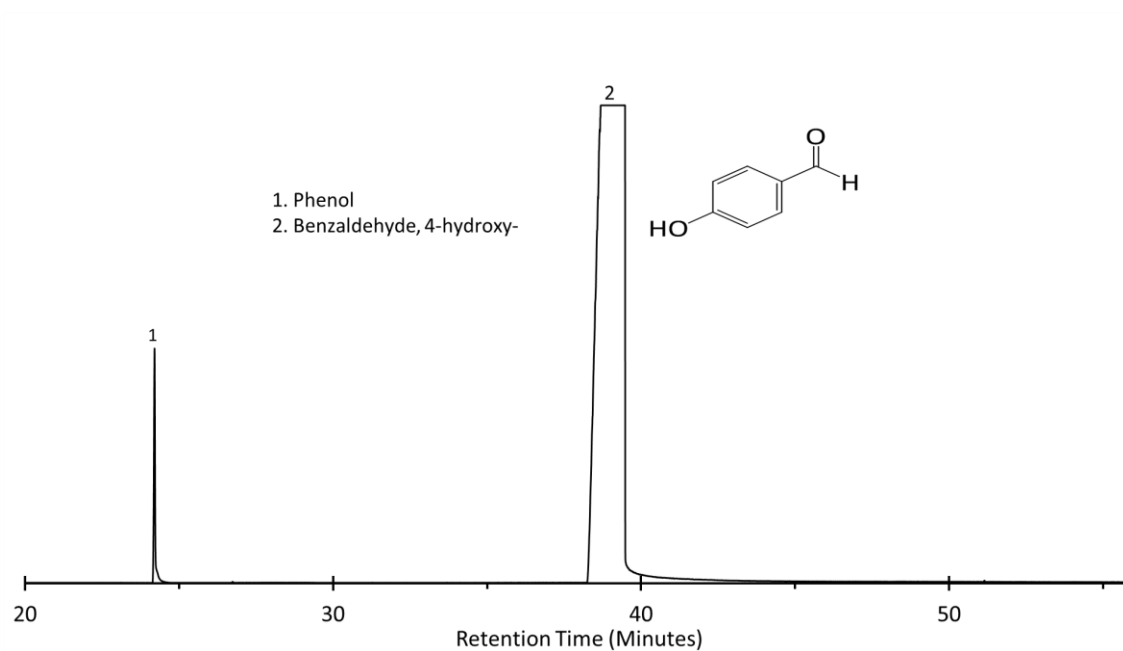


Fig. 6. Pyrolysis-GC/MS chromatograph of 4-hydroxybenzaldehyde pyrolyzed at 500°C. Chromatograph of 4-hydroxybenzaldehyde indicates that it is unreactive at these conditions.

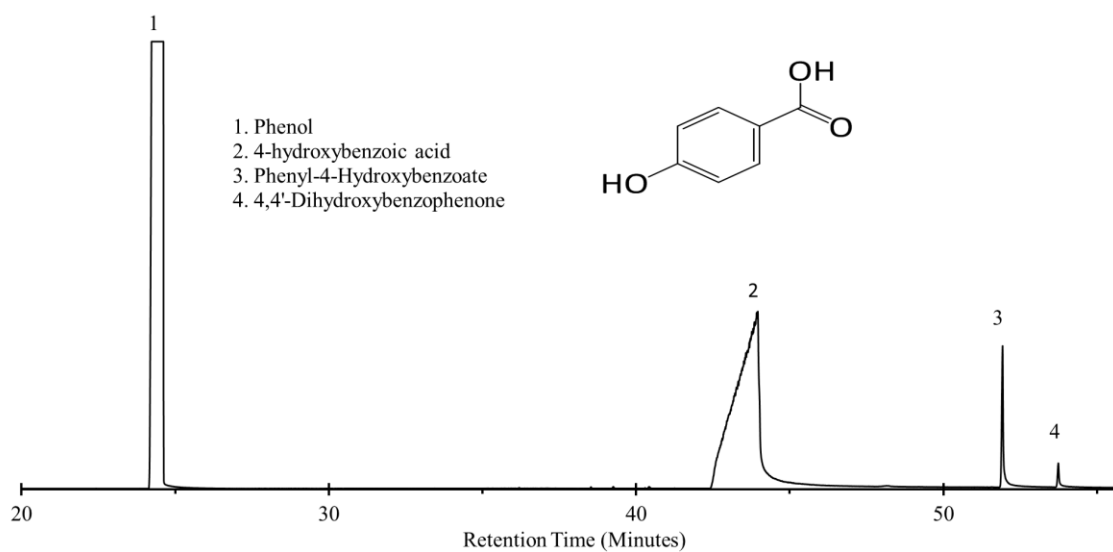


Fig. 7. Pyrolysis-GC/MS chromatograph of 4-hydroxybenzoic acid pyrolyzed at 500°C. Phenol was the only decomposition product detected under these conditions.

Fig. 8 summarizes the dimers produced from the phenolic alcohol and carboxylic acid, which provides insight into the role of oxidation in promoting polymerization of phenolic

monomers. In particular, the dimers formed by 4-hydroxybenzyl alcohol contain aromatic and aliphatic C-C bonds. While a detailed pathway is not fully elucidated, the carbon bonds formed for the 4,4'-methylene bisphenol and 4,4'-ethylene diphenol were likely the result of radical polymerization. These reactions, and the overall reactivity of the aliphatic –OH group, has been noted in computational and experimental studies on reactions of p-coumaryl alcohol [53]. The oligomer products detected for 4-hydroxybenzoic acid indicate aromatic carbonyl and C-O bonds were the most prevalent bonds of the dimers. The formation of the aromatic ester linkage (i.e. the aromatic C-O bond) is not surprising as that particular condensation reaction has been used to polymerize 4-hydroxybenzoic acid [49,50].

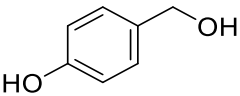
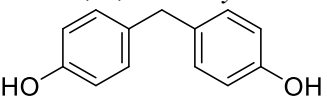
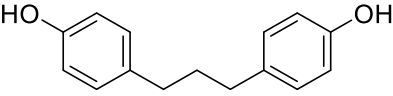
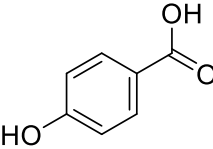
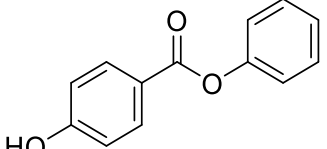
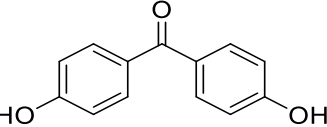
Initial Compound	Identified Phenolic Oligomer
<p><i>4-hydroxybenzyl alcohol</i></p> 	<p><i>Phenol, 4,4'-methylenebis</i></p>  <p>Carbon Bond: Aromatic C-C</p>
	<p><i>4,4'-Ethylenediphenol</i></p>  <p>Carbon Bond: Aliphatic C-C</p>
<p><i>4-hydroxybenzoic acid</i></p> 	<p><i>Phenyl-4-hydroxybenzoate</i></p>  <p>Carbon Bonds: Aromatic C-O; Aromatic Carbonyl</p>
	<p><i>4,4'-dihydroxybenzophenone</i></p>  <p>Carbon Bond: Aromatic Carbonyl</p>

Fig. 8. Identified phenolic dimers formed during micropyrolysis of 4-hydroxybenzoic acid and 4-hydroxybenzyl alcohol.

The formation of these dimers is consistent with the previous NMR analyses. Hydroxyl groups present in the gas phase during non-oxidative pyrolysis are thought to undergo condensation/ polymerization reactions resulting in a high concentration of C-C bonds. However, oxidation of hydroxyl groups to aromatic carbonyls would result in fewer hydroxyl groups available for condensation to oligomers. The diminishing amount of aromatic and aliphatic C-C bonds under oxidative conditions (as measured by  $^{13}\text{C}$  NMR) is strong evidence that oxidative pyrolysis reduces the formation pathway of these oligomers. Likewise,  $^{13}\text{C}$  NMR analysis indicates an increase in aromatic C-O bonds under oxidative conditions. The additional formation of aromatic C-O bonds could be the result of hydroxyl groups first oxidizing to carboxylic acids, then subsequently polymerizing in reactions with  $-\text{OH}$  groups. This condensation reaction would produce an oligomer with both an aromatic C-O bond (in particular an aromatic ether) and aromatic carbonyl, as occurs for phenyl-4-hydroxybenzoate formed from the 4-hydroxybenzoic acid. Again, condensation of 4-hydroxybenzoic acid has been studied as a pathway for production of polymers, supporting this hypothesis [49,50]. Thus, oxidation of phenolic compounds to produce aromatic carboxylic acids followed by polymerization is consistent with the increase of aromatic C-O bonds and carbonyl bonds.

The model compound study offers insight into the role of oxygen functionality and the formation of phenolic oligomers. The results suggest a tradeoff between production of functional groups that discourage polymerization (i.e., aldehydes) and those that encourage polymerization (i.e., acids). Although other functional groups (e.g. vinyl, methyl, etc.) likely play roles in polymerization of phenolic compounds during pyrolysis, these results offer evidence that oxidation influences formation of phenolic oligomers.

## Conclusions

This study found that autothermal pyrolysis of red oak only marginally influenced the chemical composition of the lignin-derived phenolic fraction of bio-oil. Ultimate analysis determined that carbon, hydrogen, and oxygen were not significantly changed under oxidative conditions. Likewise, GPC analysis of phenolic oligomers from autothermal pyrolysis showed little change in molecular weight compared to conventional pyrolysis. However,  $^{31}\text{P}$  NMR analysis revealed a loss in hydroxyl groups while  $^{13}\text{C}$  NMR analysis showed an increase in carbonyl functionality. Taken together, these results indicate phenolic compounds were partially oxidized during autothermal pyrolysis. Pyrolysis of model compounds representative of phenolic alcohols, aldehydes and acids indicate that oxygen functionality can impact polymerization reactions. Moderate levels of oxidation, as might occur at the low equivalence ratios of autothermal pyrolysis, can both discourage and encourage polymerization depending on the degree of oxidation. These results indicate that autothermal operation only marginally changes the chemical composition of the phenolic compounds found in bio-oil.

## Acknowledgements

This paper is based upon work supported by the Department of Energy under Award Number EE0008326. It was prepared as an account of work sponsored by an agency of the United States Government. Neither the United States Government nor any agency thereof, nor any of their employees, makes any warranty, express or implied, or assumes any legal liability or responsibility for the accuracy, completeness, or usefulness of any information, apparatus, product, or process disclosed, or represents that its use would not infringe privately owned rights. Reference herein to any specific commercial product, process, or service by trade name, trademark, manufacturer, or otherwise does not necessarily constitute or imply its endorsement,



recommendation, or favoring by the United States Government or any agency thereof. The views and opinions of authors expressed herein do not necessarily state or reflect those of the United States Government or any agency thereof.

The authors would also like to thank Patrick Johnston, Sean Rollag, and Ryan Smith of the Bioeconomy Institute for insightful discussions.

### References

- [1] R.C. Brown, T.R. Brown, *Biorenewable Resources: Engineering New Products from Agriculture: Second Edition*, John Wiley & Sons, Inc., Hoboken, NJ, USA, 2014. <https://doi.org/10.1002/9781118524985>.
- [2] R.C. Brown, *Thermochemical Processing of Biomass: Conversion into Fuels, Chemicals and Power*, John Wiley & Sons, Ltd, Chichester, UK, 2011. <https://doi.org/10.1002/9781119990840>.
- [3] D.J. McClelland, A.H. Motagamwala, Y. Li, M.R. Rover, A.M. Wittrig, C. Wu, J.S. Buchanan, R.C. Brown, J. Ralph, J.A. Dumesic, G.W. Huber, Functionality and molecular weight distribution of red oak lignin before and after pyrolysis and hydrogenation, *Green Chem.* 19 (2017) 1378–1389. <https://doi.org/10.1039/C6GC03515A>.
- [4] A.J. Yanez, P. Natarajan, W. Li, R. Mabon, L.J. Broadbelt, Coupled Structural and Kinetic Model of Lignin Fast Pyrolysis, *Energy and Fuels*. 32 (2018) 1822–1830. <https://doi.org/10.1021/acs.energyfuels.7b03311>.
- [5] J.P. Polin, C.A. Peterson, L.E. Whitmer, R.G. Smith, R.C. Brown, Process intensification of biomass fast pyrolysis through autothermal operation of a fluidized bed reactor, *Appl. Energy*. 249 (2019) 276–285. <https://doi.org/10.1016/J.APENERGY.2019.04.154>.
- [6] J.P. Polin, H.D. Carr, L.E. Whitmer, R.G. Smith, R.C. Brown, Conventional and autothermal pyrolysis of corn stover: Overcoming the processing challenges of high-ash agricultural residues, *J. Anal. Appl. Pyrolysis*. 143 (2019) 104679. <https://doi.org/10.1016/j.jaap.2019.104679>.
- [7] W. Tsang, R.F. Hampson, Chemical Kinetic Data Base for Combustion Chemistry. Part I. Methane and Related Compounds, *J. Phys. Chem. Ref. Data*. 15 (1986) 1087–1279. <https://doi.org/10.1063/1.555759>.
- [8] N.M. Marinov, A detailed chemical kinetic model for high temperature ethanol oxidation, *Int. J. Chem. Kinet.* 31 (1999) 183–220. [https://doi.org/10.1002/\(SICI\)1097-4601\(1999\)31:3<183::AID-KIN3>3.0.CO;2-X](https://doi.org/10.1002/(SICI)1097-4601(1999)31:3<183::AID-KIN3>3.0.CO;2-X).

- [9] Y.S. Choi, P.A. Johnston, R.C. Brown, B.H. Shanks, K.H. Lee, Detailed characterization of red oak-derived pyrolysis oil: Integrated use of GC, HPLC, IC, GPC and Karl-Fischer, *J. Anal. Appl. Pyrolysis*. 110 (2014) 147–154. <https://doi.org/10.1016/j.jaap.2014.08.016>.
- [10] D.E. Dugaard, R.C. Brown, The transport phase of pyrolytic oil exiting a fluidized bed reactor, *Sci. Therm. Chem. Biomass Convers.* (2006) 1189–1202.
- [11] J.M. Piskorz, P.D. Radlein, Pyrolysis of Biomass–Aerosol Generation: Properties, Applications and Significance for Process Engineers, in: R.P.C. Overend, E. Chornet (Eds.), *Biomass A Growth Oppor. Green Energy Value-Added Prod. Vol. 2*, Elsevier Science, Oxford, UK, 1999: pp. 1153–1159.
- [12] P.S. Marathe, R.J.M. Westerhof, S.R.A. Kersten, Fast pyrolysis of lignins with different molecular weight: Experiments and modelling, *Appl. Energy*. 236 (2019) 1125–1137. <https://doi.org/10.1016/J.APENERGY.2018.12.058>.
- [13] J. Montoya, B. Pecha, F.C. Janna, M. Garcia-Perez, Micro-explosion of liquid intermediates during the fast pyrolysis of sucrose and organosolv lignin, *J. Anal. Appl. Pyrolysis*. 122 (2016) 106–121. <https://doi.org/10.1016/j.jaap.2016.10.010>.
- [14] A.R. Teixeira, K.G. Mooney, J.S. Kruger, C.L. Williams, W.J. Suszynski, L.D. Schmidt, D.P. Schmidt, P.J. Dauenhauer, Aerosol generation by reactive boiling ejection of molten cellulose, *Energy Environ. Sci.* 4 (2011) 4306. <https://doi.org/10.1039/c1ee01876k>.
- [15] J.A. Tiarks, C.E. Dedic, T.R. Meyer, R.C. Brown, J.B. Michael, Visualization of physicochemical phenomena during biomass pyrolysis in an optically accessible reactor, *J. Anal. Appl. Pyrolysis*. (2019) 104667. <https://doi.org/10.1016/J.JAAP.2019.104667>.
- [16] P.R. Patwardhan, R.C. Brown, B.H. Shanks, Understanding the fast pyrolysis of lignin, *ChemSusChem*. 4 (2011) 1629–1636. <https://doi.org/10.1002/cssc.201100133>.
- [17] X. Bai, K.H. Kim, R.C. Brown, E. Dalluge, C. Hutchinson, Y.J. Lee, D. Dalluge, Formation of phenolic oligomers during fast pyrolysis of lignin, *Fuel*. 128 (2014) 170–179. <https://doi.org/10.1016/j.fuel.2014.03.013>.
- [18] V.A. Bhanu, K. Kishore, Role of oxygen in polymerization reactions, *Chem. Rev.* 91 (1991) 99–117. <https://doi.org/10.1021/cr00002a001>.
- [19] D. Meier, O. Faix, State of the art of applied fast pyrolysis of lignocellulosic materials — a review, *Bioresour. Technol.* 68 (1999) 71–77. [https://doi.org/10.1016/S0960-8524\(98\)00086-8](https://doi.org/10.1016/S0960-8524(98)00086-8).
- [20] R. Ma, M. Guo, X. Zhang, Chapter 6: Oxidative Valorization of Lignin, in: *RSC Energy Environ. Ser.*, 2018: pp. 128–158. <https://doi.org/10.1039/9781788010351-00128>.

- [21] P.C. Rodrigues Pinto, E.A. Borges da Silva, A.E. Rodrigues, Lignin as Source of Fine Chemicals: Vanillin and Syringaldehyde, in: *Biomass Convers.*, Springer Berlin Heidelberg, Berlin, Heidelberg, 2012: pp. 381–420. [https://doi.org/10.1007/978-3-642-28418-2\\_12](https://doi.org/10.1007/978-3-642-28418-2_12).
- [22] J.D.P. Araújo, C.A. Grande, A.E. Rodrigues, Vanillin production from lignin oxidation in a batch reactor, *Chem. Eng. Res. Des.* 88 (2010) 1024–1032. <https://doi.org/10.1016/j.cherd.2010.01.021>.
- [23] M. Fache, B. Boutevin, S. Caillol, Vanillin Production from Lignin and Its Use as a Renewable Chemical, *ACS Sustain. Chem. Eng.* 4 (2016) 35–46. <https://doi.org/10.1021/acssuschemeng.5b01344>.
- [24] W. Deng, H. Zhang, X. Wu, R. Li, Q. Zhang, Y. Wang, Oxidative conversion of lignin and lignin model compounds catalyzed by CeO<sub>2</sub>-supported Pd nanoparticles, *Green Chem.* 17 (2015) 5009–5018. <https://doi.org/10.1039/c5gc01473e>.
- [25] J.C. Villar, A. Caperos, F. García-Ochoa, Oxidation of hardwood kraft-lignin to phenolic derivatives with oxygen as oxidant, *Wood Sci. Technol.* 35 (2001) 245–255. <https://doi.org/10.1007/s002260100089>.
- [26] F. Asgari, D.S. Argyropoulos, Fundamentals of oxygen delignification. Part II. Functional group formation/elimination in residual kraft lignin, *Can. J. Chem.* 76 (1998) 1606–1615. <https://doi.org/10.1139/cjc-76-11-1606>.
- [27] J. Luo, P. Melissa, W. Zhao, Z. Wang, Y. Zhu, Selective Lignin Oxidation towards Vanillin in Phenol Media, *ChemistrySelect.* 1 (2016) 4596–4601. <https://doi.org/10.1002/slct.201600758>.
- [28] W. Schutyser, J.S. Kruger, A.M. Robinson, R. Katahira, D.G. Brandner, N.S. Cleveland, A. Mittal, D.J. Peterson, R. Meilan, Y. Román-Leshkov, G.T. Beckham, Revisiting alkaline aerobic lignin oxidation, *Green Chem.* 20 (2018) 3828–3844. <https://doi.org/10.1039/c8gc00502h>.
- [29] A.G. Demesa, A. Laari, I. Turunen, M. Sillanpää, Alkaline Partial Wet Oxidation of Lignin for the Production of Carboxylic Acids, *Chem. Eng. Technol.* 38 (2015) 2270–2278. <https://doi.org/10.1002/ceat.201400660>.
- [30] A. Azarpira, J. Ralph, F. Lu, Catalytic Alkaline Oxidation of Lignin and its Model Compounds: a Pathway to Aromatic Biochemicals, *BioEnergy Res.* 7 (2014) 78–86. <https://doi.org/10.1007/s12155-013-9348-x>.
- [31] K.H. Kim, R.C. Brown, X. Bai, Partial oxidative pyrolysis of acid infused red oak using a fluidized bed reactor to produce sugar rich bio-oil, *Fuel.* 130 (2014) 135–141. <https://doi.org/10.1016/j.fuel.2014.04.044>.

- [32] K.H. Kim, X. Bai, M. Rover, R.C. Brown, The effect of low-concentration oxygen in sweep gas during pyrolysis of red oak using a fluidized bed reactor, *Fuel*. 124 (2014) 49–56. <https://doi.org/10.1016/j.fuel.2014.01.086>.
- [33] S. Jiang, X. Hu, L. Wu, L. Zhang, S. Wang, T. Li, D. Xia, C.-Z. Li, Oxidative pyrolysis of mallee wood biomass, cellulose and lignin, *Fuel*. 217 (2018) 382–388. <https://doi.org/10.1016/J.FUEL.2017.12.075>.
- [34] D. Li, C. Briens, F. Berruti, Oxidative pyrolysis of kraft lignin in a bubbling fluidized bed reactor with air, *Biomass and Bioenergy*. 76 (2015) 96–107. <https://doi.org/10.1016/j.biombioe.2015.03.007>.
- [35] E.J. Roberts, S.E. Habas, L. Wang, D.A. Ruddy, E.A. White, F.G. Baddour, M.B. Griffin, J.A. Schaidle, N. Malmstadt, R.L. Brutchey, High-Throughput Continuous Flow Synthesis of Nickel Nanoparticles for the Catalytic Hydrodeoxygenation of Guaiacol, *ACS Sustain. Chem. Eng.* 5 (2017) 632–639. <https://doi.org/10.1021/acssuschemeng.6b02009>.
- [36] D. Carpenter, T. Westover, D. Howe, S. Deutch, A. Starace, R. Emerson, S. Hernandez, D. Santosa, C. Lukins, I. Kutnyakov, Catalytic hydroprocessing of fast pyrolysis oils: Impact of biomass feedstock on process efficiency, *Biomass and Bioenergy*. 96 (2017) 142–151. <https://doi.org/10.1016/j.biombioe.2016.09.012>.
- [37] B. Scholze, C. Hanser, D. Meier, Characterization of the water-insoluble fraction from fast pyrolysis liquids (pyrolytic lignin), *J. Anal. Appl. Pyrolysis*. 58–59 (2001) 387–400. [https://doi.org/10.1016/S0165-2370\(00\)00173-X](https://doi.org/10.1016/S0165-2370(00)00173-X).
- [38] R. Ma, Y. Xu, X. Zhang, Catalytic oxidation of biorefinery lignin to value-added chemicals to support sustainable biofuel production, *ChemSusChem*. 8 (2015) 24–51. <https://doi.org/10.1002/cssc.201402503>.
- [39] M.R. Rover, P.A. Johnston, L.E. Whitmer, R.G. Smith, R.C. Brown, The effect of pyrolysis temperature on recovery of bio-oil as distinctive stage fractions, *J. Anal. Appl. Pyrolysis*. 105 (2014) 262–268. <https://doi.org/10.1016/j.jaap.2013.11.012>.
- [40] D.L. Dalluge, L.E. Whitmer, J.P. Polin, Y.S. Choi, B.H. Shanks, R.C. Brown, Comparison of direct and indirect contact heat exchange to improve recovery of bio-oil, *Appl. Energy*. 251 (2019) 113346. <https://doi.org/10.1016/J.APENERGY.2019.113346>.
- [41] H. Ben, A.J. Ragauskas, NMR characterization of pyrolysis oils from kraft lignin, *Energy and Fuels*. 25 (2011) 2322–2332. <https://doi.org/10.1021/ef2001162>.
- [42] A. Granata, D.S. Argyropoulos, 2-Chloro-4,4,5,5-tetramethyl-1,3,2-dioxaphospholane, a Reagent for the Accurate Determination of the Uncondensed and Condensed Phenolic Moieties in Lignins, *J. Agric. Food Chem.* 43 (1995) 1538–1544. <https://doi.org/10.1021/jf00054a023>.

- [43] J.K. Lindstrom, J. Proano-Aviles, P.A. Johnston, C.A. Peterson, J.S. Stansell, R.C. Brown, Competing reactions limit levoglucosan yield during fast pyrolysis of cellulose, *Green Chem.* 21 (2019) 178–186. <https://doi.org/10.1039/C8GC03461C>.
- [44] L.G. Akim, J.L. Colodette, D.S. Argyropoulos, Factors limiting oxygen delignification of kraft pulp, *Can. J. Chem.* 79 (2001) 201–210. <https://doi.org/10.1139/cjc-79-2-201>.
- [45] S. Constant, A.E. Frissen, R. Boelens, H.L.J. Wienk, P. de Peinder, R.J.A. Gosselink, W.J.J. Huijgen, D.S. van Es, R.J.H. Grisel, P.C.A. Bruijninx, B.M. Weckhuysen, New insights into the structure and composition of technical lignins: a comparative characterisation study, *Green Chem.* 18 (2016) 2651–2665. <https://doi.org/10.1039/c5gc03043a>.
- [46] Anderson Guerra, Ilari Filpponen, A. Lucian A. Lucia, D.S. Argyropoulos, Comparative Evaluation of Three Lignin Isolation Protocols for Various Wood Species, (2006). <https://doi.org/10.1021/JF062433C>.
- [47] D. Li, F. Berruti, C. Briens, Autothermal fast pyrolysis of birch bark with partial oxidation in a fluidized bed reactor, *Fuel*. 121 (2014) 27–38. <https://doi.org/10.1016/j.fuel.2013.12.042>.
- [48] Y. Pu, S. Cao, A.J. Ragauskas, Application of quantitative  $^{31}\text{P}$  NMR in biomass lignin and biofuel precursors characterization, *Energy Environ. Sci.* 4 (2011) 3154–3166. <https://doi.org/10.1039/c1ee01201k>.
- [49] F. Higashi, T. Mashimo, Direct polycondensation of hydroxybenzoic acids with thionyl chloride in pyridine, *J. Polym. Sci. Part A Polym. Chem.* 24 (1986) 1697–1701. <https://doi.org/10.1002/pola.1986.080240726>.
- [50] K. Kimura, S. Kohama, Y. Yamashita, Novel Direct Polycondensation of 4-Hydroxybenzoic Acid by Means of Reaction-Induced Crystallization of Oligomers under Nonstoichiometric Condition, *Macromolecules*. 36 (2003) 5043–5046. <https://doi.org/10.1021/ma0258307>.
- [51] T. Hosoya, H. Kawamoto, S. Saka, Secondary reactions of lignin-derived primary tar components, *J. Anal. Appl. Pyrolysis*. 83 (2008) 78–87. <https://doi.org/10.1016/J.JAAP.2008.06.003>.
- [52] V. Srinivasan, N. Nagaraju, Catalytic decomposition of benzyl alcohol using copper aluminate, *J. Chem. Sci.* 107 (1995) 87–94. <https://doi.org/10.1007/BF02862977>.
- [53] R. Asatryan, H. Bennadji, J.W. Bozzelli, E. Ruckenstein, L. Khachatryan, Molecular Products and Fundamentally Based Reaction Pathways in the Gas-Phase Pyrolysis of the Lignin Model Compound p-Coumaryl Alcohol, *J. Phys. Chem. A*. 121 (2017) 3352–3371. <https://doi.org/10.1021/acs.jpca.7b01656>.

## CHAPTER 5. EFFECT OF TEMPERATURE ON PYROLYSIS OF FERROUS SULFATE PRETREATED CORN STOVER

Chad A. Peterson<sup>1</sup>, Sean S. Rollag<sup>2</sup>, Jake K. Lindstrom<sup>3</sup>, Robert C. Brown<sup>1,2,3</sup>

<sup>1</sup>*Department of Mechanical Engineering, Iowa State University, Ames, IA 50011, United States*

<sup>2</sup>*Department of Chemical and Biological Engineering, Iowa State University, Ames, IA, USA*

<sup>3</sup>*Bioeconomy Institute, Iowa State University, Ames, IA 50011, United States*

Modified from a manuscript in preparation for submission to Fuel Processing Technology

### Abstract

Corn stover is an important feedstock for second generation bio-refineries. However, its high ash content significantly reduces the yield of valuable anhydrosugars during fast pyrolysis. To passivate the high alkali and alkaline earth metal (AAEM) content, the use of ferrous sulfate as pre-treatment significantly improves sugar yield and reactor operability during fast pyrolysis. This novel pre-treatment combined with autothermal operation, in which the enthalpy for pyrolysis is internally generated through partial oxidation reactions, has the potential to greatly improve the prospects for production of cellulosic sugar from lignocellulosic biomass. The optimal temperature for conventional pyrolysis, which produces little sugar, is about 500°C. However, the temperature dependence of pyrolytic sugar production and degradation are not well known and the optimal temperature for maximum bio-oil and sugar yield may be different than for conventional pyrolysis. This study investigates the effect of temperature on pyrolysis products in the range of 400-550°C. Valuable bio-oil products, including sugars and phenolic oil, were found to be temperature dependent. Hydrolysable sugar reached a maximum yield of 15.6 wt.% at 450°C, whereas phenolic oil was maximized at 500°C with a yield of 9.2 wt.%. This indicates that an ideal reactor temperature should be between 450-500°C, with tradeoffs in

product selectivity with increasing temperature. As a result, this provides valuable information on processing conditions and will improve process scale-up.

## **Introduction**

Lignocellulosic biomass has received considerable attention as feedstock to produce advanced biofuels [1]. Fast pyrolysis, which is conventionally defined as the rapid decomposition of biomass in the absence of oxygen, has emerged as a promising approach, deconstructing plant biopolymers into bio-oil suitable for upgrading to transportation fuels [2]. The carbohydrate polymers (i.e. cellulose and hemicellulose) break down to monomeric sugars and light oxygenated compounds [3,4]. Lignin produces a wide range of phenolic monomers and oligomers, complicating efforts to understand its thermal deconstruction [5,6]. Bio-oil consists of hundreds of compounds including sugars, ketones, aldehydes, carboxylic acids, and phenolic compounds. Additional fast pyrolysis products include non-condensable gases (NCG) and biochar.

Conventional pyrolysis of lignocellulose yields very little sugar because alkali and alkaline earth metals (AAEM) in the biomass catalyze fragmentation of pyranose and furanose rings to light oxygenated molecules [7]. Extensive washing to remove these metals or pretreatment with acid impregnation to passivate their catalytic activity mitigates fragmentation of sugars [7,8]. Acid pretreatment of high ash feedstocks increases sugar yields as much as ten-fold. However, AAEM also appears to catalyze depolymerization of lignin in the biomass. Removal or passivation of AAEM has the unintended consequence of reducing the rate of lignin devolatilization compared to its rate of melting, which results in char agglomeration [9,10]. Char agglomeration reduces reactor throughput and may force reactor shutdown. Rollag et al. [11] discovered that pretreating biomass with ferrous sulfate both passivates AAEM by reacting with

the sulfate anion and promotes lignin depolymerization through the catalytic activity of the ferrous iron [12,13]. Pretreatment of biomass with ferrous sulfate produced pyrolytic sugar yields comparable to acid pretreatment while eliminating char agglomeration and reactor fouling characteristic of the acid pretreatment. In tests with corn stover, ferrous sulfate pretreatment dramatically shifted products from the aqueous phase (e.g. furans and acids) to more valuable anhydrosugars [11,14]. This dramatic increase in sugar yields and reactor operability offers the prospect of large-scale production of cellulosic sugar from lignocellulosic biomass.

Rollag et al. [11] conducted their pyrolysis experiments with ferrous sulfate pretreated biomass in both inert and low equivalence ratio (oxidative) environments. Traditionally, oxygen is excluded during fast pyrolysis under the assumption that bio-oil yield would be dramatically reduced [15]. However, recent studies at Iowa State have found that bio-oil yields were only slightly impacted upon admitting air at equivalence ratio of less than about 10% [14,16]. At these equivalence ratios, partial oxidation of pyrolysis products releases enough energy to provide the enthalpy for pyrolysis. Experiments indicate that much of the enthalpy for pyrolysis comes from oxidation of biochar, in total consuming less than 10% of the energy content of the biomass processed [14,16]. Consequently, autothermal pyrolysis offers additional processing benefits as auxiliary heat conveyance equipment is no longer necessary.

Although temperature is known to strongly impact the yield and distribution of pyrolysis products [17–19], its influence on pyrolysis yields under autothermal operation and with pretreated biomass has not been previously explored. Relevant temperature studies on pretreated biomass are scarce, likely from poor operability, as most research has focused on a single temperature (450-500°C) [8,10]. A single study from Oudenhoven et al.[21] did explore the effect of temperature on acid washed pinewood, finding sugar yield increased with temperature



from 23 wt.% to 29 wt.% at 360°C and 480°C, respectively. However, with additional increase in temperature, sugar yield decreased to less than 20 wt.% at 530 & 580°C. Notably, the study also conducted this temperature analysis on untreated pinewood finding sugar yield was not temperature dependent and was consistently between 4.5-6 wt.%, with no trend between temperature. This single study gives evidence that pretreatment makes select products (i.e. sugars) more temperature dependent than untreated feedstocks. In addition, given the autothermal (oxidative) operation of the current study, the effect of oxygen introduces another variable that is underexplored. The poor understanding of the underlying oxidation reactions during autothermal pyrolysis is evident as several attempts resulted in detrimental losses of valuable bio-oil [15,20]. Thus, by conducting autothermal pyrolysis at multiple temperatures, the underlying oxidation reactions should be apparent. As a result, exploring the effects of temperature on pretreated biomass coupled with autothermal processing will improve operability and scale-up efforts.

This work focuses on the characterization and product optimization of the fast pyrolysis products of iron-sulfate pretreated corn stover at four temperatures: 400, 450, 500, and 550°C. While studies optimizing bio-oil yield in the past have been conducted on the effect of temperature, the introduction of a novel pretreatment coupled with autothermal pyrolysis offers a new set of operating parameters. To analyze the products, numerous analytical techniques (e.g. GC/MS, HPLC, GPC, IC, etc.) were used to gain a better understanding of temperature effects. With the goal of maximizing valuable sugar and phenolic oil yield, this work will aid in future scale-up of pretreated biomass pyrolysis.

## Methods

### Biomass pretreatment

All experiments used Zea mays (corn stover) biomass collected using multi-pass harvesting [34]. The bales were initially ground using a hammer mill with a 3.2 mm screen, followed by additional processing with a knife mill through a 1.6 mm screen. The ferrous sulfate treatment was made by dissolving a known amount of sulfate into 1 kg of water. Then, with a syringe pump, this solution was continuously sprayed onto the biomass while mixing using an Erweka paddle mixer. The resulting solution spray and biomass mixing resulted in a 1:1 water to biomass ratio. Total ferrous sulfate loading was 7.5 wt. % (biomass basis), which was determined to fully passivate the AAEM content. After pretreatment, the samples were dried at 105°C until moisture content was below 10 wt. %.

Table 1 Corn stover compositional properties. All values reported as received.

<b>Proximate Analysis</b>	<b>wt. %</b>
Moisture	4.5
Volatiles	79.2
Fixed Carbon	12.6
Ash Content	8.3
<b>Ultimate Analysis</b>	<b>wt. %</b>
Carbon	40.7
Hydrogen	5.1
Sulfur	0.0
Nitrogen	0.5
Oxygen	-

### Continuous pyrolysis reactor and fractional recovery

A bubbling fluidized bed reactor, with a 3.8 cm diameter reactor and height of 40 cm was used for the pyrolysis experiments. The reactor was initially loaded with 600 grams of 600-1200 µm diameter silica sand. Biochar was recovered using two cyclones immediately following the reactor. After the cyclones, the hot bio-oil vapors entered a staged condenser train. Stage fraction

1 (SF1) is a shell-in tube condenser operated at 130°C. Stage fraction 2 (SF2) is a hot electrostatic precipitator operated at 120°C and 15 kV. These first two stage fractions are generally referred to as the bio-oil heavy ends, composed of anhydrosugars and phenolic compounds [22]. The vapors then enter an additional shell-in tube heat exchanger at 0°C (SF3), followed by an ESP operated at -15°C and 15 kV electric potential (SF4). The last two stage fractions are collectively called the bio-oil light ends, containing light organic compounds and the aqueous fraction. Quantification of the non-condensable gases (NCG) was performed using a micro-GC (Varian CP-4900) and a drum-type gas meter. The results from SF1 and SF2 are summarized into a collective bio-oil heavy ends. Likewise, SF3 and SF4 containing the aqueous fraction are collectively called the bio-oil light ends.

For each pyrolysis experiment, the reactor was fluidized with 20 standard liters per minute (SLPM) of nitrogen and air based on desired equivalence ratio. After initial reactor heating, biomass feed rate was started at 0.5 kg/hr for 20 minutes, then ramped to 1 kg/hr for a fifty minute steady state.

For autothermal operation, the air (oxygen) admitted into the reactor is intended to balance the endothermic pyrolysis reactions with exothermic oxidation reactions. To determine the quantity of air required, air is progressively introduced into the reactor until the reactor heater output reaches baseline parasitic levels [16]. For these experiments, the equivalence ratio is defined as the mass of air fed into the reactor over the amount needed for stoichiometric combustion, which was calculated as 0.10. This corresponded to a gas flow rate of 5.6 SLPM of air at a biomass feed rate of 1 kg/hr. The remaining sweep gas was balanced with 14.4 SLPM of nitrogen.

## **Product analysis**

### **Liquid-Liquid Extractions**

Phenolic compounds were recovered from the first two stage fractions (heavy ends) through liquid-liquid extractions. Samples were analyzed in duplicates. Five grams of bio-oil were mixed with equal mass of water in 50 mL centrifuge tubes. These were heated to 65°C for 20 minutes and subsequently vortexed for four minutes followed by centrifugation (Fischer Scientific accuSpin 1) at 3000 RPM for 20 minutes to achieve phase separation. The aqueous phase, containing water-soluble carbohydrates from the bio-oil heavy ends, was decanted and kept separate for HPLC and GFC analyses. Likewise, this first extraction mass is subsequently recorded. The remaining heavy organic phase, consisting of water-insoluble phenolic compounds, was again washed with equal mass of water, to remove any remaining water-soluble components. This water-soluble portion was decanted and again kept separate for HPLC and GFC analyses. The use of two consecutive water washes was previously determined to remove the non-phenolic compounds [23]. The remaining insoluble portion, consisting primarily of phenolic compounds, was dried in a vacuum oven at 40°C at a pressure of 6 in-Hg for 15 hours to drive off any residual moisture before subsequent chemical analysis. Any additional mass loss from vacuum drying was subsequently included in the second extract mass.

### **Gel permeation chromatography**

Gel permeation chromatography (GPC) analysis was performed using a Dionex Ultimate 3000 High Performance Liquid Chromatograph. Two types of columns, MesoPore (3 mm inner diameter, 300x7.5 mm; 200–25000 Da) and PLgel (3 mm inner diameter; 300x7.5 mm; 100–4000 Da), were used in series at 25°C with tetrahydrofuran (THF) as the mobile phase (flow rate: 1 mL min<sup>-1</sup>). Phenolic compounds extracted from the bio-oil using the liquid extractions (approximately 20 mg) were dissolved in 10 mL of THF. Then, the phenolic compounds

recovered from the SF1 and SF2 were combined and filtered through a 0.45  $\mu\text{m}$  polytetrafluoroethylene (PTFE) filter prior to GPC analysis. Measurements were performed using a diode array detector. The GPC columns were calibrated with twelve polystyrene standards in the molecular weight range of 162–38640 Da.

### **Ultimate Analysis**

Ultimate analysis was used to determine the carbon, hydrogen, sulfur, nitrogen, and oxygen (by difference) of the bio-oil stage fractions and bio-char. For each sample, 5 mg was weighed into tin capsules and placed into an Elementar Analyzer (vario MICRO cube). The instrument measured mass fractions of carbon, hydrogen, sulfur, and nitrogen in a sample, with oxygen content determined by difference for the bio-oil components. All samples were prepared in at least duplicates. Oxygen content was not calculated for the biochar consistent with high ash feedstocks [24].

### **Proximate Analysis**

The moisture, volatile, and total inorganic (ash) content of the biochar was determined using proximate analysis procedures in a TGA. Briefly, the moisture content was the mass loss of the biochar up to 105°C, with the volatile content defined as mass loss in an inert environment up to 900°C. Fixed carbon was determined as the mass loss after the introduction of air at 900°C. Ash content was the residual material after this inert and oxidative decomposition.

The ferrous sulfate treatment added additional mass to the biochar in the form of the sulfate salts and ferrous iron. Thus, the mass of sulfate salts was subtracted from the determined volatile content mass as they decompose to sulfur dioxide at temperatures exceeding 600°C [25]. Likewise, the mass of ferrous iron was subtracted from the ash content. These two data corrections allowed for the determined values to be presented on a biomass basis.

### **Sugar quantification**

Sugar yields were determined by acid hydrolysis for the different stage fractions. For the analysis, 60 mg of bio-oil was weighed into a vial followed by the addition of 6 ml of 400 mM sulfuric acid. The samples were hydrolyzed at 125°C for 44 minutes followed by rapid cooling to prevent any additional degradation reactions. Then, the samples were filtered using a 0.45  $\mu\text{m}$  microfiber filter into a 2 mL vial. The samples then underwent analysis and quantification using High-Performance Liquid Chromatography (Dionex Ultimate 3000 series HPLC) calculating glucose, xylose, and sorbitol yields [26]. Sugar analysis of bio-oil samples was performed in at least four replicates. Additional analysis, using the same procedure, was conducted on the liquid extracted product from bio-oil heavy ends. Given this homogenous liquid, only duplicates were performed.

### **Gas Chromatography**

Liquid bio-oil was analyzed using a 5975C GC/MSD coupled to an Agilent 7890 GC connected to a Polyarc® reactor (Activated Research Company) followed by an FID. The system was outfitted with Phenomenex DB-1701 fused silica capillary columns (60m x 0.25mm ID, 0.25  $\mu\text{m}$  film thickness). The GC injector operated isothermally at 280°C with a split ratio of 10, with a constant helium (99.999%) flow rate of 3 mL min<sup>-1</sup>. The temperature program for the oven started at 35°C with a 3-minute hold, then heated up to 280°C at 5°C min<sup>-1</sup> and held for 4 minutes. The MS operated with electron impact ionization operating at 280°C. Mass to charge ratio values (m/z) were recorded over a range of 35 - 650 m/z at a rate of 2 seconds per scan. Recorded peaks were identified using the 2008 NIST library. The tandem use of the PolyArc and FID allowed for direct quantification of identified compounds using an internal standard (phenanthrene).

Sample preparation called for 100 mg of bio-oil dissolved in 3 ml of methanol with 0.51 wt. % phenanthrene for the internal standard. After thorough mixing, the solution was injected on the instrument using an autosampler.

### **Karl Fisher**

The moisture content of the bio-oil was determined by Karl Fischer titration (Mettler Toledo V30S Compact Volumetric KF Titrator). For heavy ends analysis, ~70 mg of bio-oil was dissolved in 1 mL of dry methanol (Hydranal). Bio-oil light ends used 20mg of sample and were directly analyzed. Data was reported on a weight percentage basis. All samples were analyzed in duplicates.

### **Gel filtration chromatography**

Gel filtration chromatography (GFC) analysis was performed using a Dionex Ultimate 3000 High Performance Liquid Chromatograph. Identical to the GPC analyses, two types of columns, MesoPore (3 mm inner diameter, 300x7.5 mm; 200–25000 Da) and PLgel (3 mm inner diameter; 300x7.5 mm; 100–4000 Da), were used in series at 25°C with water as the mobile phase (flow rate: 1 mL min<sup>-1</sup>). For this, 10 mg of the extracted bio-oil heavy ends (section 2.3.1) was dissolved in 10 mL of water. The samples were filtered and analyzed using a diode array detector.

### **Ion Chromatography**

The Ion Chromatograph (IC) was a Dionex ICS3000 equipped with a conductivity detector and an Anion Micromembrane Suppressor AMMS-ICE 300. The suppressor regenerate used was 5mM tetrabutylammonia Hydroxide (TBAOH) at a flow rate of 3 ml/min. The eluent used was 1.0 mM heptafluorobutyric acid with IonPac® ICE-AS1 4x50 mm guard column and an IonPac® ICE-AS1 4x250 mm analytical column with a flow rate of 0.120 mL/min at 19°C. Organic acid standards were purchased from Inorganic Ventures. The standard contained acetate,

propionate, formate, and glycolate at ~200.0 mg/L each. A calibration curve was made by diluting the standard to five final concentration values: 10, 25, 67, 100, and 200 mg/L.

The SF3 bio-oil samples were prepared (100mg) using 36 mL deionized water and 1.5 mL of methanol. The SF4 bio-oil (100mg) had to be diluted with 48 mL deionized water and 1.5mL of methanol to fall within the calibration curve. All samples were filtered before IC analysis.

## **Results**

### **Influence of temperature on grouped pyrolysis products**

Mass closure for all runs was 90% on a biomass and oxygen basis. This denominator includes the mass of feedstock fed and the additional oxygen. The biochar yield has the mass of the pretreatment subtracted, as the ferrous sulfate will remain in the biomass (biochar) structure.

From Fig. 1, the yield of biochar decreased from 28.8 wt. % to only 14.0 wt. % as temperature increased from 400°C to 550°C. Likewise, as the temperature increased, the yield of NCG increased from 16.9 wt. % to 24.9 wt. %. This inverse relationship between NCG and biochar yield is from the biomass biopolymers being fully depolymerized. Given the recalcitrant structure of biomass, lignin biopolymers require elevated temperatures to fully depolymerize, as evident with lignin derived products increasing with temperature [21].



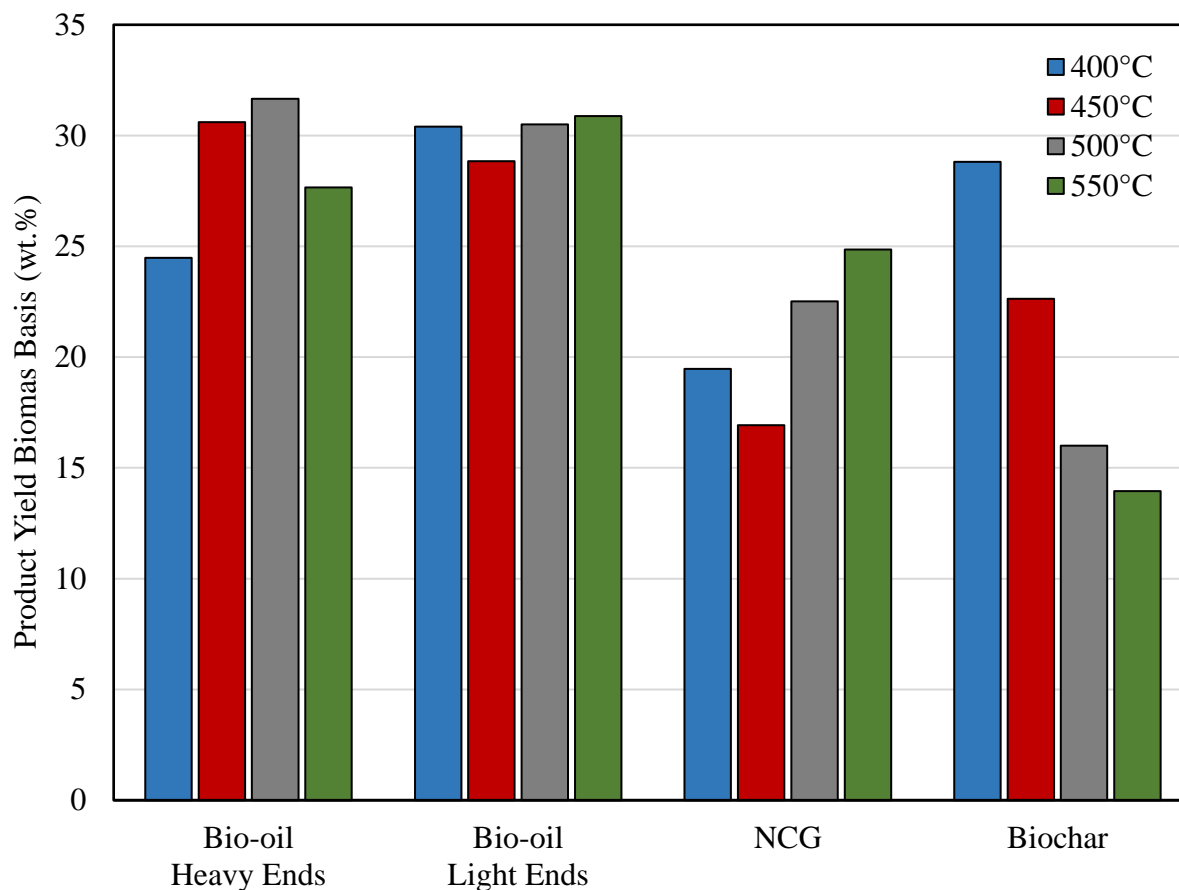


Fig. 1. Yield of pyrolysis products as a function of temperature. Biochar and NCG yield had an inverse relationship while total bio-oil yield reached a maximum at 500°C.

Total bio-oil yield ranged from 54.9 to 62.2 wt. %, with maximum yield occurring at 500°C. This was no surprise as maximum bio-oil production around 450-500°C is commonly reported for conventional (anoxic) pyrolysis [17,22,27]. At these intermediate temperatures, it is thought to balance the devolatilization of biomass while avoiding significant secondary cracking of bio-oil vapors to NCG. The yield of bio-oil light ends (SF3 & SF4) was relatively constant at 28.8-30.9 wt. % while heavy ends (SF1 & SF2) was more variable at 24.5-31.7 wt. %, with peak yield at 500°C. Given the importance of the bio-oil heavy ends, containing phenolic compounds and anhydrosugars, the variation in yield indicates these components are more temperature dependent than the bio-oil light ends (aqueous fraction).

From Table 2, the elemental composition of the bio-oil heavy ends was essentially unchanged with pyrolysis temperature. The carbon content slightly increased with temperature from 49.6 to 52.5 wt. %, with a corresponding decrease in oxygen, though this increase (3%) was minimal. Hence, this increase in carbon with the student t-test ( $\alpha=0.05$ ) was not found to be statistically significant. Trace amounts of sulfur were detected in the bio-oil heavy ends, suggesting that a small amount of biochar (containing ferrous sulfate) may have been carried from the cyclones to condensers. Overall, the elemental analysis indicates that despite yield changes (24.5-31.7 wt.%) the composition remains consistent.

Carbon content of the light ends increased slightly with temperature, from 18% to 21.4%. Interestingly, carbon content of the light ends was substantially lower at 450°C (14.6%) compared to the other temperatures. However, the large sample standard deviation makes the value not statistically significantly ( $\alpha=0.05$ ) from 400°C. Thus again, the elemental composition indicates minor differences in the bio-oil light ends.

Biochar carbon content decreased with temperature from 46.8 to 30.9 wt. % on a biochar basis. This indicates at elevated temperatures, the biomass is fully depolymerized, leaving behind only the non-volatile ash and residual fixed carbon. As previously mentioned, biochar data is presented as received, with oxygen content not accounted for, consistent with previous work of high ash biochars [24]. This as received analysis is necessary as the large inorganic content makes it difficult to calculate an accurate oxygen content without additional analytical techniques (e.g. X-ray fluorescence).

Of note, from the moisture balance most of the water (>90%) was collected in the bio-oil light ends. Given the operation of the condenser system, this is expected. Additional discussion of the moisture balance of the bio-oil light ends is discussed in a subsequent section.

Table 2 Elemental composition of bio-oil fractions and biochar. All weight percentages are presented on as received basis. Bracket value is the sample standard deviation.

Pyrolysis Component	Temperature (°C)	Yield (g/100g biomass)	Ultimate Analysis (wt. %)					KF Moisture (%)
			Carbon	Hydrogen	Sulfur	Nitrogen	Oxygen (difference)	
Heavy Ends	400	24.5	49.6 [0.6]	5.6 [0.1]	0.2 [0.1]	0.4 [0.1]	44.2 [0.8]	5.6 [0.3]
	450	30.6	49.6 [0.9]	5.5 [0.3]	0.0 [0.1]	0.6 [0.1]	44.2 [1.1]	4.2 [0.3]
	500	31.7	51.2 [0.4]	6.0 [0.2]	0.0 [0.1]	0.7 [0.1]	42.1 [0.4]	4.3 [0.3]
	550	27.7	52.6 [0.4]	5.7 [0.2]	0.3 [0.1]	0.7 [0.1]	40.8 [0.6]	4.2 [0.1]
Light Ends	400	30.4	18.0 [0.8]	5.6 [1.6]	0.1 [0.2]	0.4 [0.2]	75.9 [2.1]	62.1 [1.5]
	450	28.8	14.6 [3.5]	5.1 [2.7]	0.1 [0.1]	0.3 [0.2]	79.9 [6.0]	64.1 [0.5]
	500	30.5	21.0 [1.0]	6.3 [1.6]	0.0 [0.1]	0.3 [0.1]	72.4 [2.5]	57.0 [0.6]
	550	30.9	21.4 [1.0]	7.3 [0.4]	0.0 [0.1]	0.4 [0.1]	71.0 [1.6]	57.6 [0.4]
Biochar	400	28.8	46.8 [0.1]	2.5 [0.1]	7.9 [0.3]	1.0 [0.1]	-	-
	450	22.6	40.5 [0.5]	2.2 [0.3]	4.2 [1.2]	1.3 [0.2]	-	-
	500	16.0	35.0 [0.2]	2.0 [0.2]	3.7 [0.1]	1.0 [0.1]	-	-
	550	14.0	33.9 [0.6]	1.4 [0.1]	9.5 [0.3]	0.9 [0.1]	-	-

## Temperature effects on bio-oil heavy ends

### Water insoluble yield

With the large increase in sugar production, liquid extractions on the heavy ends fraction was performed to determine a subsequent aqueous fraction of anhydrosugars suitable for upgrading. Likewise, the raffinate would be a phenolic oil fraction suitable for upgrading to fuels. Given the low moisture content of the bio-oil heavy ends, less than 1.5 wt. % on a biomass basis, the extract yield is expected to be primarily water-soluble sugars.

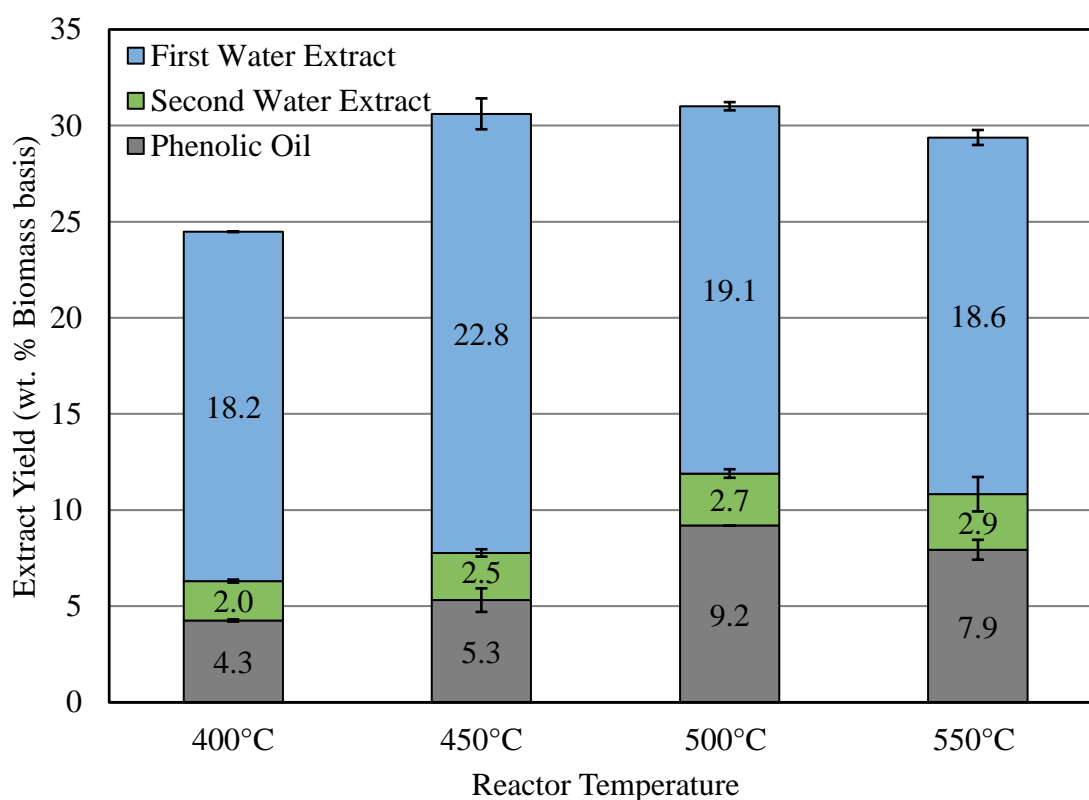


Fig. 2. Liquid extractions on bio-oil heavy ends indicate yield of phenolic oil increased with increasing temperature. Yield of the second water extract includes mass loss from the vacuum oven drying procedure. Error bars represent sample standard deviation from liquid-liquid extractions.

As shown in Fig. 2, yield of phenolic oil reached a maximum at 500°C. The increasing phenolic fraction is likely from increased depolymerization of lignin, though mostly to gas, at elevated temperatures [28]. Phenolic oil yield slightly decreased from 500°C to 550°C,

indicating that additional cracking of the phenolic vapors could have occurred. Zhou et al. [29] determined with fast pyrolysis of untreated pine, pyrolytic lignin yield (water insoluble fraction) reached a maximum at 530°C, then subsequently decreased at 580°C. The notion of phenolic oil cracking to produce additional NCG appears to occur based on the increased yield of NCG at 550°C. In a similar fashion, oxidation rates would be faster at elevated temperatures and phenolic compounds could have been oxidized producing carbon oxides and water.

The water-soluble fraction was measured to be much greater than the insoluble portion for the bio-oil heavy ends. This is not surprising as the ferrous sulfate pretreatment has now drastically increased the yield of water-soluble sugars present in the heavy ends [11]. Even accounting for water, water soluble yield is greater than 20 wt.% for all temperatures. The yield of this water soluble extract reached a maximum at 450°C (25.4 wt.%), with a subsequent decrease in yield as temperature increased. Analysis of this liquid extract is discussed in the following sections.

### **Effect of temperature on sugar yield**

It was hypothesized that enhanced sugar yields arising from ferrous sulfate pretreatment of biomass would lower the optimum temperature for sugar production, based on the expectation that the rate of secondary reactions that crack sugars would be reduced [30]. Furthermore, lower temperatures would reduce the rate that sugars oxidize under autothermal conditions compared to char oxidation. Biochar oxidation could have a significantly lower activation energy (from mass transfer effects) as compared to the oxidation of bio-oil vapors. Thus, even a small decrease in temperature would drastically lower than oxidation rate of bio-oil vapors while biochar oxidation would have a much smaller decrease.

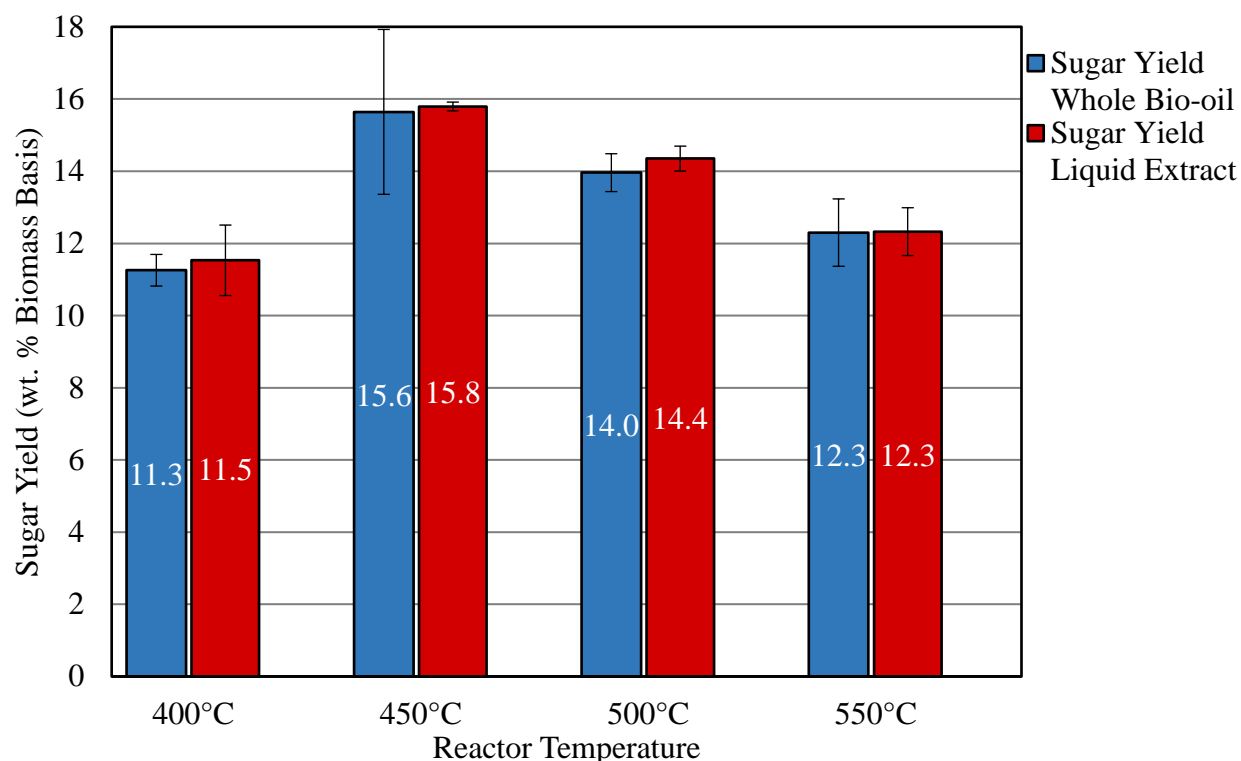


Fig. 3. Sugar yield as determined through HPLC analysis. Whole bio-oil represents direct quantification of sugar yield in bio-oil heavy ends. Liquid extract yield was based on sugar concentration and mass of liquid extractions. The agreement in yield between the two indicates sugars are readily extracted during the water wash. Error bars represent sample standard deviation.

Total hydrolysable sugar yield (Fig 3.) had a maximum yield at 450°C (15.6 wt.%), and a subsequent decrease in yield with reactor temperature. The decreasing sugar yield at temperatures hotter than 450°C is likely from gas phase degradation and oxidation of the sugar products. While performed under inert conditions, a similar trend was seen with Oudenhoven et al. [21], finding sugar yield was maximized at an intermediate temperature (480°C) and decreased at elevated temperatures (530 and 580°C). These results indicate at temperatures greater than 500°C, oxidation and decomposition reaction rates are fast enough to affect product yields despite short vapor residence times (<1 second). Conversely, the low yield at 400°C could be from the cellulose and hemicellulose biopolymers only partially depolymerizing, as the solid (biomass) residence time in the reactor was not sufficient to fully convert the biopolymers. Thus,

while 400°C would offer the slowest oxidation and decomposition rates of the temperature used here, the biomass particle may not properly devolatilize leaving behind unreacted material in the biomass (now biochar) structure [28,31]. In contrast, at elevated temperatures (500 and 550°C), the biopolymers were likely fully depolymerized and well ventilated, followed by cracking and oxidation in the gas phase reducing the overall yield.

In addition to the reported sugar yield from the bio-oil, the water-soluble liquid extract was hydrolyzed and analyzed on HPLC. Not surprisingly, the sugar yield for the liquid extract is nearly identical to the whole bio-oil analysis. Likewise, the standard deviation of these liquid samples was lower than that of whole bio-oil, indicating the homogenous liquid solution better represents the actual yield. With nearly identical yields between the two, this indicates near perfect liquid extraction of the sugars from whole bio-oil. As a result, this proves valuable anhydrosugars can be easily extracted from bio-oil for future upgrading [32].

#### **Molecular weight distribution of liquid extract**

From the previously determined sugar content, over 50% of the liquid extracted mass from the heavy ends is sugar. While this hydrolysable sugar content represents a significant mass portion, a substantial fraction is still unaccounted for. With the iron catalyst present in the biomass, radical polymerization reactions of pyrolysis products may be forming large anhydro-oligomers [33]. Likewise, water-soluble oligosaccharides (e.g. cellobiose or cellotriose) may be present in this liquid extract. Consequently, it was hypothesized with increasing temperature these oligosaccharides would diminish as elevated temperatures would crack these oligosaccharides to monomeric products.

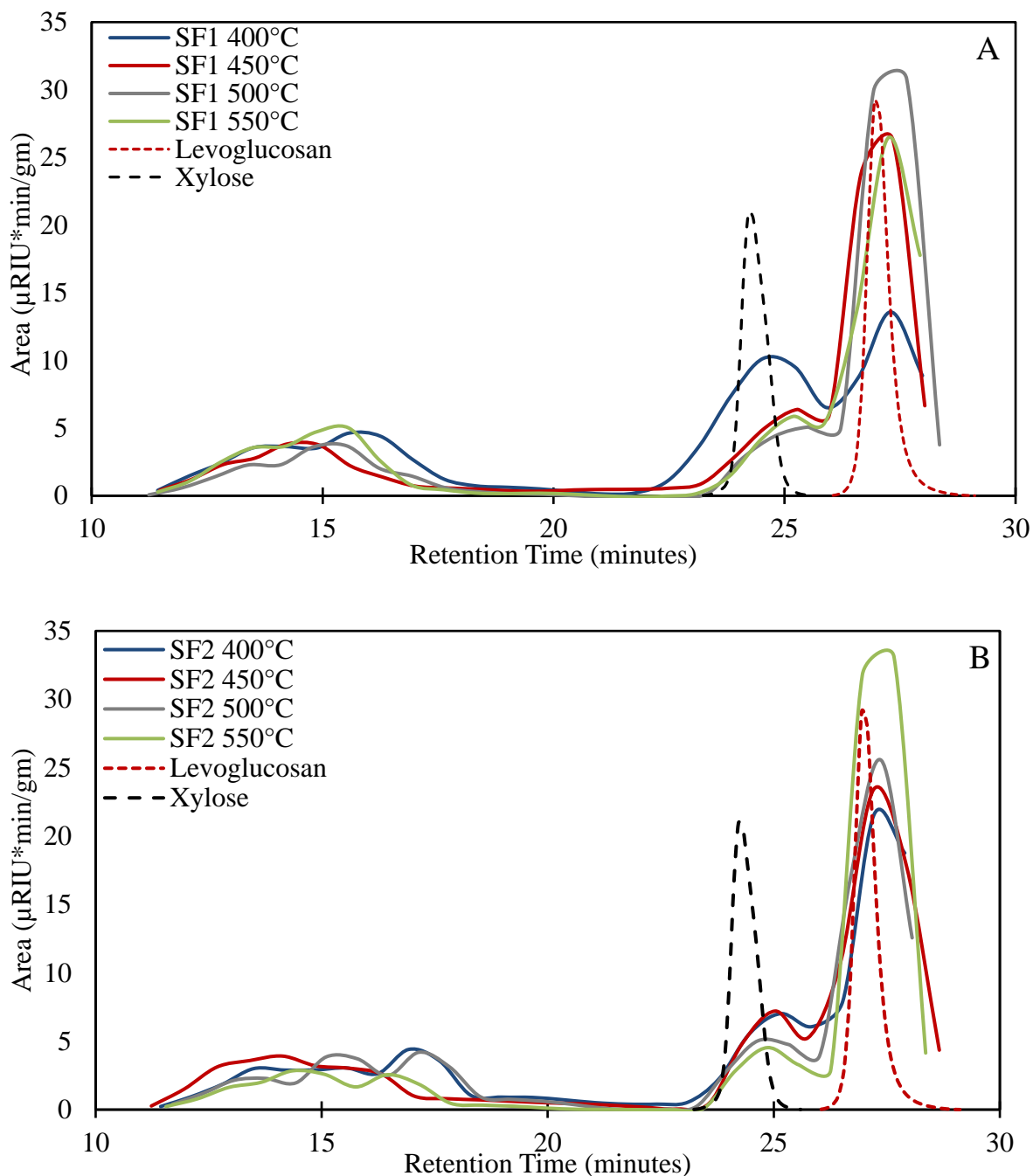


Fig. 4. GFC of liquid extract product from SF1 (A) and SF2 (B). At retention times lower than 20 minutes, large water-soluble oligomers were present at all four temperatures. The presence of these peaks indicates polymerization reactions could have occurred.

As depicted in Fig. 4, both SF1 and SF2 had large peaks present for levoglucosan (~27 minutes) and xylose (~24.5 minutes). Identification of these sugars was confirmed with HPLC analysis and from standards of xylose and levoglucosan ran on GFC. Below a retention time of



20 minutes, additional peaks were measured. Difficulties in identification complicates determining an accurate degree of polymerization or molecular weight; however, their presence indicates that radical polymerization of pyrolysis products may have occurred. Given there are no discernable trends or differences between stage fractions or temperature, these large molecular weight compounds do not appear temperature dependent. This would indicate that water soluble oligosaccharides are present, and reactor temperature does not affect their formation. Consequently, it is possible these form during the condensation of the hot pyrolytic vapors. While quantification was not possible with GFC, these peaks likely represent a significant mass portion of the liquid extract product.

### **Molecular weight distribution of phenolic oil**

With increasing temperature, secondary cracking reactions of the phenolic oligomers would reduce the molecular weight of products. In particular, cleavage of functional groups from the aromatic rings is expected, reducing the molecular weight [22].

The GPC chromatographs (Fig 5.) of the four temperatures are quite similar. There are likely phenolic monomers present, from the minor shoulder at 210 Da, and subsequent double peaks representative of phenolic oligomers at approximately 300 and 420 Da. With the chromatographs being nearly identical, temperature did not appear to change the polymerization/condensation reactions of the phenolic compounds in the pyrolyzer.

The number average ( $M_n$ ) and weight average ( $M_w$ ) was calculated for the phenolic oil samples and shown in Table 3. With increasing temperature, both the  $M_w$  and  $M_n$  decreased, while the polydispersity showed no discernible trend (1.74-1.61). The decrease in average molecular weight could be caused by additional functional groups (e.g. methoxy, methyl, hydroxyl) being cleaved off the aromatic rings, reducing the molecular weight. The notion of methoxy groups being lost is supported by Rover et al.[22], that determined with increasing

reactor temperature methoxy phenol yield decreased. The decrease in molecular weight with temperature is in contrast to the work of Zhou et al.[29], that determined with organosolv lignin molecular weight increased with pyrolysis temperature. However, given pyrolysis of technical lignin behaves much differently than whole biomass, with thermal ejection of phenolic oligomers readily occurring, experimental differences are to blame. Therefore, the slight decrease in molecular weight with temperature is best explained by the loss of phenolic functional groups.

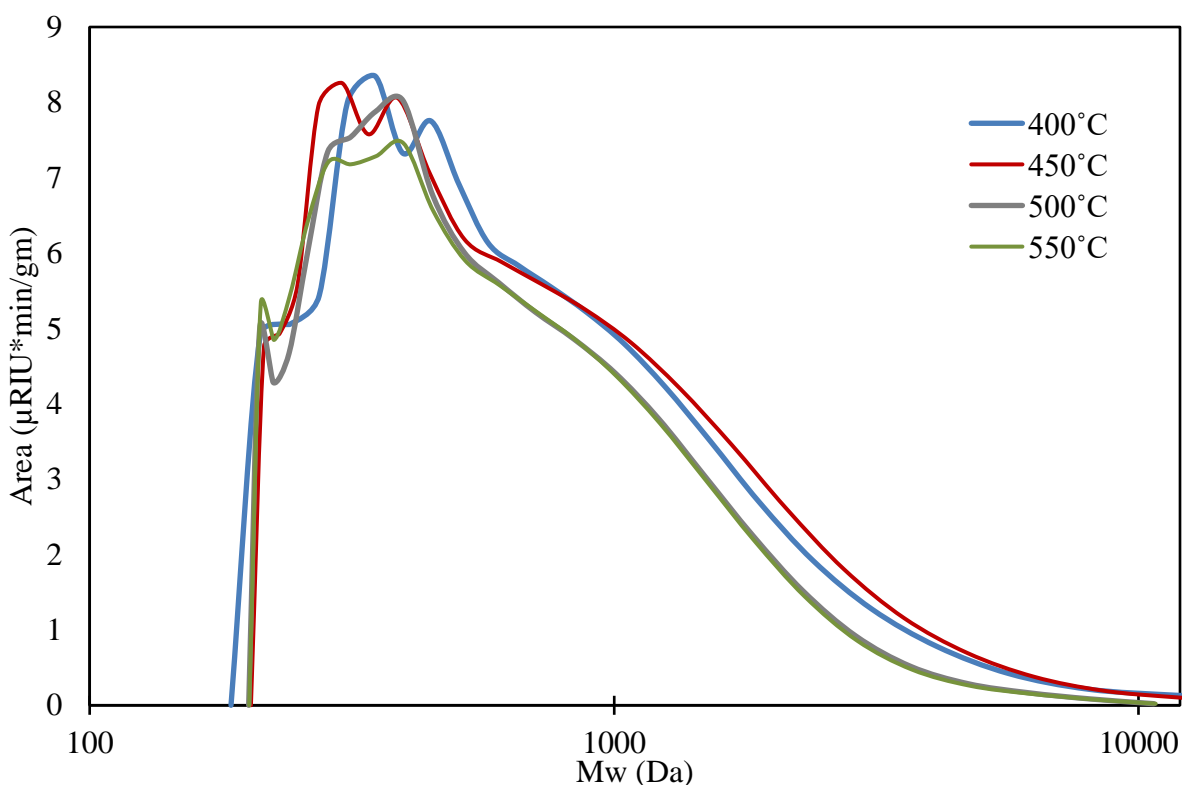


Fig. 5. Relative molecular weight of the phenolic oil showed minimal differences between temperatures.

Table 3 Molecular weight of the liquid extracted phenolic compounds decreased with increasing temperatures.

Temperature	Number Average Mn	Weight Average Mw	Polydispersity
400°C	434	715	1.66
450°C	405	704	1.74
500°C	388	622	1.61
550°C	382	612	1.61

### Temperature effect on bio-oil light ends

Bio-oil light ends were expected to contain carboxylic acids and other light oxygenated compounds. Given these components are typically derived from the hemicellulose fraction (e.g. acetyl groups produce acetic acid [4]) bio-oil light end composition was expected to be relatively consistent. This hypothesis assumes that hemicellulose is the least recalcitrant of the biopolymers [34], implying it would readily depolymerize at the temperatures used. While not as valuable as the sugars and phenolics collected in the heavy ends, there is still potential for future upgrading of the bio-oil light ends [35].

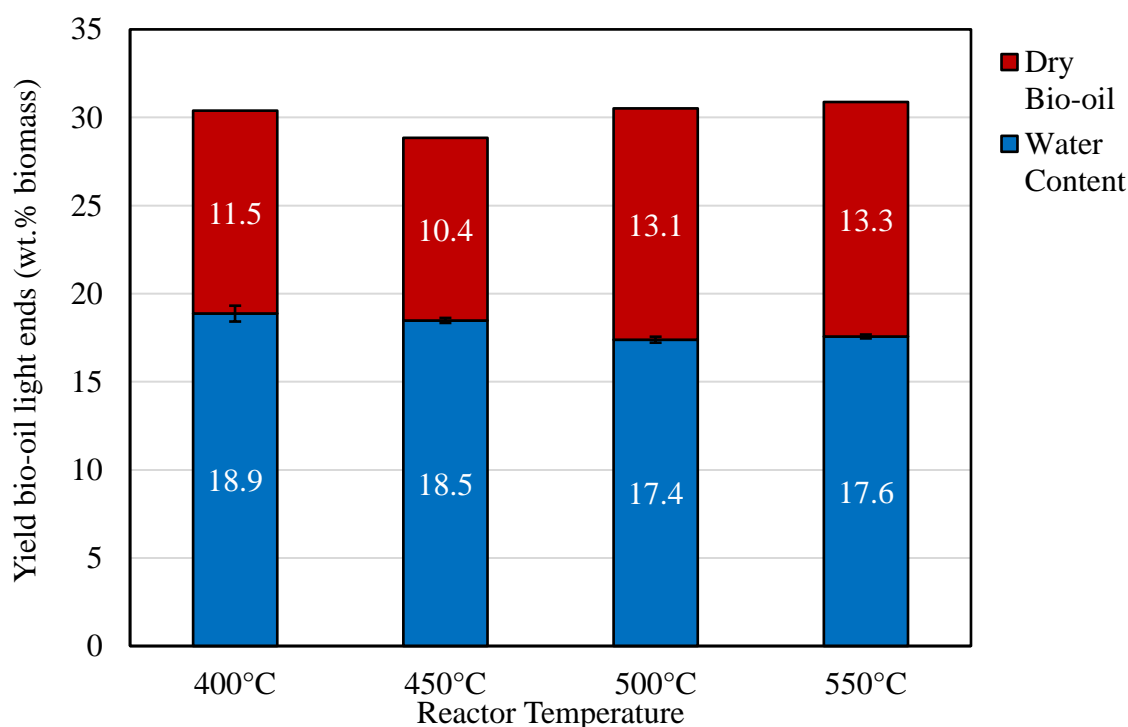


Fig. 6. Water content composed a significant fraction of the bio-oil light ends. Dry bio-oil content was calculated as the difference between water and total bio-oil yield. Error bars represent sample deviation from Karl Fisher analysis.

Given the fractional condenser system, nearly two thirds of the bio-oil light ends is water (Fig. 6). From this moisture balance, there appears to be a slight decrease in water content with increasing temperature. However, the difference was not statistically significant using the student

t-test ( $\alpha=0.05$ ). With the large presence of water, the dry bio-oil content was calculated by difference from the measured moisture content.

Ion Chromatography (IC) was used to quantify the yield of four carboxylic acids (Fig. 7). Total acid yield was 1.94-2.37 wt. %, representing ~20% (dry basis) of the bio-oil light end components. Of the four acids quantified, acetic acid comprised greater than 75% of the mass. Interestingly, while the yields were very consistent for three temperatures, 450°C had a much lower yield of acetic acid. Given acetic acid yield is mainly determined by the initial content of acetyl groups [36], this could indicate acetic acid was consumed through oxidation.

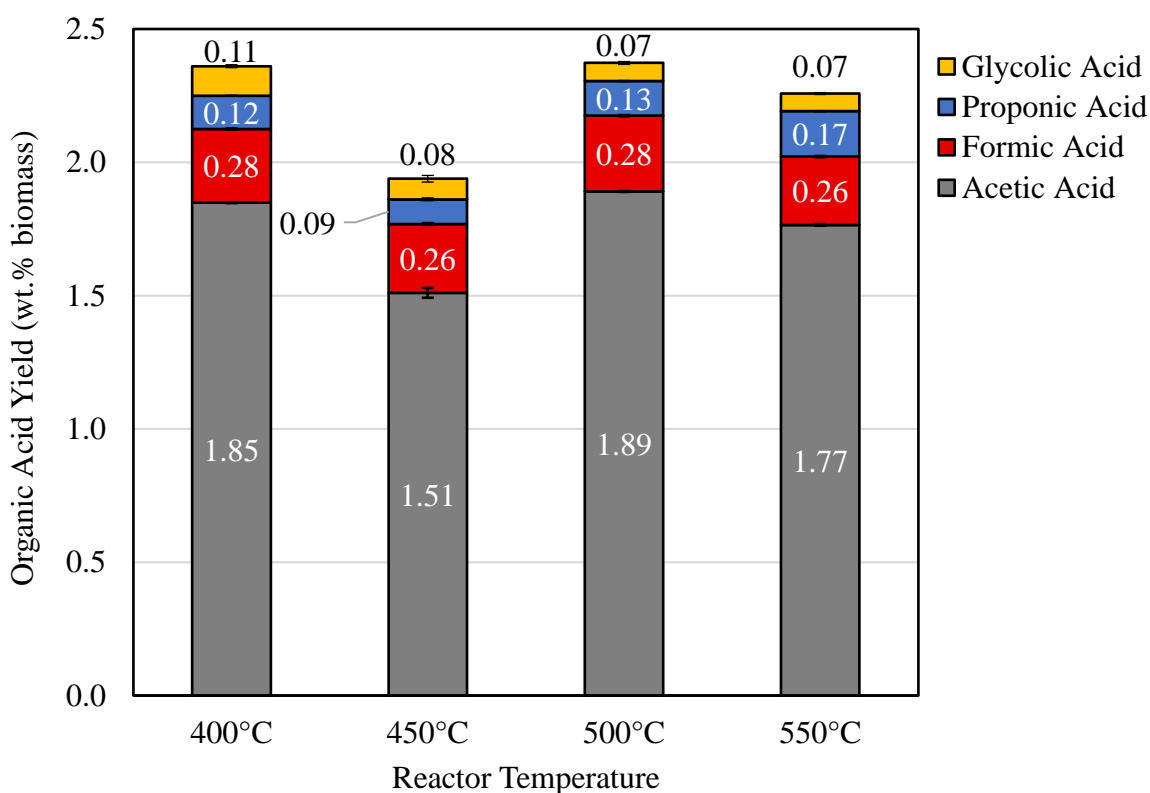


Fig. 7. Light organic acids were primarily composed of acetic acid. These four select carboxylic acids comprised 20% of the dry bio-oil light end components. Error bars represent sample standard deviation.

Partial analysis was also conducted on the bio-oil light ends using GC-MS/FID. Of note, given the inherent complexity of bio-oil, complete identification and quantification was not performed [37]. From the GC results (Fig. 8), yield of the select identified products was 0.82-

2.39 wt.%, with the minimum and maximum at 450°C and 550°C, respectively. With increasing temperature, it is expected that secondary cracking of sugar products would result in additional formation of light oxygenated compounds [30]. The significant increase in these products at 550°C indicates that sugar products are decomposing to produce these various light oxygenated compounds. This observation is consistent with the carbon content and dry bio-oil yield being the greatest at 550°C.

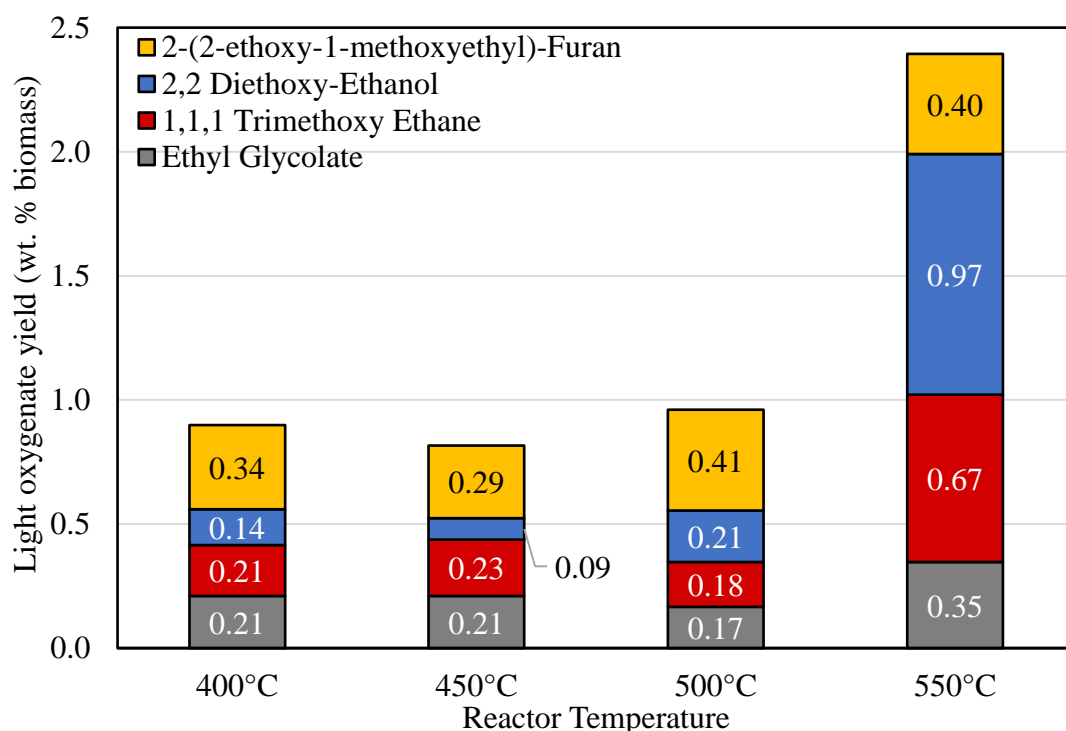


Fig. 8. Minor compositional analysis of bio-oil light ends from GC-MS/FID. The identified compounds represent the four most concentrated products in the bio-oil light ends.

### Comparison of pyrolysis co-products

#### Effect of pyrolysis temperature on biochar

With increasing reaction temperature, total biochar yield decreased from 28.8 to 14.0 wt. %. This decrease in temperature was from the biomass fully depolymerizing at elevated temperatures. From the proximate analysis (Fig. 9), there was a decrease in volatile matter from 9.1 wt.% to just 1.3 wt.% (biomass basis) as temperature increased. The decrease in volatile

matter is the result of the biopolymers fully devolatilizing with increasing temperature. A similar decrease was measured with the fixed carbon from 12.4 wt.% to 4.6 wt.% at 400 and 550°C, respectively. Given biomass fixed carbon content was measured as 12.6 wt.%, oxidation of the biochar was likely occurring. With the large decrease in fixed carbon, the upwards of 8 wt.%, this would indicate biochar oxidation is providing significant energy towards the enthalpy for pyrolysis. Overall, these results indicate with increasing temperature the biomass is fully devolatilized leaving behind only trace amounts of carbonaceous material and residual ash.

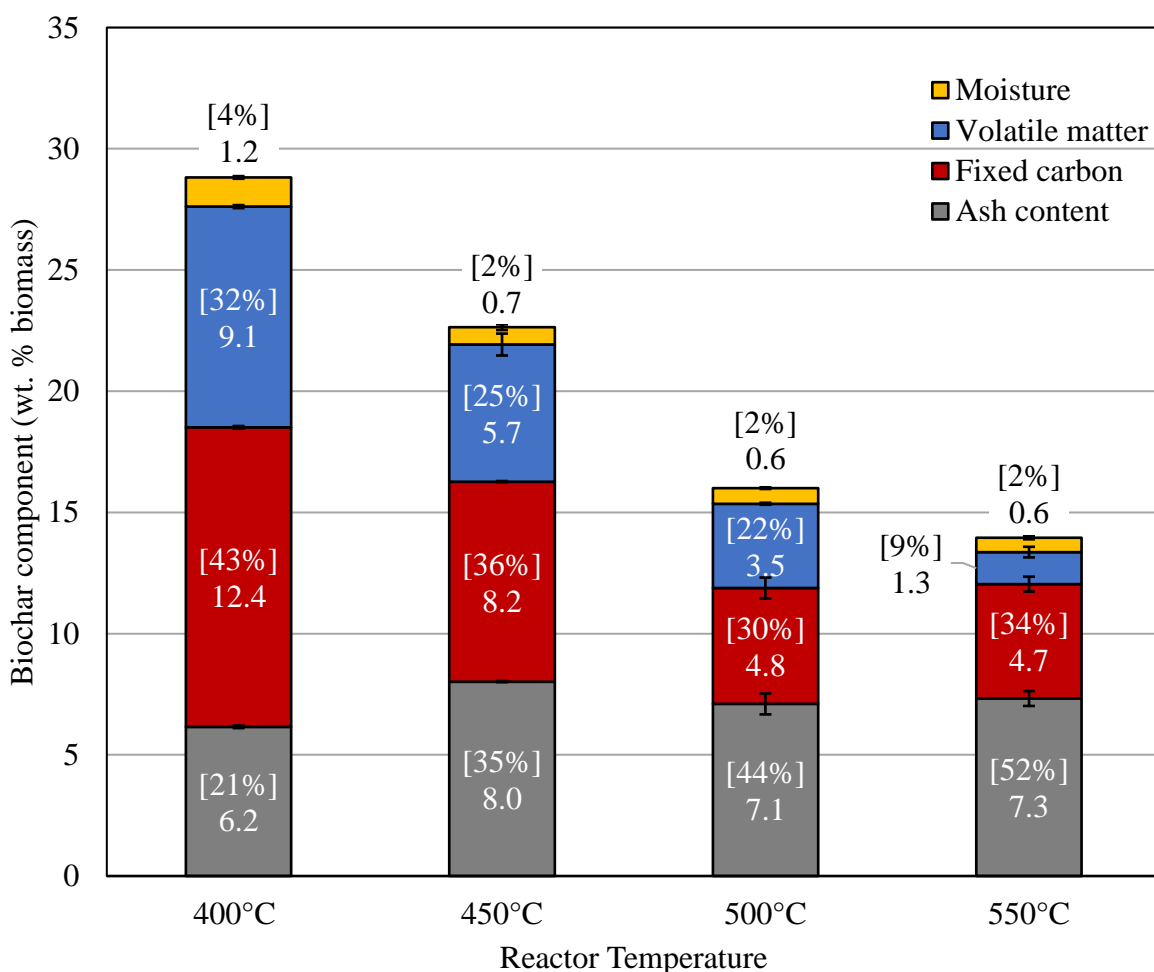


Fig. 9. Comparison of the proximate analysis of the biochar. The component mass is reported on a biomass basis and the bracket value indicates on a biochar basis. The mass of the ferrous sulfate treatment was accounted for. Error bars are sample standard deviation.

### **Comparison of non-condensable gases**

It was hypothesized with increasing temperature, the yield of NCG would increase as the secondary cracking rate of bio-oil vapors would be faster. This concept is commonly seen with untreated feedstocks finding NCG yield increases with reactor temperature [22].

From the measured NCG, it was not surprising the maximum yield was achieved at 550°C (24.9 wt. %). At these elevated temperatures, the biomass is fully devolatilized followed by additional secondary cracking of the pyrolytic bio-oil vapors producing NCG. While there was a general trend that NCG yield increased with temperature, gas yield decreased from 19.5 wt.% to 16.9 wt.% at 400°C and 450°C, respectively. The yield decrease contradicts the assumption that elevated temperatures, with faster decomposition rates, produce additional NCG from the degradation of bio-oil vapors. However, the use of a pretreatment, thus affecting pyrolysis products, may be responsible for this behavior. Oudenhoven et al.[21] pyrolyzed acid washed pine and had a similar decrease in gas yield from 16 wt.% to 14.1 wt.% at 430 and 480°C, respectively. With additional increase in temperature, the gas yield increased to 27.1 wt.% at 530°C [21]. This similar observation could indicate competing decomposition versus devolatilization reactions may be occurring in the solid biomass phase. As with the sugar yield, if bio-oil vapors cannot readily volatilize out of the biomass particle, decomposition reactions in the biomass particle could produce NCG.

From Fig. 10, the majority of gases measured were CO<sub>2</sub> and CO, accounting for greater than 96% of the gas yield. A small fraction of methane, ethylene, and ethane was measured, with total mass yield of only 0.4-0.8 wt. %, increasing with reactor temperature. This low yield of valuable flammable gases (ethane, ethylene, and methane) is similar to the yields (<1 wt.%) of untreated corn stover pyrolysis [14].

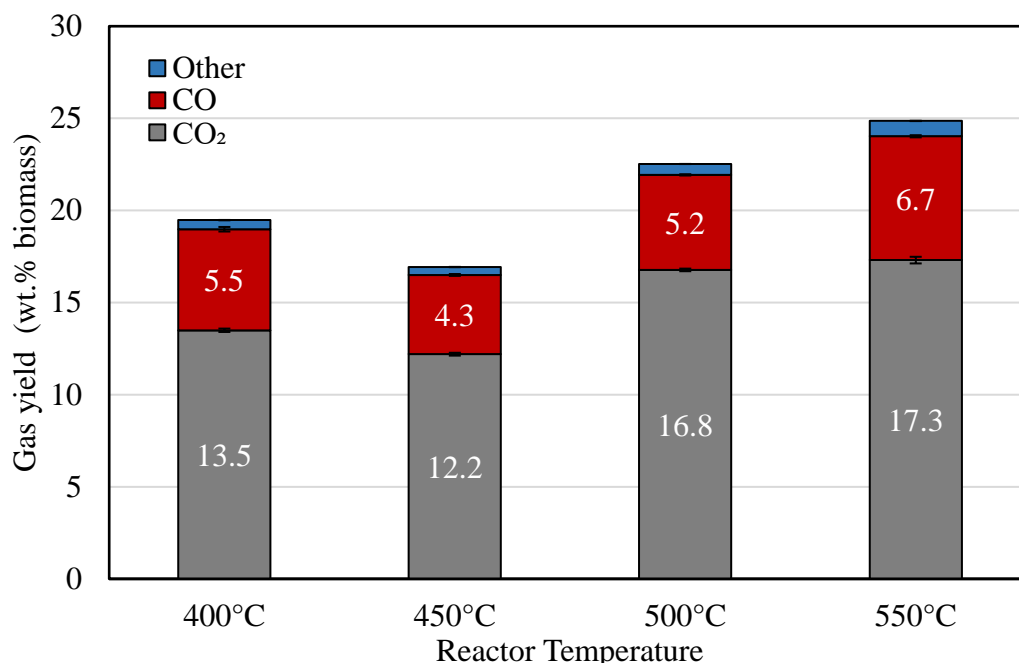


Fig. 10. Yield of non-condensable gases reached at maximum at the hottest temperature used. Other includes methane, ethylene, and ethane. Error bars are sample standard deviation from MicroGC gas measurements.

## Conclusions

Although temperature studies have been performed in the past, this work demonstrates that pretreated biomass coupled with autothermal processing offers a new set of operational parameters. By utilizing a ferrous sulfate treatment, substantial gains in sugar yields were observed as the native AAEM no longer catalytically cracked the pyranose sugars. Sugar yield reached a maximum at an intermediate temperature (450°C) and subsequently decreased as the oxidation and decomposition reaction rates increased with temperature. However, the yield of phenolic oil was maximized at 500°C, indicating a tradeoff between sugars and phenolic oil. This implies that a potential two stage processing, with primary pyrolysis at 450°C followed by additional devolatilization of the biochar at higher temperature (>550°C), could be beneficial for increasing the yield of bio-oil heavy ends. Nevertheless, these results provide valuable insight that the oxidation and decomposition reactions associated with autothermal pyrolysis are



temperature dependent. This work will aid directly in the scale-up of autothermal pyrolyzers and tailoring of pyrolysis products.

### **Acknowledgements**

This paper is based upon work supported by the Department of Energy under Award Number EE0008326. It was prepared as an account of work sponsored by an agency of the United States Government. Neither the United States Government nor any agency thereof, nor any of their employees, makes any warranty, express or implied, or assumes any legal liability or responsibility for the accuracy, completeness, or usefulness of any information, apparatus, product, or process disclosed, or represents that its use would not infringe privately owned rights. Reference herein to any specific commercial product, process, or service by trade name, trademark, manufacturer, or otherwise does not necessarily constitute or imply its endorsement, recommendation, or favoring by the United States Government or any agency thereof. The views and opinions of authors expressed herein do not necessarily state or reflect those of the United States Government or any agency thereof.

### **References**

- [1] R.C. Brown, T.R. Brown, *Biorenewable Resources: Engineering New Products from Agriculture: Second Edition*, John Wiley & Sons, Inc., Hoboken, NJ, USA, 2014. <https://doi.org/10.1002/9781118524985>.
- [2] R.C. Brown, *Thermochemical Processing of Biomass: Conversion into Fuels, Chemicals and Power*, John Wiley & Sons, Ltd, Chichester, UK, 2011. <https://doi.org/10.1002/9781119990840>.
- [3] J.K. Lindstrom, J. Proano-Aviles, P.A. Johnston, C.A. Peterson, J.S. Stansell, R.C. Brown, Competing reactions limit levoglucosan yield during fast pyrolysis of cellulose, *Green Chem.* 21 (2019) 178–186. <https://doi.org/10.1039/C8GC03461C>.

- [4] P.R. Patwardhan, R.C. Brown, B.H. Shanks, Product distribution from the fast pyrolysis of hemicellulose, *ChemSusChem*. 4 (2011) 636–643. <https://doi.org/10.1002/cssc.201000425>.
- [5] D.J. McClelland, A.H. Motagamwala, Y. Li, M.R. Rover, A.M. Wittrig, C. Wu, J.S. Buchanan, R.C. Brown, J. Ralph, J.A. Dumesic, G.W. Huber, Functionality and molecular weight distribution of red oak lignin before and after pyrolysis and hydrogenation, *Green Chem.* 19 (2017) 1378–1389. <https://doi.org/10.1039/C6GC03515A>.
- [6] A.J. Yanez, P. Natarajan, W. Li, R. Mabon, L.J. Broadbelt, Coupled Structural and Kinetic Model of Lignin Fast Pyrolysis, *Energy and Fuels*. 32 (2018) 1822–1830. <https://doi.org/10.1021/acs.energyfuels.7b03311>.
- [7] N. Kuzhiyil, D. Dalluge, X. Bai, K.H. Kim, R.C. Brown, Pyrolytic Sugars from Cellulosic Biomass, *ChemSusChem*. 5 (2012) 2228–2236. <https://doi.org/10.1002/cssc.201200341>.
- [8] B. Pecha, P. Arauzo, M. Garcia-Perez, Impact of combined acid washing and acid impregnation on the pyrolysis of Douglas fir wood, *J. Anal. Appl. Pyrolysis*. 114 (2015) 127–137. <https://doi.org/10.1016/J.JAAP.2015.05.014>.
- [9] D.L. Dalluge, T. Daugaard, P. Johnston, N. Kuzhiyil, M.M. Wright, R.C. Brown, Continuous production of sugars from pyrolysis of acid-infused lignocellulosic biomass, *Green Chem.* 16 (2014) 4144–4155. <https://doi.org/10.1039/c4gc00602j>.
- [10] K.H. Kim, R.C. Brown, X. Bai, Partial oxidative pyrolysis of acid infused red oak using a fluidized bed reactor to produce sugar rich bio-oil, *Fuel*. 130 (2014) 135–141. <https://doi.org/10.1016/j.fuel.2014.04.044>.
- [11] S.A. Rollag, J.K. Lindstrom, R.C. Brown, Pretreatments for the continuous production of pyrolytic sugar from lignocellulosic biomass, *Chem. Eng. J.* 385 (2020) 123889. <https://doi.org/10.1016/j.cej.2019.123889>.
- [12] J.A. Tiarks, C.E. Dedic, T.R. Meyer, R.C. Brown, J.B. Michael, Visualization of physicochemical phenomena during biomass pyrolysis in an optically accessible reactor, *J. Anal. Appl. Pyrolysis*. (2019) 104667. <https://doi.org/10.1016/J.JAAP.2019.104667>.
- [13] S. Zhou, R.C. Brown, X. Bai, The use of calcium hydroxide pretreatment to overcome agglomeration of technical lignin during fast pyrolysis, *Green Chem.* 17 (2015) 4748–4759. <https://doi.org/10.1039/c5gc01611h>.
- [14] J.P. Polin, H.D. Carr, L.E. Whitmer, R.G. Smith, R.C. Brown, Conventional and autothermal pyrolysis of corn stover: Overcoming the processing challenges of high-ash agricultural residues, *J. Anal. Appl. Pyrolysis*. 143 (2019) 104679. <https://doi.org/10.1016/j.jaap.2019.104679>.
- [15] D. Li, F. Berruti, C. Briens, Autothermal fast pyrolysis of birch bark with partial oxidation in a fluidized bed reactor, *Fuel*. 121 (2014) 27–38. <https://doi.org/10.1016/j.fuel.2013.12.042>.

- [16] J.P. Polin, C.A. Peterson, L.E. Whitmer, R.G. Smith, R.C. Brown, Process intensification of biomass fast pyrolysis through autothermal operation of a fluidized bed reactor, *Appl. Energy*. 249 (2019) 276–285. <https://doi.org/10.1016/J.APENERGY.2019.04.154>.
- [17] D. Mourant, C. Lievens, R. Gunawan, Y. Wang, X. Hu, L. Wu, S.S.A. Syed-Hassan, C.Z. Li, Effects of temperature on the yields and properties of bio-oil from the fast pyrolysis of mallee bark, *Fuel*. 108 (2013) 400–408. <https://doi.org/10.1016/j.fuel.2012.12.018>.
- [18] M. Garcia-Perez, X.S. Wang, J. Shen, M.J. Rhodes, F. Tian, W.J. Lee, H. Wu, C.Z. Li, Fast pyrolysis of oil mallee woody biomass: Effect of temperature on the yield and quality of pyrolysis products, *Ind. Eng. Chem. Res.* 47 (2008) 1846–1854. <https://doi.org/10.1021/ie071497p>.
- [19] M. Amutio, G. Lopez, M. Artetxe, G. Elordi, M. Olazar, J. Bilbao, Influence of temperature on biomass pyrolysis in a conical spouted bed reactor, *Resour. Conserv. Recycl.* 59 (2012) 23–31. <https://doi.org/10.1016/j.resconrec.2011.04.002>.
- [20] S. Zhao, Y. Luo, Y. Su, Y. Zhang, Y. Long, Experimental investigation of the oxidative pyrolysis mechanism of pinewood on a fixed-bed reactor, *Energy and Fuels*. 28 (2014) 5049–5056. <https://doi.org/10.1021/ef500612q>.
- [21] S.R.G. Oudenhoven, C. Lievens, R.J.M. Westerhof, S.R.A. Kersten, Effect of temperature on the fast pyrolysis of organic-acid leached pinewood; the potential of low temperature pyrolysis, *Biomass and Bioenergy*. 89 (2016) 78–90. <https://doi.org/10.1016/j.biombioe.2015.12.019>.
- [22] M.R. Rover, P.A. Johnston, L.E. Whitmer, R.G. Smith, R.C. Brown, The effect of pyrolysis temperature on recovery of bio-oil as distinctive stage fractions, *J. Anal. Appl. Pyrolysis*. 105 (2014) 262–268. <https://doi.org/10.1016/j.jaap.2013.11.012>.
- [23] M.R. Rover, P.A. Johnston, T. Jin, R.G. Smith, R.C. Brown, L. Jarboe, Production of Clean Pyrolytic Sugars for Fermentation, *ChemSusChem*. 7 (2014) 1662–1668. <https://doi.org/10.1002/cssc.201301259>.
- [24] C.E. Brewer, K. Schmidt-Rohr, J.A. Satrio, R.C. Brown, Characterization of biochar from fast pyrolysis and gasification systems, *Environ. Prog. Sustain. Energy*. 28 (2009) 386–396. <https://doi.org/10.1002/ep.10378>.
- [25] H. Tagawa, Thermal decomposition temperatures of metal sulfates, *Thermochim. Acta*. 80 (1984) 23–33. [https://doi.org/10.1016/0040-6031\(84\)87181-6](https://doi.org/10.1016/0040-6031(84)87181-6).
- [26] P.A. Johnston, R.C. Brown, Quantitation of sugar content in pyrolysis liquids after acid hydrolysis using high-performance liquid chromatography without neutralization, *J. Agric. Food Chem.* 62 (2014) 8129–8133. <https://doi.org/10.1021/jf502250n>.
- [27] A. V. Bridgwater, D. Meier, D. Radlein, An overview of fast pyrolysis of biomass, *Org. Geochem.* (1999). [https://doi.org/10.1016/S0146-6380\(99\)00120-5](https://doi.org/10.1016/S0146-6380(99)00120-5).

- [28] J.K. Lindstrom, Analyzing and exploiting biomass thermal deconstruction, Iowa State University, 2019. <https://lib.dr.iastate.edu/etd/17242>.
- [29] S. Zhou, M. Garcia-Perez, B. Pecha, S.R.A. Kersten, A.G. McDonald, R.J.M. Westerhof, Effect of the fast pyrolysis temperature on the primary and secondary products of lignin, *Energy and Fuels*. 27 (2013) 5867–5877. <https://doi.org/10.1021/ef4001677>.
- [30] A. Fukutome, H. Kawamoto, S. Saka, Kinetics and molecular mechanisms for the gas-phase degradation of levoglucosan as a cellulose gasification intermediate, *J. Anal. Appl. Pyrolysis*. 124 (2017) 666–676. <https://doi.org/10.1016/J.JAAP.2016.12.010>.
- [31] P. Gable, R.C. Brown, Effect of biomass heating time on bio-oil yields in a free fall fast pyrolysis reactor, *Fuel*. 166 (2016) 361–366. <https://doi.org/10.1016/J.FUEL.2015.10.073>.
- [32] M.R. Rover, A. Aui, M.M. Wright, R.G. Smith, R.C. Brown, Production and purification of crystallized levoglucosan from pyrolysis of lignocellulosic biomass, *Green Chem*. 21 (2019) 5980–5989. <https://doi.org/10.1039/c9gc02461a>.
- [33] M.H. Stenzel-Rosenbaum, T.P. Davis, V. Chen, A.G. Fane, Synthesis of poly(styrene) star polymers grown from sucrose, glucose, and cyclodextrin cores via living radical polymerization mediated by a half-metallocene iron carbonyl complex, *Macromolecules*. 34 (2001) 5433–5438. <https://doi.org/10.1021/ma0021803>.
- [34] J.K. Lindstrom, A. Shaw, X. Zhang, R.C. Brown, Condensed Phase Reactions During Thermal Deconstruction, in: *Thermochem. Process. Biomass*, John Wiley & Sons, Ltd, Chichester, UK, 2019: pp. 17–48. <https://doi.org/10.1002/9781119417637.ch2>.
- [35] A.K. Starace, B.A. Black, D.D. Lee, E.C. Palmiotti, K.A. Orton, W.E. Michener, J. ten Dam, M.J. Watson, G.T. Beckham, K.A. Magrini, C. Mukarakate, Characterization and Catalytic Upgrading of Aqueous Stream Carbon from Catalytic Fast Pyrolysis of Biomass, *ACS Sustain. Chem. Eng*. 5 (2017) 11761–11769. <https://doi.org/10.1021/acssuschemeng.7b03344>.
- [36] X. Zhou, W. Li, R. Mabon, L.J. Broadbelt, A mechanistic model of fast pyrolysis of hemicellulose, *Energy Environ. Sci*. 11 (2018) 1240–1260. <https://doi.org/10.1039/c7ee03208k>.
- [37] Y.S. Choi, P.A. Johnston, R.C. Brown, B.H. Shanks, K.H. Lee, Detailed characterization of red oak-derived pyrolysis oil: Integrated use of GC, HPLC, IC, GPC and Karl-Fischer, *J. Anal. Appl. Pyrolysis*. 110 (2014) 147–154. <https://doi.org/10.1016/j.jaap.2014.08.016>.

## **CHAPTER 6. GENERAL CONCLUSION**

Investigation of the underlying oxidation reactions associated with autothermal pyrolysis provided clarity on its operation. While the initial goal was to determine the products oxidizing during autothermal operation, this work showed that inherent differences in biomass feedstock lead to operational differences. This dissertation leveraged previous work regarding pure gas phase and gas-solid phase reactions to derive reaction kinetics associated autothermal pyrolysis. With these rates, the overall operation of an autothermal pyrolyzer can be improved. The four chapters and future work are discussed below.

### **Chapter 1**

This chapter summarized thermochemical processing of biomass and previous attempts at autothermal pyrolysis. The chapter examines the oversights and challenges that previous works had when trying to operate a pyrolyzer in the presence of oxygen. In particular, early attempts at autothermal pyrolysis found that oxygen significantly decreased the yield of valuable bio-oil. Likewise, attempts at modeling autothermal pyrolysis were hampered as experimental data was lacking. However, the work performed in recent years at Iowa State challenged this notion that the introduction of oxygen into the reactor was detrimental. With this success, the need to understand the underlying oxidation reactions was evident leading to the work in this dissertation.

### **Chapter 2**

This chapter explored the oxidation rates of six fast pyrolysis produced biochars in two experimental apparatuses. The biochars were a combination of woody and herbaceous materials with varying ash content, allowing for relationships to be built on compositional parameters. The TGA results indicated that the oxidation rate between a low ash feedstock (red oak) and high ash

(switchgrass) varied by a factor of three under a kinetically limited regime. Though, with increasing temperature ( $>500^{\circ}\text{C}$ ), mass transfer effects started to dominate the overall reaction rate and differences in composition became negligible. The oxidation rate was found to best correlate with potassium content and should be used as the key parameter in modeling char oxidation.

Additional oxidation studies were performed using a fluidized bed reactor finding a similar relationship between the oxidation rate and potassium content. The molar production of  $\text{CO}_2$  vs  $\text{CO}$  was measured during these experiments finding the composition of the biochar appeared to affect the formation of these carbon oxides. This observation is important as fully oxidizing to  $\text{CO}_2$  vs  $\text{CO}$  releases greater energy per mole of oxygen, which is important in starved oxygen environments found during autothermal pyrolysis. This work provided direct evidence that compositional parameters will impact the operation of biomass autothermal pyrolysis.

### **Chapter 3**

Current published gas phase reactions have limited application to autothermal pyrolysis as the mechanisms were not validated for this low temperature operation. Likewise, the products of pyrolysis (i.e. sugars) have little to no relevant combustion data. Thus, the reaction rates of three ideal pyrolysis products, xylose, levoglucosan, and acetic acid, was explored in this work.

The complexity of deriving elementary reactions led to global rates being derived; however, even these rates offer an improvement over current published works. The oxidation and decomposition rates were determined using a fluidized bed reactor with application of the two phase theory of fluidization. Given this novel application of the two-phase theory, the decomposition rate of levoglucosan was compared to previous published works to validate the

system. From the oxidation rate, even among just these three species, the rate varied by an order of magnitude at 500°C. Enthalpy calculations also determined that incomplete combustion represents an inefficient usage of oxygen. This is notable as the equivalence ratio for autothermal pyrolysis is impacted by this inefficient combustion.

## **Chapter 4**

While complete oxidation of products is taking place during autothermal pyrolysis (forming CO<sub>2</sub> and H<sub>2</sub>O), this chapter explored the potential of partial oxidation reactions of the lignin fraction from red oak autothermal pyrolysis. Using multiple analytical techniques and model compound studies, these partial oxidation reactions were detailed.

From these results, it was determined that phenolic hydroxyl groups are oxidizing producing a higher fraction of aromatic carbonyl groups (aldehydes, ketones, carboxylic acids). These oxidized functional groups then underwent condensation reactions different from the typical reactions observed during non-oxidative pyrolysis. These observations were bolstered with model compound studies of different oxidation states, finding the oxidation of phenolic compounds would result in differences in the phenolic oligomers formed.

## **Chapter 5**

From the previous kinetic studies, optimization of pyrolysis products (i.e. sugars) during autothermal operation was performed using pretreated ferrous sulfate corn stover. Based on the oxidation rates from Chapter 3, this study was performed under the guiding hypothesis that a lower operational temperature would optimize sugar yield. Previous research has been conducted on maximizing bio-oil production, but this work focused on a pretreated biomass and autothermal operation proving its novelty.

A semi-detailed analysis of the products found that the valuable sugar fraction (primarily levoglucosan and xylose) was maximized at an intermediate temperature of 450°C. This temperature balanced fully depolymerizing the biomass, while minimizing the oxidation and decomposition of the bio-oil vapors. With increasing temperature, it was evident the biomass became fully depolymerized, as char yield decreased from 28 wt.% to just 14 wt.% from 400 to 550°C, respectively. This work can be used as the basis for future work on the effect of temperature during autothermal operation.

### **Future Work**

Determining and understanding the underlying reactions of autothermal pyrolysis will improve process scale-up. As detailed in Chapter 5, product yield of sugar was optimized based on the information provided from the kinetic rate studies. Likewise, the rates of the bio-oil vapors and biochar oxidation can be used to develop computational models further improving the design and operability of autothermal pyrolyzers. This work does open the door to future studies, as in-depth studies of oxidation of the gas phase products still needs improvement. Likewise, oxidation studies on mixtures of pyrolysis products could be used for validation and further improvement of these gas phase kinetics.



**APPENDIX A. NOMENCLATURE CHAPTER 3**

$A$ =cross-sectional area reactor ( $m^2$ )

$Ar$ =Archimedes number

$d_{b,i}$ =Initial bubble diameter (m)

$d_m$ =Maximum bubble diameter (m)

$d_s$ =diameter sand (m)

$d_b$ =bubble diameter (m)

$g$ =gravitational acceleration ( $m/s^2$ )

$H_{rec}$ =Reactor height (m)

$U_b$ =velocity of bubble (m/s)

$U_o$ =Superficial gas velocity (m/s)

$U_{umf}$ =minimum fluidization velocity (m/s)

$V_b$ =Gas percentage in bubble phase

$\rho_g$ =density of fluidizing gas ( $kg/m^3$ )

$\rho_s$ =density of sand

$\mu_g$ = dynamic viscosity gas, ( $kg/m-s$ )

$V_b$ =Bubble velocity (m/s)

$B$ =bubble

$I$ =initial

$G$ =gas

$S$ =sand

$R$ =reactor

## **APPENDIX B. SUPPLEMENTAL INFORMATION CHAPTER 3**

### **Reactor model**

The two-phase theory modeled the fluidized bed as a set of CSTRs and PFRs. From the proposed correlations the gas percentage allocated to the PFR is calculated versus reactor height. Shown in Figure B.1 is the gas percentage calculated for the PFR versus reactor height, with the dashed line (at 0.05m) indicating the location of the liquid injection port. The two conditions displayed are typical of that used for the decomposition and oxidation studies. The gas calculations indicate that after a height of 0.10m, the bubbles have fully coalesced in the bed and a subsequent minimum is reached for the gas allocated to the PFR. Given the liquid injection location is near this fully developed gas flow, when calculating the gas percentage in the PFR, an average is taken from 0.05m to the maximum height of 0.42m. From the gas percentage in the PFR (bubble phase), the remaining gas is allocated to the emulsion phase and modeled as a CSTR. With this fully developed flow at 0.10m, a single CSTR and PFR was assumed to model the fluidized bed.

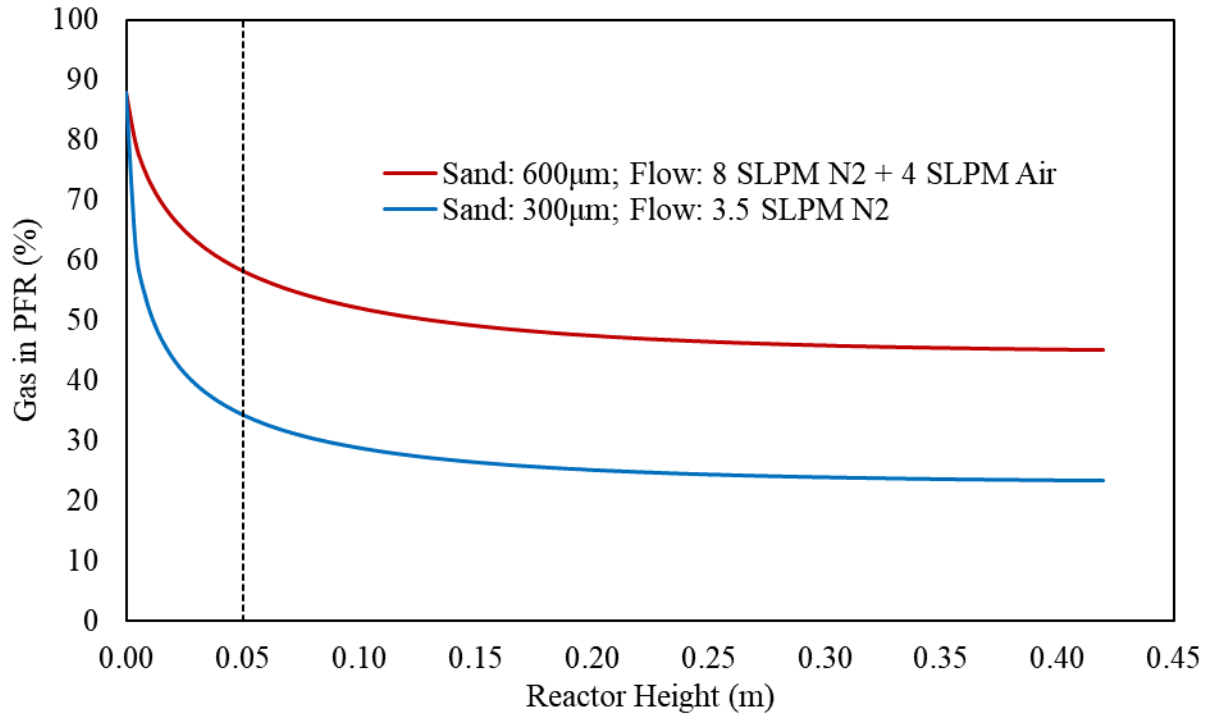


Figure B.1 Gas percentage allocated to the PFR versus reactor height for typical operating conditions. Dashed line at 0.05m indicates location of liquid injection. After a height of 0.10m bubbles have fully coalesced causing the bed to slug.

To calculate the kinetic rate coefficient at each temperature and flow condition, the gas percentage allocated to CSTR and PFR was based on fluidizing gas flow and steam expansion from the liquid injection. Then, a residence time is calculated for the PFR from the average bubble velocity, again taken as the average from 0.05m to 0.42m, and the CSTR residence time calculated from the gas volume flowrate over CSTR reactor volume. With the simplification that a single parallel CSTR and PFR can model the fluidized bed, and one additional PFR for the transfer line, the rate coefficient is easily calculated using a non-linear solver from the three ideal reactors.

Table B.1 Experimental conditions used for acetic acid oxidation trials.

<b>Temperature (°C)</b>	<b>Air Flow (SLPM)</b>	<b>Nitrogen Flow (SLPM)</b>	<b>Liquid Flow (g/min)</b>	<b>Acetic Acid Concentration (%)</b>	<b>Equivalence Ratio</b>
450-1	5.0	7.0	4.3	30	1.03
450-2	5.0	7.0	4.2	30	1.07
500-1	5.0	7.0	3.9	30	1.16
500-2	5.0	7.0	4.0	30	1.12
500-3	3.7	8.3	3.0	30	1.12
550-1	5.0	7.0	3.3	30	1.34
550-2	5.0	7.0	3.9	30	1.15

With levoglucosan being a solid at room temperature, a 21 wt.% solution was made with water to allow for feeding into the reactor. The experimental conditions for the levoglucosan trials are shown in Table S.2. Table S.3 contains the xylose parameters.

Table B.2 Operational conditions used for levoglucosan oxidation.

<b>Temperature (°C)</b>	<b>Air Flow (SLPM)</b>	<b>Nitrogen Flow (SLPM)</b>	<b>Liquid Flow (g/min)</b>	<b>Levoglucosan Concentration (%)</b>	<b>Equivalence Ratio</b>
450	4.4	7.6	4.9	20.9	1.03
500	4.4	7.6	5.1	20.9	0.98
550	4.4	7.6	5.1	20.9	0.98

Table B.3 Operational parameters used for oxidation experiments of xylose.

<b>Temperature (°C)</b>	<b>Air Flow (SLPM)</b>	<b>Nitrogen Flow (SLPM)</b>	<b>Liquid Flow (g/min)</b>	<b>Xylose Concentration (%)</b>	<b>Equivalence Ratio</b>
430	1.7	10.3	4.92	8.3	1.11
465	1.7	10.3	5.05	8.3	1.08
500	1.7	10.3	5.06	8.3	1.08